Title
Mechanical signaling and Patterning Stem Cell-derived Vascular Cells

Author
Wong, Lian Elizabeth

Publication Date
2018

Peer reviewed|Thesis/dissertation

UNIVERSITY OF CALIFORNIA, MERCED

Mechanical Signaling and Patterning Stem Cell-derived Vascular Cells

A dissertation submitted in partial satisfaction of the requirements for the degree of Doctor of Philosophy

in

Materials and Biomaterials Science Engineering

by

Lian Elizabeth Wong

Committee in charge:
Professor Kara McCloskey, Primary Advisor
Professor Christopher Viney, Committee Chair
Professor Ajay Gopinathan
Professor Adam Engler

2018

Mechanical Signaling and Patterning Stem Cell-derived Vascular Cells

The Dissertation of Lian Elizabeth Wong is approved, and it is acceptable in quality and form for publication on microfilm and electronically

_____

Professor Kara McCloskey, Primary Advisor

_____

Professor Ajay Gopinathan

_____

Professor Adam Engler

_____

Professor Christopher Viney, Committee Chair

University of California, Merced
2018

ACKNOWLEDGEMENTS

First, I would like to acknowledge my funding sources, the National Science Foundation (NSF) Grant 0965918 IGERT: Cellular and Molecular Mechanics and BioNanotechnology and the NSF-CREST: Center for Cellular and Biomolecular Machines Fellowship. I would also like to thank UC Merced for awarding me the Graduate Dean's Dissertation Fellowship.

Second, I would like to thank my committee members, Dr. Ajay Gopinathan and Dr. Adam J. Engler for their support and insight. I would also like to thank my chair, Dr. Christopher Viney, for his continued encouragement since my undergraduate years.

Third, I would like to thank my supervisor, Dr. Kara E. McCloskey, for allowing me all the opportunities I have gained thus far.

Fourth, I would like to thank all members of the McCloskey lab, from Dr. Silin Sa, Dr. Drew E. Glaser, and Dr. William Turner who have taught me everything I know, to my lab mates and all my undergraduates who have helped me with all those experiments.

And finally, I would like to thank Norman, my family, and friends for their continued support.

CURRIVULUM VITAE

EDUCATION

Ph.D., Materials and Biomaterials Science Engineering Dec. 2018
University of California, Merced

- Studies focusing on how microenvironment signaling affect vascular cell fate to produce microvascular networks from embryonic and induced pluripotent stem cells. When differentiated into vascular cells they can be used for patient specific therapies, drug screenings, disease modeling, and tissue engineering applications

B.S., Bioengineering May 2013
University of California, Merced

AWARDS/FELLOWSHIPS

- Graduate Dean's Dissertation Fellowship 2018
- BEST Bobcat Summer Award, 2017
- NSF-CREST: Center for Cellular and Biomolecular Machines Fellowship, 2016
- Bobcat Travel Award; School of Engineering, UC Merced, 2016
- Annual UC Systemwide Bioengineering Symposium Travel Award; UC Santa Cruz, 2015
- NSF-IGERT: Cellular and Molecular Mechanics and BioNanotechnology (grant with UIUC) Fellowship, 2014-2016
- NSF-funded nanoBIO node; UIUC, 2014

PUBLICATIONS

5. **Wong, L.**, McCloskey, K. E. (in preparation). Substrate Stiffness Directs Diverging Vascular Fates.
4. **Wong, L.**, Pegan, J., Gabela-Zuniga, B., Khine, M., McCloskey K. (2017). Leaf-inspired microcontact printing vascular patterns. *Biofabrication* 2017 Jun 1;9(2):021001. doi: 10.1088/1758-5090/aa721d
3. Glaser, D.E., Turner, W.S., Madfis, N., **Wong, L.**, Zamora, J., White, N., Reyes, S., Burns, A.B., Gopinathan, A., McCloskey, K.E. (2016). Multifactorial Optimizations for Directing Endothelial Fate from Stem Cells. *PLoS ONE* 2016 Dec 1;11(12):e0166663. doi: 10.1371/journal.pone.0166663. eCollection 2016
2. Sa, S., **Wong, L.**, McCloskey, K. E. (2014). Combinatorial fibronectin and laminin signaling promote highly efficient cardiac differentiation of human embryonic stem cells. *BioResearch Open Access*, *3*(4), 150–61. doi:10.1089/biores.2014.0018
1. Blancas, A. A., **Wong, L.**, Glaser, D. E., & McCloskey, K. E. (2013). Specialized tip/stalk-like and phalanx-like endothelial cells from embryonic stem cells. *Stem Cells and Development*, *22*(9), 1398–407. doi:10.1089/scd.2012.0376

ORAL PRESENTATIONS

- Singh GS, **Wong LE**, Hatano R, McCloskey KE. *Perfusable Vasculature Enhanced by Cardiomyocyte Co-Culture*, UC-Systemwide Bioengineering Symposium in Riverside, CA. June 2018

- **Wong LE**, Glaser DE, McCloskey KE. *Role for Stiffness in Vascular Fate*, Biomedical Engineering Society (BMES) Annual Meeting, Tampa, FL. October 2015
- **Wong LE**, Glaser DE, McCloskey KE. *Role for Stiffness in Vascular Fate*, UC-Systemwide Bioengineering Symposium in Santa Cruz, CA. June 2015
- **Wong LE**, Glaser DE, Choi Y, Pegan J, Engler A, Sim J, Pruitt B, Khine M, McCloskey KE. *Role for Stiffness in Vascular Fate*, Tissue Engineering and Regenerative Medicine International Society-AM in Washington, D.C.. December 2014
- **Wong LE**, Glaser DE, Choi Y, Pegan J, Engler A, Sim J, Pruitt B, Khine M, McCloskey KE. *Role for Stiffness in Vascular Fate*, American Society of Mechanical Engineers (ASME): Nanoengineering for Medicine and Biology Global Conference in San Francisco, CA. January 2014
- DeMarco D, **Wong LE**, Magpantay R, Heinzen I, Limsakoune V, Tung VC. *Carbon-Based Transparent Conductors for Solar Cells*, Innovate to Grow in Merced, CA. May 2013

ADDITIONAL SKILLS DEVELOPMENT

- **Supervisory Certificate Program** in Merced, CA. August 2015–April 2018
- **Student Leadership Council** for IGERT-CMMB, UIUC. 2015
- **NSF-Emergent Behaviors of Integrated Cellular Systems (EBICS) Science and Technology Center-Trainee,** Multi-institutional. August 2014–present
    - Contribute to ongoing collaborations with MIT (Dr. Roger Kamm) to study *in vitro* vasculature formation in microfluidic devices
    - Present findings to internal and industry advisory boards, as well as NSF representations at annual meetings
- **Center of Integrated Nanomechanical Systems (COINS) Intern,** UC Merced. Tissue Engineering Laboratory, Dr. Kara E. McCloskey. May 2013–August 2013
    - Investigate the effect of stiffness on vascular differentiation using a novel mouse ESC line on polyacrylamide gels
- **NSF-funded Emerging Frontiers in Research and Innovation-Multicellular and Interkingdom Signaling (EFRI-MIKS) Summer Experience,** Stanford University. Force Sensing and Remodeling in Multicellular Tissues, Dr. Beth L. Pruitt. June 2012–August 2012
    - Optimize protocols for microcontact printing on different substrates such as glass, PDMS sheets, and PDMS micropost arrays, Study the forces produced by mouse embryonic fibroblasts and human microvascular endothelial cells using PDMS micropost arrays

TEACHING EXPERIENCE

Teaching Assistant, UC Merced, Fall 2017. ENGR 045: Introduction to Materials
Teaching Assistant, UC Merced, Fall 2016. BIOE 114: Tissue Engineering and MSE 111: Kinetics and Processing
Teaching Assistant, UC Merced, Spring 2016. BIOE 104: Biotransport

Teaching Assistant, UC Merced, Fall 2013. BIOE 030: Introductory to Bioengineering and BIOE 104: Biotransport

INVITED LECTURES

Guest Lecturer: Tissue Engineering and Design (BIOE 114/BEST214); UC Merced Material Stiffness and Cell Fate and Bionano Hub Tool Online Training. October 2016
Guest Lecturer: Tissue Engineering and Design (BIOE 114/BEST214); UC Merced Material Stiffness and Cell Fate. March 2015
Guest Lecturer: Tissue Engineering and Design (BIOE 114/BEST 214); UC Merced High Through-put Biological Data. February 2015
Guest Lecturer: Tissue Engineering and Design (BIOE 114/BEST 214); UC Merced Cell and Tissue Culture. March 2013

POSTER PRESENTATIONS

Wong LE, Pegan J., Gabela-Zuniga B., Khine M., McCloskey KE. *Leaf-inspired Microcontact Printing Vascular Patterns*, Biomedical Engineering Society (BMES) in Phoenix, AZ. October 2017
Wong LE, Chua, J., Glaser DE, McCloskey KE. *Role for Stiffness in Vascular Fate*, National Labs Day in Merced, CA. October 2016
Wong LE, Chua, J., Glaser DE, McCloskey KE. *Role for Stiffness in Vascular Fate*, Biomedical Engineering Society (BMES) Annual Meeting in Minneapolis, MN. October 2016
Wong LE, Zamora J, McCloskey KE. *Role for Stiffness in Vascular Fate*, Emergent Behaviors of Integrated Cellular Systems Annual Retreat in St. Charles, IL. July 2016
Wong LE, Hatano R, Whisler J, Chan V, Asada H, Kamm R, McCloskey KE. *Stem-Cell Derived Endothelial and Cardiac Cells for Vascularizing of Muscle*, Emergent Behaviors of Integrated Cellular Systems NSF site visit in Cambridge, MA. December 2015
Wong LE, Glaser DE, McCloskey KE. *Role for Stiffness in Vascular Fate*, Emergent Behaviors of Integrated Cellular Systems Annual Retreat in Atlanta, GA. June 2015
Wong LE, Glaser DE, McCloskey KE. *Role for Stiffness in Vascular Fate*, IGERT Annual Symposium in Champaign, IL. May 2015
Sa S, **Wong LE**, McCloskey KE. *Combinatorial Fibronectin and Laminin Signaling Promote Highly Efficient Cardiac Differentiation of Human Embryonic Stem cells*, Tissue Engineering and Regenerative Medicine International Society-AM in Washington, D.C.. December 2014
Wong LE, Glaser DE, Choi Y, Pegan J, Engler A, Sim J, Pruitt B, Khine M, McCloskey KE. *Effect of Stiffness on Vascular Differentiation,* UC-Systemwide Bioengineering Symposium in Irvine, CA. June 2014
Wong LE, Glaser DE, Engler AJ, Choi YS, McCloskey KE. *Effect of Stiffness on Vascular* Differentiation, IGERT Annual Symposium in Champaign, IL. May 2014
Wong LE, Glaser DE, Engler AJ, Choi YS, McCloskey KE. *Effect of Stiffness on Vascular Differentiation*, Biomedical Engineering Society (BMES) Annual Meeting in Seattle, WA. September 2013

SERVICE, OUTREACH AND MENTORING EXPERIENCE

- **Mentor for GRAD-EXCEL Program**, UC Merced. Met one-on-one with first-year doctoral students bi-monthly to promote early success by coaching and engagement as they acclimate to UC Merced and their graduate students during their first academic year. August 2016–May 2018
- **General member** for Chancellor's Advisory Committee on the Status of Women, UC Merced. September 2016–present
- **Graduate Student Representative** for Society of Asian Scientists and Engineers (SASE), UC Merced. February 2016
- **Graduate Student Representative** for Research Week Committee, UC Merced. September 2015–August 2016
- **Graduate Student Representative** for Graduate Research Orientation Week Committee, UC Merced. September 2015–August 2016
- **Global Cardboard Challenge Judge**, Sonora, CA. Sonora High School Engineering projects. October 2015
- **Mentor** a diverse group of 9 students in undergraduate research, UC Merced. Provide hands-on training in cell culture techniques, laboratory techniques, notebook keeping, critical thinking, troubleshooting, group meeting presentations, and professional development. 2014–2018
- **Team Member for Team Get S.E.T. (Science, Engineering and Technology)**, UC Merced. Worked with a team of six to design extracurricular activities to aid in the teaching of kinematic concepts for Merced County Schools. Designed and improved an air pressure cannon to meet safety requirements and developed accompanying worksheets for high school students. August 2011-December 2011
- **Mentor for Peer Mentor Program, UC Merced.** Met one-on-one with freshmen weekly to discuss any challenges they may be facing in their first year of college. Tracked mentee's progress throughout their first year and provided guidance and encouragement to help them succeed academically. October 2010-August 2011

ABSTRACT

Mechanical signaling and Patterning Stem Cell-derived Vascular Cells

by

Lian Elizabeth Wong

in

Materials and Biomaterials Science Engineering

UNIVERSITY OF CALIFORNIA, MERCED

Committee in charge:
Professor Kara McCloskey, Primary Advisor
Professor Christopher Viney, Committee Chair
Professor Ajay Gopinathan
Professor Adam Engler

2018

Stem cells, including embryonic stem cells (ESC) and induced pluripotent stem (iPS) cells, have been speculated as tools for studying development as well as prospective sources for tissue engineering. However, a major challenge in building tissues and organs is the lack of a vascular system. The development of the vascular system in vivo, starts with ESC differentiating into vascular progenitor cells (VPC), which further differentiates into endothelial cells (EC) and smooth muscle cells (SMC). Studying EC differentiation and the synergistic effects of molecular, cellular, and physical cues that drive blood vessel formation can provide researchers with the means to develop larger tissues in vitro, as well as therapies against vascular diseases in adults. The guidance of stem cell differentiation has largely relied on biochemical factors, but the precise combinatorial signals in the vascular niche has yet to be defined. In this study, mechanical signaling and patterning was explored by probing various components in the microenvironment. Specifically, I 1) studied stiffness directed vascular differentiation, 2) generated vascular patterns with use of biomimicry; 3) optimized human stem cell EC differentiation to form vascular networks.

TABLE OF CONTENTS

ACKNOWLEDGEMENTS iv
CURRICULUM VITA v
ABSTRACT x
LIST OF FIGURES AND TABLES..... xiii

Chapter 1: Introduction 1
1.1 Background 1
1.1.1 Vasculogenesis in the embryo 1
1.1.2 Vascular progenitor cells 2
1.1.3 Biochemical signaling 3
1.1.4 Mechanical signaling 4
1.1.5 Assembly of 3D vascular networks 6
1.1.6 Patterning cells 7
1.1.7 Small-diameter vascular grafts 7
1.2 Goal and Overview of the Dissertation 8
Chapter 2: Substrate Stiffness Directs Diverging Vascular Fates 10
2.1 Introduction 11
2.2 Methods 13
2.2.1 Mouse embryonic stem cell culture 13
2.2.2 Polyacrylamide hydrogel fabrication 13
2.2.3 Characterizing material properties of polyacrylamide hydrogels 14
2.2.4 Induction of Mouse Embryonic Stem Cells to Mesodermal Lineage 14
2.2.5 Immunofluorescence 16
2.2.6 RNA-Seq 16
2.2.7 Inhibitor assay 16
2.2.8 Statistical analysis 16
2.3 Results 16
2.4 Discussion 22
Chapter 3: Leaf-inspired microcontact printing vascular patterns 24
3.1 Introduction 25
3.1.1 Generation of perfusable microvessels 25
3.1.2 Microcontact printing 25
3.2 Methods 26
3.2.1 Mask 26
3.2.2 Leaf mold 26
3.2.3 Vascular stamp 26
3.2.4 Microcontact printing 27
3.2.5 Validation of printed fibronectin 28
3.2.6 Cell culture 28
3.2.7 Immunofluorescence staining and microscopy 28
3.2.8 Collagen gels 28

3.2.9 Matrigel 28
3.3 Results 29
3.4 Conclusions 32
Chapter 4: Generation of Endothelial Cells from Human Stem Cells to Form Perfusable Vascular Networks 33
4.1 Introduction 33
4.1.1 *In vitro* microvasculature 33
4.2 Methods 34
4.2.1 Primary cell culture 34
4.2.2 Mouse embryonic stem cell culture 34
4.2.3 Induction of mouse embryonic stem cells to mesodermal lineage 34
4.2.4 Human stem cell culture 35
4.2.5 Human stem cell induction towards KDR+ VPC (stage 1) 35
4.2.6 Human stem cell induction towards VE-cadherin+ EC (stage 2) 35
4.2.7 Induction of human stem cells towards smooth muscle cells 36
4.2.8 Human stem cell induction towards cardiomyocytes 36
4.2.9 Microfluidic device fabrication 37
4.2.10 Microvascular network formation 38
4.2.11 Vessel quantification 38
4.2.12 Statistical analysis 39
4.3 Results 39
4.4 Conclusions 47
Chapter 5: Electrospinning *Bombyx Mori* Silk with Poly(ethylene oxide) 48
5.1 Introduction 48
5.1.1 Silk fibroin 48
5.1.2 Electrospinning 49
5.1.3 Lumenized muscle 49
5.2 Methods 50
5.2.1 Silk processing and spinning solution 50
5.2.2 Electrospinning 50
5.2.3 Scanning electron microscopy (SEM) 51
5.2.4 X-ray diffraction 51
5.2.5 Primary cell culture 51
5.2.6 Quantifying Cell Alignment 51
5.2.7 Muscle-endothelial bundle device 52
5.3 Results 52
5.3.1 Silk characterization using SEM 52
5.3.2 X-ray diffraction analysis 54
5.3.3 In vitro cell interactions 55
5.4 Conclusions 57
Chapter 6: Conclusions 58
References 61

LIST OF FIGURES

Figure 1: Development of the vasculature 3
Figure 2: VEGFR2 or Flk1 is a possible receptor 4
Figure 3: The mechanisms in which these physical forces 5
Figure 4: Microenvironmental factors direct stem cell fate 9
Figure 5: Mechanotransduction signaling 12
Figure 6: Polyacrylamide hydrogel formation 14
Figure 7: Overview of induction process to examine the role of stiffness 15
Figure 8: Flk-1+ VPC-A3 on Zebraxis on day 8 in stage 2 17
Figure 9: Flk-1+ VPC-A3 on 1 vs. 10kPa and 10 vs. 34 kPa Zebraxis 18
Figure 10: Flk-1+ VPC-A3 on single stiffness matrices at day 7 in stage 2 18
Figure 11: Flk-1+ VPC-A3 and R1 differentiation on single stiffness substrates from day 3-10 in stage 2 19
Figure 12: Gene expression of 10 kPa compared to TCP populations 20
Figure 13: Inhibitor assay on Flk-1+ VPC-A3 outgrowths 21
Figure 14: Proposed mechanism of low stiffness directed EC differentiation. 23
Figure 15: Leaf mask 27
Figure 16: Schematic of the stamping process 27
Figure 17: Images of the patterned cells 29
Figure 18: Resolution of the PDMS stamp 30
Figure 19: Pattern transfer to collagen gels 31
Figure 20: Pattern transfer to Matrigel 31
Figure 21: Optimized protocol for hESC-H9 for EC 36
Figure 22: Differentiation protocol for hIPS for SMC 36
Figure 23: hESC-H9 derived cardiomyocytes stained with cTNT 37
Figure 24: Microfluidic device fabrication 37
Figure 25: Quantification of vessel statistics 39
Figure 26: HUVEC and NHLF form perfusable microvasculature 40
Figure 27: mESC-derived tip/stalk and phalanx EC and NHLF in fibrin gels 40
Figure 28: Vascular progenitor cells in fibrin gels 41
Figure 29: Induction of human ESC cells into VPC (stage 1) into KDR+ cells 42
Figure 30: hESC-H9 derived EC and NHLF in fibrin gels 43
Figure 31: Investigating different accessory cell types co-cultured with HUVEC in microfluidic devices 44
Figure 32: Muscle strip device 50
Figure 33: Processing *Bombyx mori* cocoons 50
Figure 34: Muscle-endothelial bundle device 52
Figure 35: Scanning electron microscope images 53
Figure 36: Histogram of diameter of electrospun fibers 53
Figure 37: X-ray diffraction patterns 54
Figure 38: Normal human lung fibroblasts plated on 55
Figure 39: Muscle-endothelial bundle 56
Table 1: Measured modulus of elasticity of polymerized polyacrylamide 14
Table 2: Cell combinations used in microfluidic devices 38

Chapter 1: Introduction

1.1 Background

The cellular microenvironment is a complex system composed of biochemical signaling, cell-to-cell signaling, and matrix components with distinct biochemical composition, architectural structure and corresponding mechanical signals. Due to this complexity, the precise combinatorial signals in the vascular niche, particularly as they change over time, have yet to be elucidated.

Understanding the various signals in the vascular niche during vasculogenesis and angiogenesis, are important in the field of medicine, as dysfunctions in the system cause numerous pathologies including atherosclerosis and tumor angiogenesis. In tissue engineering, recapitulating the vascular environment is essential to be able to generate a thick enough tissue to facilitate organ regeneration. The fundamental building block to both vasculogenesis and angiogenesis are endothelial cells (EC), which line all blood vessels and are responsible for regulating metabolism, development, healing, regeneration, and immune response in the body. Their multifaceted nature is coupled with the presence of other important cell types, like smooth muscle cells (SMC) and fibroblasts that form each blood vessel.

By deriving vascular EC from stem cells, they can be applied to therapeutic applications, including new vessel formation or for use in drug testing *in vitro*. ESC and iPS are known for their self-renewing properties and their ability to differentiate into all cell types in the body. These characteristics make ESC and iPS appealing tools for therapeutic strategies and developmental models. The derivation of EC from ESC/iPS can be utilized in regenerative therapies to treat cardiovascular diseases, like revascularization of ischemic tissue in patients exhibiting other vascular damage [2, 3]. The capability of stem cells to become any cell type in the body is an exciting tool in regenerative medicine, but also poses a challenge to mimic the vascular niche in the differentiation process.

The development of embryonic vascular networks is temporally and spatially coordinated through various soluble signals in the surrounding microenvironment which provides differentiation, migration, and positioning cues. The guidance of stem cell fate has largely relied on biochemical signals, such as growth factors, and is typically confined to a 2D environment. Recently, the extracellular ‘niche’, including its mechanical environment, has been shown to influence the fate of stem cells *in vitro* [1]. Understanding how mechanical signals in both 2D and 3D microenvironments will enable the study of normal and pathological development processes for the future of regenerative medicine.

1.1.1 Vasculogenesis in the embryo

The development of the vasculature is vital once the growing embryo reaches a size in which passive diffusion cannot adequately supply cells with oxygen and nutrients. Vasculogenesis describes the process of *de novo* formation of blood vessels in the

embryo that arise from endothelial precursor cells (EPC) or angioblasts derived from the mesoderm to form a primitive vascular plexus and form the first blood vessel network [2]. The vascular plexus undergoes further remodeling (angiogenesis) where growth, migration, sprouting, and pruning of these progenitor cells leads to the development of a functional circulatory system. As the network matures, pericytes and SMC stabilize the network and provide contractile support and integrity to the newly formed vessels [3, 4]. Vasculogenesis within the embryo is spatially divided within extra- or intra- embryonic compartments. Extraembryonic vasculogenesis initially forms by the blood islands assembling within the mesodermal layer of the yolk sac [5]. Blood islands form a functional network that facilitates the transfer of nutrients from the yolk sac to the embryo. Intraembryonic vasculogenesis has been shown to occur throughout the mesoderm layer, with the endocardium being the first endothelial structure formed at 7.3 days post-coitum (dpc) [2]. As the heart enlarges, the coronary vasculature is formed to supply nutrients and remove waste from the newly forming heart tissue. Endothelial and smooth muscle precursor cells that develop the heart tube undergo epithelial-to-mesenchymal transformations to give rise to capillaries, arteries, and veins of the coronary vasculature [6].

1.1.2 Vascular progenitor cells

The differentiation of the vasculature is divided into three stages: determination, differentiation, and maturation. Vascular smooth muscle cells (VSMC) and pericytes share a common progenitor with EC [7], and are the primary cells derived from vascular progenitor cells (VPC). The distinction between VCMC and pericytes reside primarily in morphology and anatomical locations. VSMC are mainly associated with arteries and veins while pericytes surround vessels with smaller diameters such as arterioles and capillaries. Expression of Flk-1 has been identified as VPC which may be used to generate pure populations of EC. Notable studies that implicate Flk-1 come from single cell studies done by Nishikawa et al., and Yamashita et al., in which ESC were induced towards Flk-1^{+} cells that gave rise to both EC and hematopoietic cells or EC and VSMC, respectively (Figure 1) [7, 8].

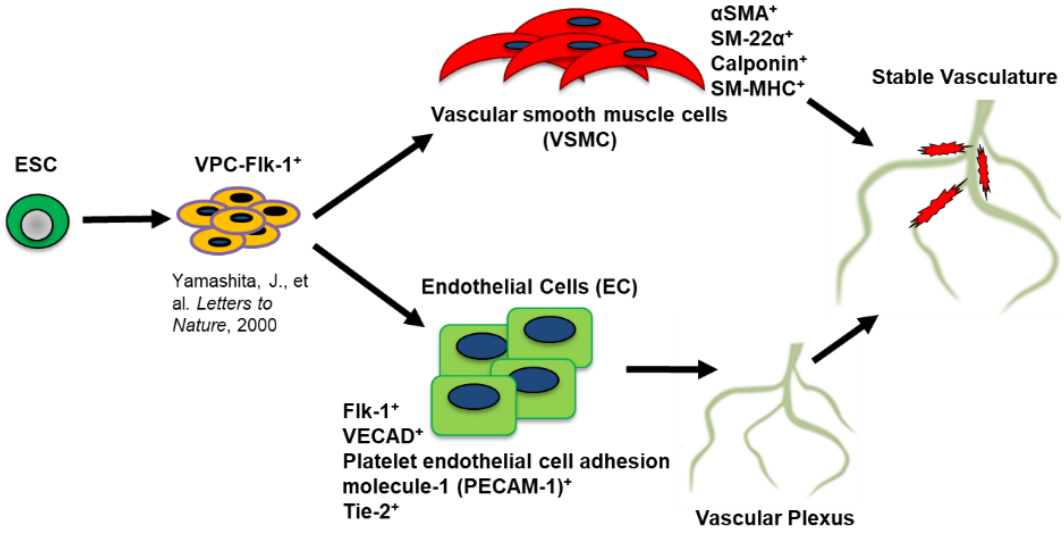

Figure 1: Development of the vasculature. EC and VSMC arise from a common progenitor that are positive for Flk-1 expression. The propagation of EC undergoes vasculogenesis that gives rise to a primitive vascular plexus. This primitive plexus stabilizes through VSMC and pruning through angiogenesis which is the process of new blood vessel formation from pre-existing ones to form a mature vascular structure.

Yamashita et al. studies note the presence of both α-SMA$^+$ (SMC) and PECAM-1$^+$ (EC) cells from a common Flk-1$^+$ progenitor four days after single cell sorting [7]. Moreover, VEGF knockout mice lacking one copy of the receptor genes have abnormal blood vessel formation and subsequently die *in utero* [9]. The absence of blood islands and blood vessel networks is observed in the yolk sac, dorsal aortae, and endocardium, indicating that VEGF/Flk-1 are required very early in development to regulate both vasculogenesis and angiogenesis through signaling cascades [10]. These cues must determine the spatial and temporal appearance of hemangioblasts from undifferentiated mesoderm, and further the maturation and assembly of these precursors into angioblasts and then into mature, quiescent blood vessels. The close development of hematopoietic and endothelial precursors may indicate that both lineages arise from a common progenitor, the hemangioblast, where studies have shown that they share several genes [6].

1.1.3 Biochemical signaling

Chemical signals mark the initiation of a developmental cascade during the early events of endothelial differentiation. Growth factors are soluble molecules that are supplemented in the medium which may prompt cells to grow, replicate, differentiate, or migrate. Without growth factor stimulation, cells are programmed towards apoptotic pathways. Mesoderm-inducing factors are critical for the differentiation of angioblasts, as suggested by the defects in the vascular lineage of embryos lacking the receptor tyrosine kinase, Flk-1 or vascular endothelial growth factor receptor-2 (VEGFR-2) [9, 11]. VEGF is the most published biochemical molecule that regulates vasculogenesis and angiogenesis *in vivo,* and influences the fate of ESC by guiding them towards an EC lineage [7, 8, 12]. Flk-1 is an important receptor that marks for mesodermal commitment, and is influenced by the presence of the following biochemical signals: bone morphogenetic protein-4 (BMP-4), fibroblast growth factor (FGF), and the Wnt ligand [13]. When VEGF binds to the Flk-1 receptor, it induces a signal cascade that activates the Ras pathway, which is believed to influence cell fate towards the vascular lineage [14].

Although BMP-4 is usually associated with osteoblast inductions, it induces undifferentiated cells towards the mesoderm and subsequently endothelial fate from Flk-1$^+$ cells [15]. It has also been reported that BMP-4 induces phosphorylation of Flk-1 and Tie-2 receptors and migration in mESC-derived EC [16]. Lastly, basic FGF (bFGF) has been used with VEGF for EC development and to promote angiogenesis [17]. EC also recruit pericytes and VSMC by releasing platelet derived growth factor (PDGF) [3]. These cell types stabilize the newly formed blood vessel. Transforming growth factor-

beta is responsible for stabilizing VSMC around the blood vessel by promoting VSMC differentiation [18].

1.1.4 Mechanical signaling

In addition to responding to biochemical factors, cells are also constantly sensing the mechanical factors in their surroundings while interacting with the local ECM. The ECM provides additional signaling to tissues for: maintaining tissue integrity, remodeling during adaptations, and repair in response to disease or injury [19]. Even though cells are in close contact with the ECM *in vivo*, cells spatially interact with the ECM differently; EC contact the basement membrane on the basal but not the apical surface [20]. Mechanotransduction is the conversion of mechanical stimuli into chemical signals that affect cellular responses such as proliferation, differentiation, migration, adhesion, and matrix reconstruction [21, 22]. Integrins are transmembrane receptors that act as mechanosensors by sensing and responding to cell-ECM connections, and facilitate inside-out and outside-in signaling pathways resulting from complex combinations of chemical or mechanical stimuli (Figure 2). Fibronectin is a known ECM protein that promotes the differentiation of EC from stem cells [23, 24], and α5β1 integrin activity enhances the secretion of VEGF, thereby providing a positive feedback loop in EC differentiation [25]. Another integrin, α5β3, has been coupled to VEGFR2 to initiate EC migration in response to VEGF binding [26].

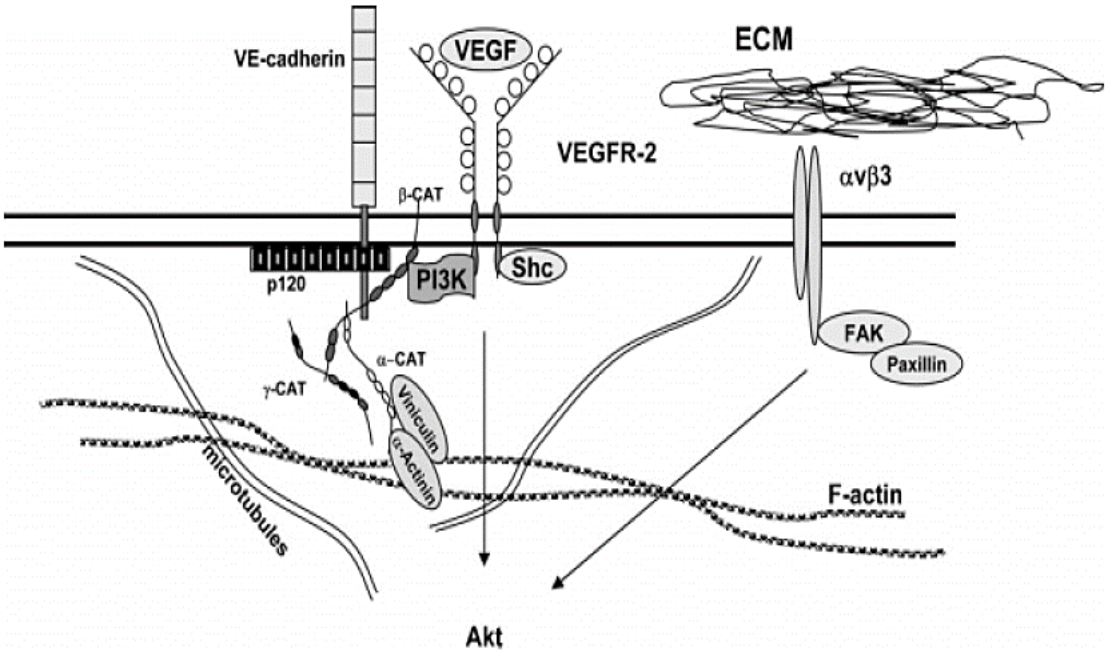

Figure 2: VEGFR2 or Flk1 is a possible receptor that can sense changes in the environment such as shear stress and release soluble factors like VEGF. α5β3 is an integrin that has been shown to sense the ECM and transmit signals inside the cell [27].

In the vascular system, vascular functions are partially maintained through forces produced by blood flow and blood pressure. The constant unidirectional flow of blood

exerts a shear stress on EC that results in changes in morphology, function, and gene expression. With the onset of forces, mechanosensors (ion channels, G protein-coupled receptors, and tyrosine kinase receptors) transmit information to the cytoskeleton to either assemble or disassemble its filaments in response (Figure 3) [28]. The extracellular domain of integrins binds directly to ECM proteins and interact with proteins inside the cell through its cytoplasmic domains. Inside the cell, there are proteins such as focal adhesion kinase (FAK), Src family kinases (SFK), and cytoskeletal proteins such as α-actinin, vinculin, etc. [13] that, together, translate the mechanical signal into a cell fate response. Shear stress also plays a role in determining arterial/venous-EC specification [29].

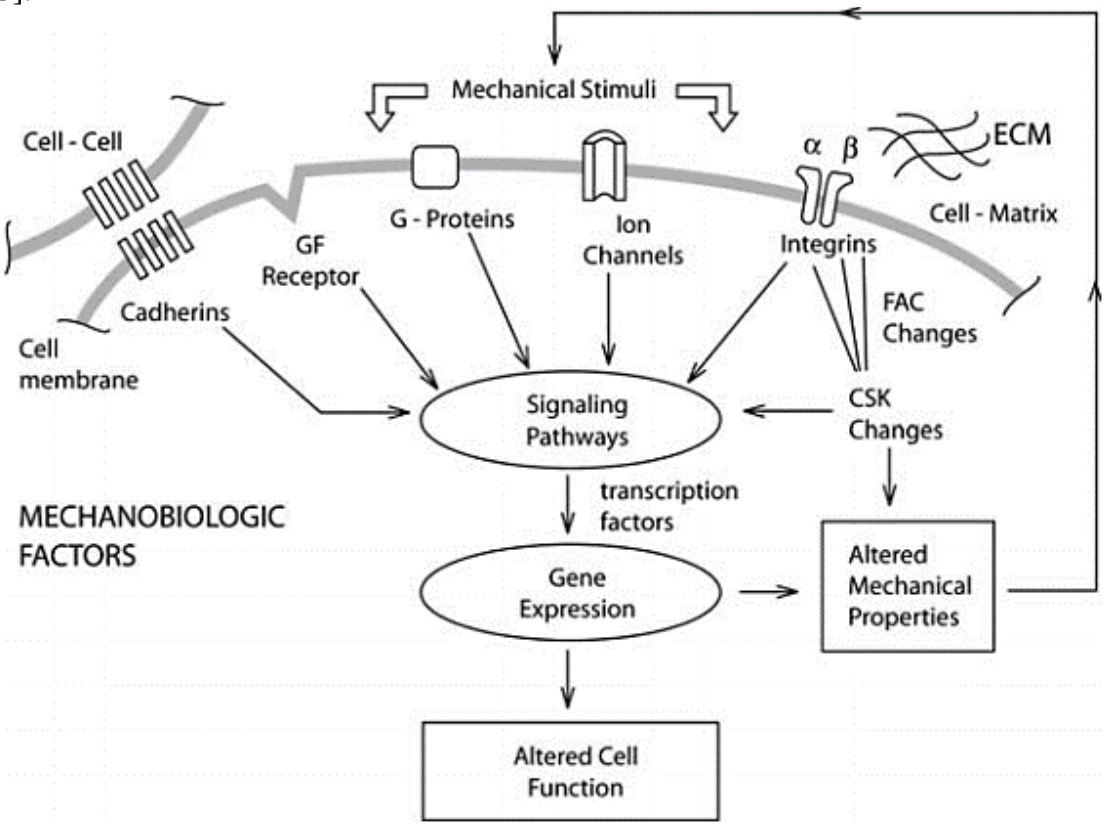

Figure 3: The mechanisms in which these physical forces are being sensed is named the study of mechanotransduction. In mature cells, it has been shown that these cells can sense the mechanical environment, however, in immature or differentiating cells it is not well understood how these mechanisms have a role in directing stem cell fate. Growth factor receptors and integrins are the most studied sensors in mechanotransduction. [30].

In vitro experiments have also developed ways to analyze these signals when EC are subjected to both shear and tensile stresses [31, 32]. EC are subjected to the blood-induced shear stresses as well as stretching forces due to constriction or dilation of vessels from VSMC or pericytes. In addition to transmembrane proteins acting as mechanosensors, the surface of EC is coated in a matrix of membrane-bound proteins called the glycocalyx which include proteoglycan(s [33]. Specifically, heparan sulfate

proteoglycan (HSPG) acts as mechanosensors for EC [34] and SMC [35]. In one study, ESC-derived EC under shear stress increased specific EC markers, such as vascular endothelial-cadherin and PECAM-1. However by using heparinase III enzyme to selectively degrade HSPG, the effects of shear stress on ESC-derived EC were abolished, suggesting that shear stress induced expression of these genes depends on HSPG [36]. Similarly, another study suggests that HSPG is also an important mechanotransducer in modulating SMC gene expression through the activation of the ERK1/2 pathway. When SMC were subjected to laminar flow shear stress there was reduced expression of several SMC markers (α-SMA, SM22, SM-MHC, smoothelin, and calponin). These effects were negated when an enzyme to cleave heparan sulfate was added, as well as an inhibitor to the ERK1/2 pathway and marker expression was not downregulated when shear stress was applied [35].

The modulus of elasticity or stiffness is a characteristic of the ECM that certain anchorage-dependent cells sense and respond to with a variety of cellular processes, including lineage specification and commitment of progenitor cells [37]. When mesenchymal stem cells are seeded on soft substrates, Flk-1 is upregulated while the stiffer substrate upregulates protein markers associated with SMC fate [38]. Softer materials also increase the migration of many cell types and form more capillary-like structures [39]. The forces that cells exert on the matrix and the mechanical resistance of the matrix gives rise to tension across the cell membrane which leads to changes in expression of genes and differentiation.

In the vascular system, the stiffness of transplanted *ex vivo* blood vessels vary significantly from healthy versus diseased endothelium and between arterial and venous environments. The healthy range of arterial EC is reported to be from 3-5 kPa while diseased stiffness are higher, ranging from 13-280 kPa [40].Porcine aorta stiffness measured by atomic force microscopy (AFM) is reported to be 5-8 kPa [41] and similarly mouse arteries are measured at 5 kPa [42, 43], while bovine carotid arteries are measured at 2.5 kPa [44]. Conversely, the diseased arteries in ApoE-null mice, a model for atherosclerosis, exhibit an increased stiffness of 28 kPa [42, 43]. Interestingly, longitudinal tensile stress of bovine veins range from 35-100 kPa [45]. These studies suggest that recapitulating the stiffness of the endothelial microenvironment is an important factor in development and diseases.

1.1.5 Assembly of 3D vascular networks

Perfusion of larger engineered biological tissues is required to ensure proper function and survival in its intended environment. However, advances in tissue engineered microvascular networks have been slow. Current limitations include the small size of lumen diameter, vessel length, complex geometries, and high vessel density requirements. Recently, a few laboratories have been able to generate perfusable vasculature by utilizing microfluidic devices made from molded polydimethylsiloxane (PDMS) seeded with human umbilical vein endothelial cells (HUVEC) and normal human lung fibroblasts (NHLF) within fibrin or collagen gels [46-48]. These gels contain angiogenic properties that subject cells to mechanical signaling through integrins

that associate with the cytoskeleton [49]. Changing the concentration of fibrinogen allows for modifications of the gels' mechanical and viscoelastic properties that lead to increased vascular-like formation [49-51]. When HUVEC are co-cultured with stromal cells, networks do not regress as quickly and maintain their stable morphology over longer times [46]. While HUVEC have been the most utilized cell type for building microvasculature *in vitro*, the use of stem cells are of particular interest as a cell source. Additionally, iPS-derived EC, would allow for pathologies associated with patient-derived tissues to be examined [52].

1.1.6 Patterning cells

One potential alternative for providing semi-structured vasculature is to transfer patterned EC as distinct layers between sheets of cell/tissues or on the surface of biomaterials. Microcontact printing proteins is a well-known technique that is utilized to control spatial patterning and cell-cell interactions [53]. However, the successful biomimetic replicate of a highly branched vascular tree requires the anatomical structure of the native vasculature include branching over various length scales. Analogous to the transport of oxygen and nutrients in the blood vessel, the leaf contains veins that transport food and water to the plant. The length scales in the leaf can also mimic our microcapillary system. The veins of the leaf can also branch into smaller and smaller tributaries, just like the vascular system. Specifically, net-veined or reticulate-veined leaves contain veins that branch from the main rib with subdivisions into finer veinlets, extending from a midrib to the edge (elm, peach, apple, cherry), or radiate fan-shaped (maple, grapes). Some leaves are even designed in a parallel configuration (tulip). These lessons from nature can be exploited to create innovative designs in building new tissues.

1.1.7 Small-diameter vascular grafts

Small-diameter (<6 mm) vascular grafts potentially serve as an alternative solution for patients who cannot undergo bypass surgeries. However, delayed re-endothelialization of commercially available non-degradable synthetic grafts [54] is a major obstacle. EC mitigate thrombus formation, and therefore, are vital for long term graft survival [55, 56]. Cell-seeded tissue engineered vessels have been shown to perform better at the blood-material interface. However, these natural grafts exhibit limited mechanical integrity without synthetic supplementation in the scaffolding [57]. Silk fibroin is a naturally occurring polymer that can be blended with different ECM proteins, growth factors, or other polymers through electrospinning techniques and has been explored as a viable substitute for blood vessels [58]. The rate of degradation can also be tuned and has been shown to be replaced by collagen and other ECM proteins within the body [59, 60]. Silk vascular grafts have been reported to have comparable mechanical properties to those of native blood vessels [58]. Silk material is easily processed, biocompatible, with tunable properties that are suitable for small-diameter vascular grafts.

1.2 Goal and Overview of the Dissertation

Blood vessels are the essential transport mechanism responsible for moving oxygen and nutrients throughout the body. For sufficient transportation, most cells are found no more than 100-200 μm from the nearest capillary [61]. This diffusion limitation significantly restricts researchers' ability to build tissues and organs for regenerative medical applications and impedes successful integration after implantation. Thus, integration of a functional vascular network is essential for tissues greater than thicknesses of 500 μm [62, 63]. Endothelial cells (EC), which line the interior surface of blood vessels, are a critical component to building vasculature *in vitro*. Smooth muscle cells (SMC) associate with blood vessels, mainly arteries, to synthesize supporting matrix and control blood pressure, with pericytes supporting the smaller vessels. By understanding the synergistic effects of molecular, cellular, and physical cues that drive blood vessel formation, we may provide the field with the means to develop larger tissues *in vitro,* as well as therapies against vascular diseases in adults.

Embryonic stem cells (ESC) and induced pluripotent stem cells (iPS) are exciting *in vitro* models, retaining the ability to differentiate into all cell types in the body, and are potential cell sources for patient specific therapies, drug screenings, and disease modeling. The guidance of stem cell differentiation from soluble signals (i.e. cytokines) has been well-examined in several cell lines [23, 64, 65] , but the precise combinatorial signals, including mechanical signaling in the vascular niche guiding vascular specification have yet to be defined (Figure 4).

It has become apparent that mechanical signaling plays a critical role in the development of many tissues differentiation [37], but its role in vascular EC or SMC fate from a common vascular progenitor cell (VPC) remains undiscovered [7]. Therefore, the goal of the work in this thesis is to investigate microenvironment niche signals for enhanced EC and vascular formation of perfusable vasculature. This thesis focuses on 1) stiffness directed differentiation, 2) microcontact printing for vascular assembly, and 3) microvasculature formation. The following chapter, Chapter 2, investigates how stiffness directs VPC towards EC or SMC, and examines a panel of mechanosensors and their effect on mechanotransduction. Chapter 3 examines signaling from topological patterns. We show how leaf veins can be used to generate a reverse mold to mimic branching vasculature by using microcontact printing. Chapter 4 examines the development of vasculature using stem cell derived-EC by looking at cell ratio, concentrations, and exogenous soluble factors, as well as, the role of supporting cell type in. Chapter 5 examines using electrospun silk as a scaffold to generate a muscle-endothelial bundle to provide perfusion through our cardiac muscle strips. The last chapter includes a discussion of the challenges and successes involved in obtaining the data presented in this dissertation.

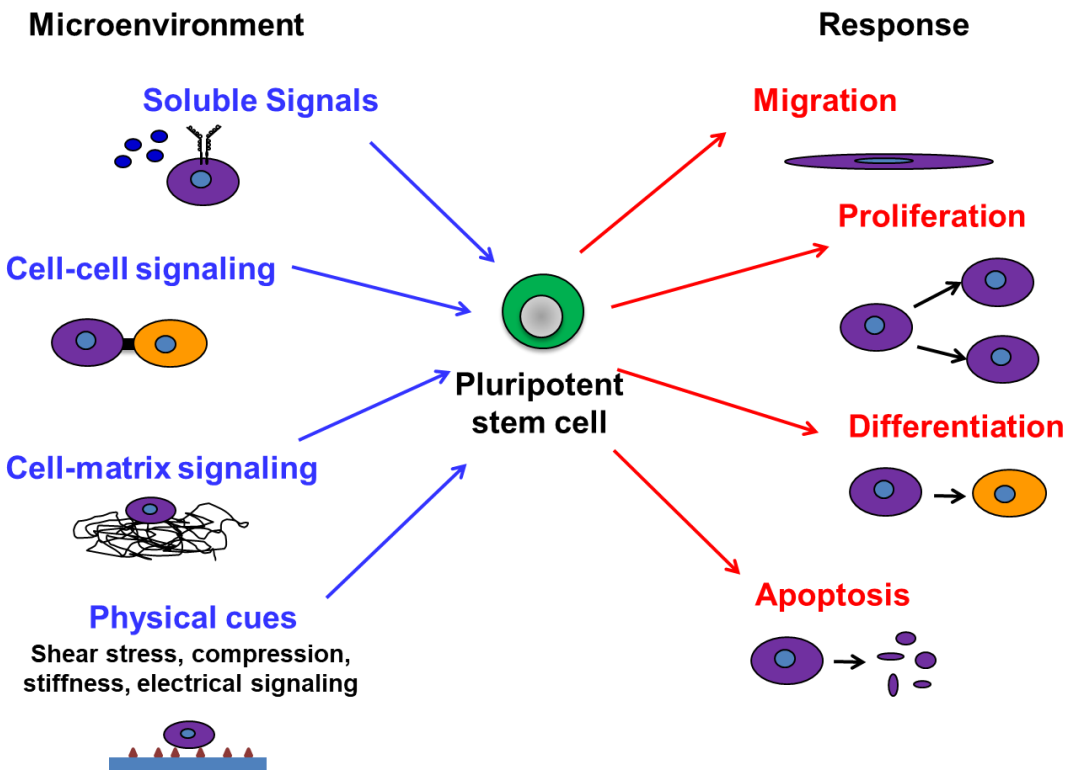

Figure 4: Microenvironmental factors direct stem cell fate. Soluble factor signaling, cell-ECM interactions, cell–cell interactions shear stress, and material stiffness can all influence stem cell commitment.

Chapter 2: Substrate Stiffness Directs Diverging Vascular Fates

ABSTRACT

In addition to providing cells sourcing for many cell therapies, ESC and induced pluripotent stem (iPS) cells are excellent cell culture systems for elucidating developmental signals. ESC and iPS cells are traditionally cultured and induced into tissue-specific derivatives on tissue culture plastic, however; it has been recently shown that the stiffness of the substrate also plays a role in directing cells towards differential cell lineages. Using our chemically-defined and staged induction methods, the putative role for stiffness in vascular fate was examined in 2 distinct ESC lines. After initial induction and purification of multipotent Flk-1+ vascular progenitor cells (VPC), the diverging endothelial cell (EC) and smooth muscle cell (SMC) populations were quantified for expression of either platelet endothelial cell adhesion molecule (PECAM-1). Here, we were able to culture mouse ESC VPC on single stiffness polyacrylamide hydrogels and observed EC and SMC emerging in a spatially distinct arrangement and identify signaling pathways that may be contributing to stiffness directed vascular differentiation.

2.1 Introduction

In vivo, cells are closely integrated with their cellular microenvironment - a complex system composed of soluble signals, cell-to-cell interactions, and extracellular matrix (ECM). The structural cells, soluble signals and ECM proteins combine to provide mechanical support, as well as signals that influence cell behavior and even cell fate. Although it has been well-known that matrix elasticity influences 2D cell migration [66], matrix elasticity has also recently been shown to provide a distinct signal that can exert effects on the lineage specification of progenitor cells [37]. Subsequently, a flurry of manuscripts have published on guiding the differentiation of epidermal stem cells [67], osteoblasts [68, 69], and neuronal [37, 70] by tuning the substrate stiffness to *in vivo* like conditions. Specifically, mesenchymal stem cells (MSC) differentiate towards adipocytes on less stiff matrices, while bone differentiation occurs on stiff matrices [37, 71].

However, with regards to the role of stiffness in directly vascular endothelial fate, only 1 direct study has been published suggesting that low stiffness (2kPa) in directing mesenchymal stem cells (MSC) towards an EC fate. Unfortunately, it was unclear whether the nanofibrous architecture was, in fact, also playing a role in cell fate specification since the experimental design simultaneously changed from high stiffness polystyrene dishes to the low stiffness nanofibrous architecture [72]. Moreover, the role of stiffness in directing embryonic stem cells or vascular progenitor cells towards and endothelial fate has not yet been examined. There are a few more studies studying the role of stiffness in smooth muscle fate, with one showing that stiff substrates had a higher expression of SMC markers from MSC (15kPa), while MSC on soft substrates had a higher expression of chondrogenic and adipogenic markers (1kPa) [73]. Another, using a nanofiber matrix showed that stiff matrices (8-15kPa) had an increase of smooth muscle actin while soft (2-5kPa) had an increase of Flk-1 expression [38]. However, Flk-1 expression is a known vascular progenitor marker that can differentiate into both EC and SMC [7], so it is unclear if a specific cell type was obtained, and rather only a commitment to becoming a vascular cell.

Despite the lack of evidence directly showing that low stiffness materials can direct EC fate from vascular progenitor cells (VPC), there are a number of studies that show that mature EC internalize vascular endothelial growth factor (VEGF) [74], as well as, upregulate the production of VEGF [75] and GATA2 [76], a VEGF2 promoter, following culture on low stiffness materials, and that this specifically replaces the Rho/ROCK signaling pathway [75] that typically leads to upregulation of VEGF. Based on these studies, we expect that low stiffness will direct EC compared to vascular SMC, but the direct effect of matrix stiffness on vascular endothelial fate has not yet been shown.

The matrix stiffness, largely sensed by integrins [77], has been shown to manipulate lineage specification and commitment of progenitor cells [37]. The forces that cells exert on the matrix, as well as, the mechanical resistance of the matrix, gives rise to tension across the cell membrane which leads to changes in expression of genes

and differentiation. Integrins are transmembrane receptors that act as mechanosensors by sensing and responding to cell-ECM connections, and facilitate inside-out and outside-in signaling pathways resulting from complex combinations of chemical or mechanical stimuli. Integrins are composed of α and β subunits, and several have been implicated to be necessary in cell differentiation. Fibronectin is a known ECM protein that promotes the differentiation of osteoblasts through its interaction with α5β1 [78, 79], but also promotes the differentiation of EC from stem cells [23, 24] and through α5β1 integrin activity. This interaction enhances the secretion of VEGF, providing a positive feedback loop in EC differentiation (Figure 5) [25]. When β1 integrins are activated, a signaling cascade occurs through FAK and other proteins which leads to the activation of Ras-ERK and mitogen-activated protein kinase pathways which has been shown in both endothelial [80] and osteoblast differentiation [81]. Another integrin, α5β3, has been coupled to VEGFR2 to initiate EC migration in response to VEGF binding when interacting with vitronectin or fibrinogen [26, 82, 83]. In contrast, cells in suspension showed reduced VEGFR2 activation in response to VEGF. Although there are known mechanosensors and signaling pathways, previous studies have only used tissue culture plastic. The effect of varied stiffness to mimic *in vivo* like conditions on these signaling processes has not been studied.

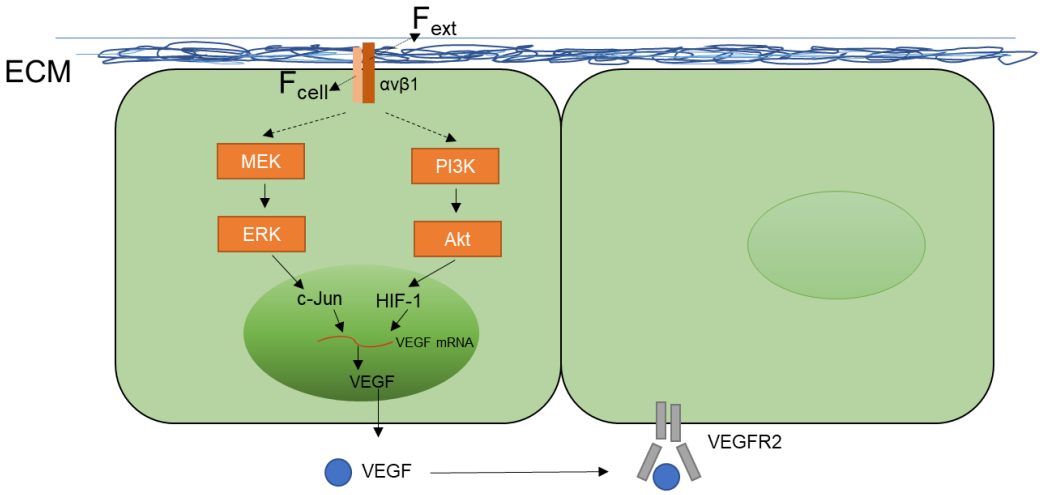

Figure 5: Mechanotransduction signaling. The cell exerts a force (F_{ext}) which is internalized (F_{cell}) at a mechanosensor (an integrin) and activates multiple intracellular signaling pathways to secrete VEGF which creates a positive feedback loop by activating VEGFR2.

In the vascular system, the stiffness of transplanted *ex vivo* blood vessels also vary significantly from healthy versus diseased endothelium and between arterial versus venous EC. Porcine aorta stiffness is reported at 5-8 kPa [41] and similarly mouse arteries are measured to be 5 kPa [84], while bovine carotid arteries are measured at 2.5 kPa [44]. However, the arteries in ApoE-null mice, a model for atherosclerosis, exhibit an increased stiffness of 28 kPa [84]. Altogether, the healthy range of arterial EC is reported to be from 3-5 kPa while diseased stiffness is significantly greater, ranging from 13-280 kPa [40], suggesting that recapitulating the stiffness of the endothelial microenvironment is an important factor in development and diseases.

To mimic this physiological environment, matrix elasticity can be altered in a variety of materials: polyethylene glycol (6-26 kPa) [85, 86], alginate (0.1-30 kPa) [87, 88], PDMS (0.1-2700 kPa) [68, 89]. Polyacrylamide gels can mimic physiological conditions by altering the concentration of bis-acrylamide and generating stiffnesses that can vary by three orders of magnitude from 0.1 kPa to 200 kPa [66, 90]. Polyacrylamide hydrogels offer an easily tunable material that mimics stiffness found *in vivo*, compared to traditional cultures on glass and plastic surfaces. Also, polyacrylamide gels exhbitg1hhrt4r4e optical properties that allow generation of images similar in quality to traditional culture platforms.

To study how stiffness affects vascular fate from stem cells, cells were cultured on polyacrylamide hydrogels as the stiffness tunable substrate. Using our novel mouse ESC that express a GFP reporter under Tie-2 and a RFP reporter under α-smooth muscle actin, we examined the role of stiffness in the diverging fate of Flk-1^+ vascular progenitor cells (VPC). By using Zebraxis, which have strips that vary in stiffness we set out to observe if the stiffness will produce endothelial-like cells or smooth muscle-like cells. Next, we examined the role of stiffness on single stiffness surfaces (10- and 40 kPa) to better quantitate endothelial or smooth muscle cell levels. The commitment of Flk-1^+ cells towards EC or SMC lineages will be quantified temporally over the course of 3-10 days. By using various inhibitors and antibody-blocking, we identify signaling pathways that may be contributing to stiffness directed vascular differentiation.

2.2 Methods

2.2.1 Mouse embryonic stem cell culture

R1 and A3 murine embryonic stem cells were maintained on 0.5% gelatin coated plates in serum-free medium containing Knockout Dulbecco's Modified Eagle Medium (KO-DMEM; Invitrogen), 15% Knockout Serum Replacer (KSR; Invitrogen), 1X Penicillin-Streptomycin (Invitrogen), 1X Non-essential Amino Acids (Invitrogen), 2mM L-glutamine (Invitrogen), 0.1mM 2-mercaptoethanol (Calbiochem), 2000 Units/ml of leukemia inhibitory factor (LIF-ESGRO; Chemicon), and 10 ng/ml of bone morphogenetic protein-4 (BMP-4; R&D Systems). Full media changes occurred every other day and cells were passaged every four to five days.

2.2.2 Polyacrylamide hydrogel fabrication

Zebraxis were generously made by Dr. Engler, according to the methods described here [91]. Acrylamide was polymerized on aminosilanized 25mm diameter coverslips. A solution containing the cross linker N,N' methylene-bis-acrylamide, acrylamide, 1/100 volume 10% ammonium persulfate, and 1/1000 volume of N,N,N,',N'-Tetramethylethylenediamine was mixed. For single stiffness, two different combinations of acrylamide and bis-acrylamide were used to make 10 and 40 kPa substrates [92]. 25 µL of the mixed solution was placed between the aminosilanized treated coverslip and a Rain-X treated glass slide. 50 µg/mL fibronectin was chemically crosslinked to the substrates using photo activating cross linker Sulfo-SANPAH (Pierce)

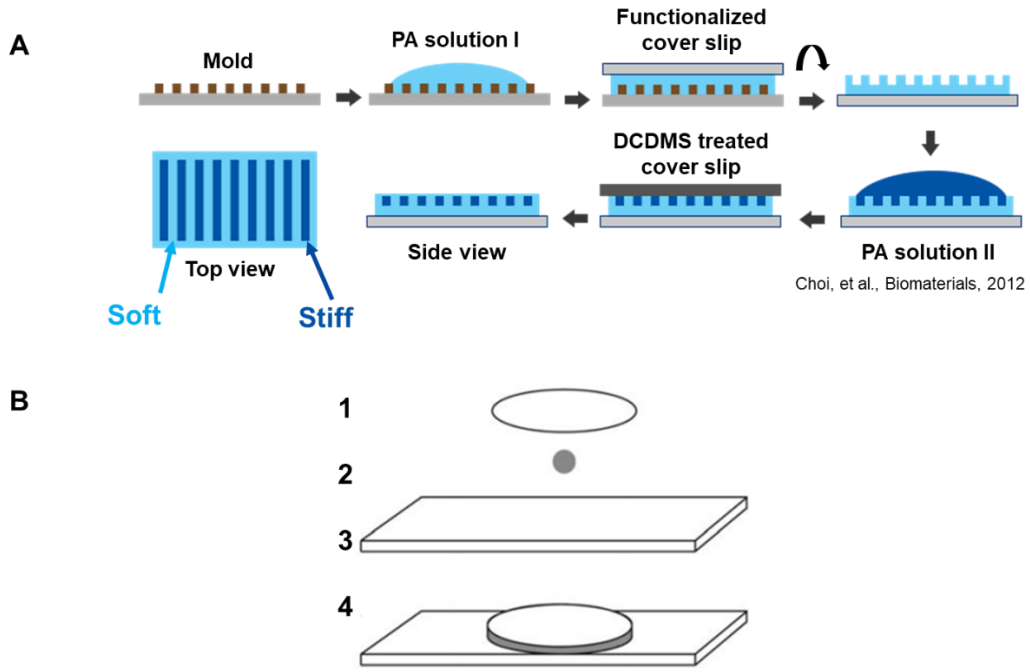

Figure 6: Polyacrylamide hydrogel formation. A) Zebraxis formation, image adapted from [91]. B) Single-stiffness polyacrylamide [92].

2.2.3 Characterizing material properties of polyacrylamide hydrogels

Indentation experiments were performed with a commercial AFM apparatus (NTEGRA Vita, NT-MDT). A spherical borosilicate glass bead with a diameter of 10 µm was used (SNL-10, Bruker). Young's modulus of elasticity, *E*, was calculated using Nanoindentation of Soft Elastic Materials on Nanohub, where force curves were obtained by the deflection of the AFM cantilever as it was unloading from the sample [93]. Poisson's ratio was assigned a value of 0.5 [94].

	Acrylamide %	Bis-Acryl %	E±SD (kPA) n=5
10 kPa	10	0.10	10±3
40 kPa	8	0.48	40±2

Table 1: Measured modulus of elasticity of polymerized polyacrylamide. This table shows the relative concentrations of acrylamide and bis-acrylamide and their measured modulus of elasticity. 1 hydrogel per sample and 5 indentations per hydrogel were assessed for these measurements.

2.2.4 Induction of Mouse Embryonic Stem Cells to Mesodermal Lineage

For dissociation, R1 mESC were harvested from 0.5% gelatin coated dishes using TrypLE (ThermoFisher) while A3 mESC were disassociated from the MEF layer and purified through a gravity separation prior to plating on 100mm tissue culture treated plates (Corning) coated with 0.050 mg/mL fibronectin (Corning). Cells were then fed with stage 1 medium containing alpha-MEM (Cellgro), 20% knockout serum

replacement (ThermoFisher), 1X penicillin-streptomycin (ThermoFisher), 1X nonessential amino acids (ThermoFisher), 2mM L-glutamine (ThermoFisher), 0.05mM 2-mercaptoethanol (Calbiochem), 5 ng/mL BMP-4 (Peprotech), and 30 ng/mL or 20 ng/mL of VEGF (Peprotech) for R1 and A3, respectively. Cells were cultured for 2 (R1) or 3 (A3) days for optimal number of Flk-1+ cells. Adherent cells were harvested using Cell Dissociation Buffer (ThermoFisher) and sorted based on expression of Flk-1 (PerCP, Biolegend) using fluorescent activated cell sorting (BD, ARIA II).

The purified Flk-1+ cells were cultured onto fibronectin-coated Zebraxis-coated slides or single stiffness polyacrylamide (PA) hydrogels or on our tissue culture plastic control Figure 7. Cell densities on substrates was varied to control total number of cells: 30,000 cells/cm^2, 20,000 cells/cm^2 and 10,000 cells/cm^2 and observed for the next 10 days in stage 2 medium consisting of 70% alpha-MEM (Mediatech), 30% DMEM (Invitrogen), 2X Nutridoma CS (Roche), 1X penicillin-streptomycin (Invitrogen), 1X nonessential amino acids (Invitrogen), 2 mM L-glutamine (Invitrogen), 0.05 mM 2-mercaptoethanol (Calbiochem), and supplemented with 30 ng/mL VEGF and 5 ng/mL BMP4 for R1 or 10 ng/mL VEGF and 10 ng/mL bFGF for A3 (as previously optimized [17]).

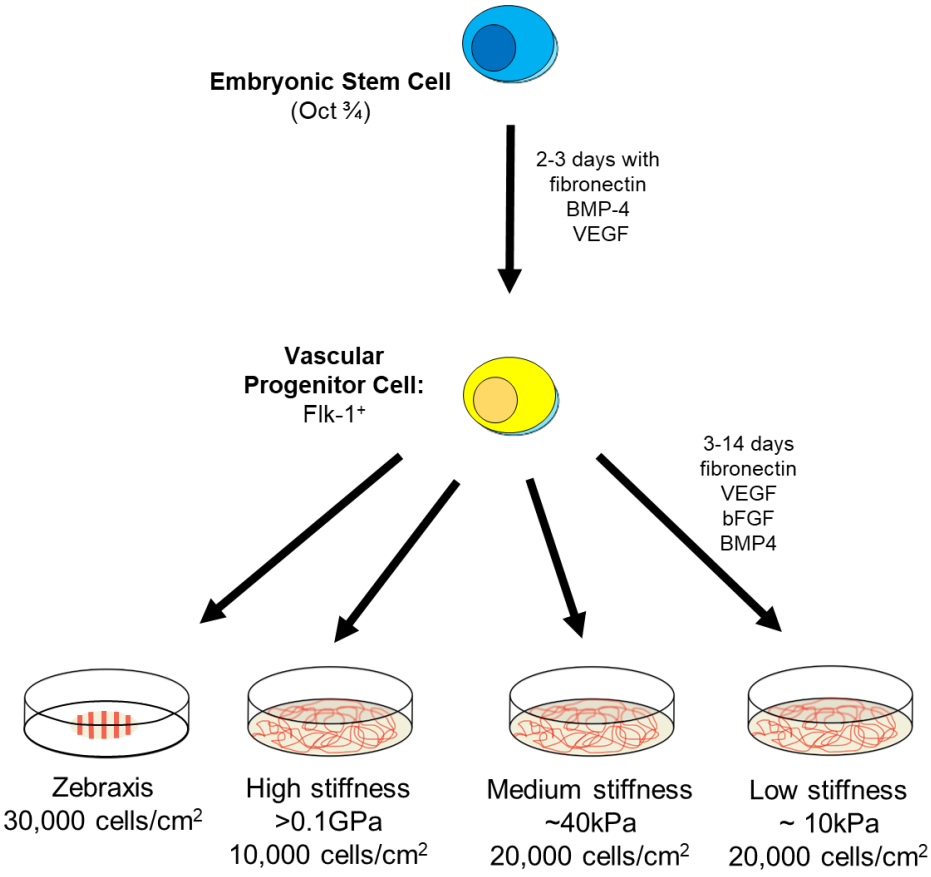

Figure 7: Overview of induction process to examine the role of stiffness. Induce R1 and A3 mESC into Flk-1+ vascular progenitor cells and plate on Zebraxis or tissue culture plastic (>0.1 GPa), 40 kPa, and 10 kPa, which are all coated with fibronectin.

2.2.5 Immunofluorescence

R1 and A3 stage 2 cells were grown from 3-10 days and fixed with 4% paraforaldeyde (Tousimis) for 5 minutes at room temperature. Cells were placed in a solution of 0.7% Triton X-100 (Fisher), 5% donkey serum (Fitzgerald), and 1% bovine serum albumin (Sigma) for another 5 minutes at room temperature to be permeabilized and block non-specific binding of the antibody. CD31 PE (rat, BD Biosciences) and primary antibody against Calponin-1 (mouse, Sigma) were used in a dilution of 1:200 and 1:30000, respectively in 1% bovine serum albumin. Secondary FITC anti-mouse (abcam) was used in a dilution at 1:300. Cells were stained for 1 hour at room temperature for both primary and secondary incubation. During secondary incubation, DAPI was added to stain the nucleus.

2.2.6 RNA-Seq

Total RNA was extracted with TRIzol reagent (Life Technologies). Ribo-Zero Gold rRNA Removal Kit (Illumina) was used to remove ribosomal RNA before preparation of sequencing libraries using the ScriptSeq RNA-Seq Library Prep Kit (Illumina). Sequencing was performed with Illumina HiSeq 4000 systems, and raw sequence reads were examined for quality using FastQC [95]. The reads were subsequently trimmed to remove adaptors and filtered for bad quality bases using Trim Galore [96, 97]. Clean sequence reads were aligned to mouse genome, mm10, using STAR aligner [98]. Gene counts were called using HTSeq (5), and differentially expressed genes were identified using DESeq2 R package [99]. Gene ontology (GO) analysis was carried out using DAVID [100, 101] to identify enriched biological functional groups and processes.

2.2.7 Inhibitor assay

Flk-1+ VPC-A3 were plated on single-stiffness surfaces for 24 hours then the media was replaced with the following inhibitors added: 5μM FAK inhibitor 14 (Tocris Bioscience), 1:200 αvβ3 (Bioss), 1:200 αvβ1 (Bioss), and 10 ug/mL αvβ6 (abcam) for another 24 hours. The cells were fixed and stained as previously explained.

2.2.8 Statistical analysis

Statistical analyses were conducted with GraphPad Prism 7 software. Two-way ANOVA with Tukey's multiple comparison for the analysis of three groups was used. Differences at $P \leq 0.05$ were considered statistically significant. P values were calculated by analysis of variance for multiple pairwise comparisons. The data are reported as mean ± SEM.

2.3 Results

Using Zebraxis with alternating channels of elevated and depressed channels (1 vs. 10 kPa and 10 vs. 34 kPa - with greater stiffnesses on the elevated channels and the

lower stiffnesses on the depressed channels), we were able to show that Flk-1+ VPC differentiated towards both Tie-2+ GFP expressing and αSMA+ RFP expressing cells on the stiffer channels on day 8 (Figure 8).

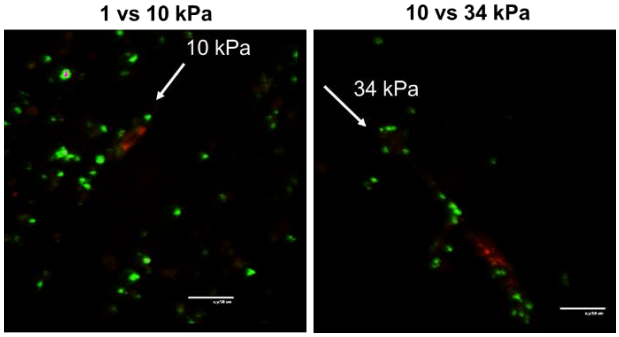

Figure 8: Flk-1+ VPC-A3 on Zebraxis on day 8 in stage 2. Confocal images of live A3-VPC on two different Zebraxis: 1vs10 kPa and 10vs34 kPa. There appears to be more Tie-2 GFP+ cells on the 1vs10 kPa compared to the 10vs34 kPa. Green: Tie-2 GFP and Red: SMA RFP+. Scale bar=50 μm.

On day 12, cells were fixed and stained with PECAM-1, SM22α, and DAPI (Figure 9). On the 1 vs. 10 kPa Zebraxis, cells were observed on only the 10 kPa stripe. However, cells on the 10 vs. 34 kPa Zebraxis were observed to be only on 34 kPa stripe. The cells consistently migrated to the elevated surface, which also happened to be the stiffer surface. The mechanism in which cells migrate upward onto an elevated ridges or channels rather than in the downward direction has been documented by other groups, but is not well-understood [36, 37]. Due to design limitations of the alternating channels, we moved to single-stiffness surfaces.

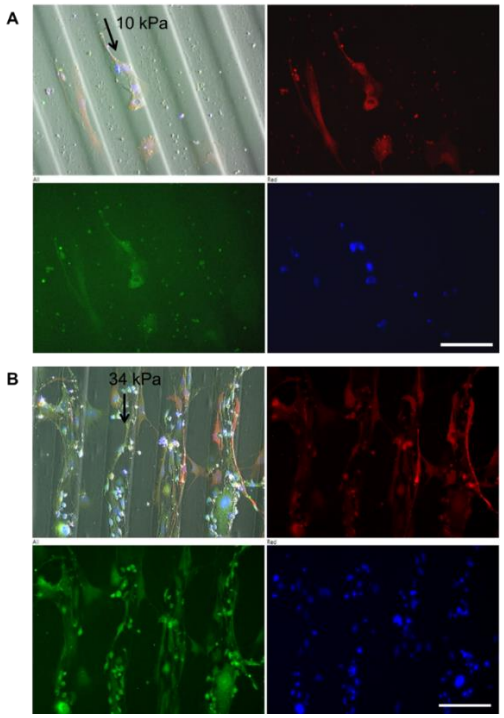

Figure 9: Flk-1+ VPC-A3 on 1 vs. 10kPa and 10 vs. 34 kPa Zebraxis on day 12 in stage 2. Cells were fixed and stained with PECAM-1 (green), SM22α (red), and DAPI (blue). The cells only adhere on the stiffer (higher) A) 10 kPa or B) 34 kPa stripe. Scale bar=200 μm.

To isolate the elastic modulus from the elevation factor, we decided to use single-stiffness polyacrylamide chips tuned to a low stiffness 10 kPa, and a higher stiffness, 40 kPa, plus tissue culture plastic (TCP) control, a very stiff material >0.1 GPa [102]. The VPC-A3 and R1 cells were differentiated and stained with endothelial markers, PECAM-1, and early smooth muscle cell markers, CNN-1 after 3, 7, and 10 days. The outgrowths of VPC were often observed as PECAM-1+ EC islands surrounded by CNN1+ positive SMC, or pure PECAM-1+ populations or pure CNN1+ populations (Figure 10). Although these are simple 2D cultures, it appears as if the cells were attempting to organize according to their native physiology with EC generating a confluent layer for lining the lumens of blood vessels with SMC loosely associated in the surrounding space.

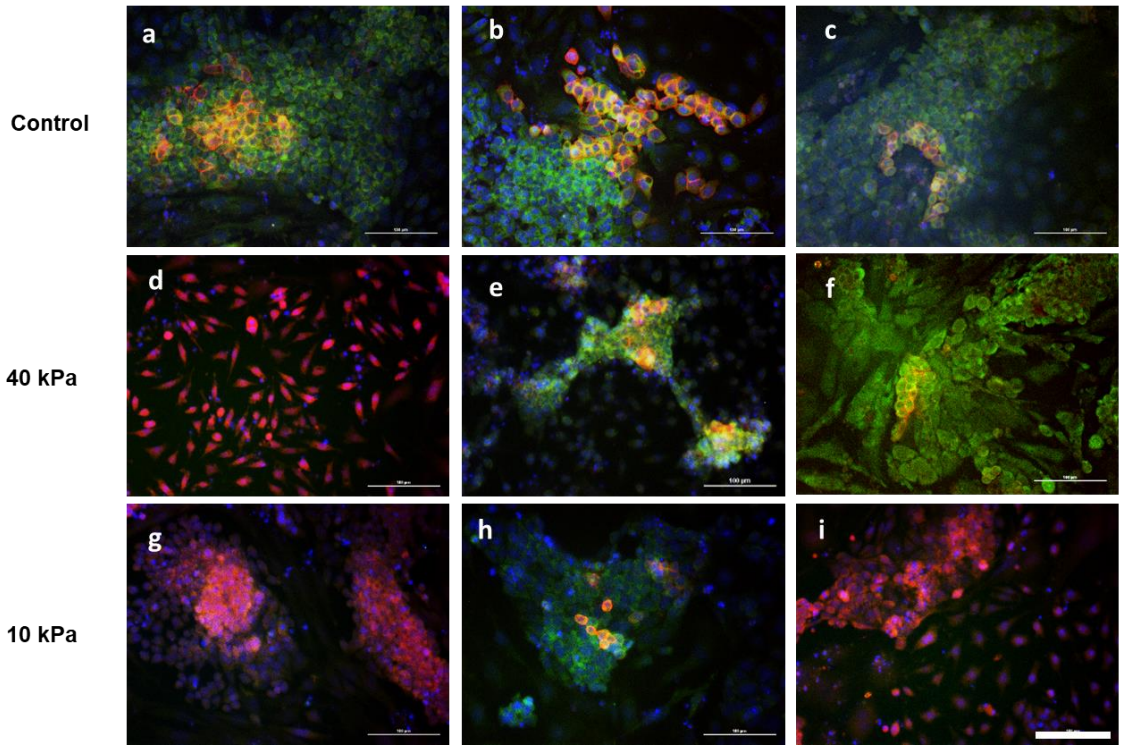

Figure 10: Flk-1+ VPC-A3 on single stiffness matrices at day 7 in stage 2. Cells were fixed and stained with PECAM-1 (red), CNN1 (green), and DAPI (blue). In some areas we see the cells organize themselves in a way where the PECAM-1+ cells are in the center with CNN-1+ cells surrounding them, but in other areas on the same chip we see pure PECAM-1+ or CNN1+ populations.

The results clearly and robustly show that stiffness does play a role in early differentiation of VPC, specifically the lower stiffness generated more PECAM-1+ (EC) cells while the greater stiffnesses (40kPa and higher) directed more VPCs towards

CNN1+ (SMC) cells (Figure 11). The trend continues onto day 7 and 10, but by day 14 we see that all CNN1+ cells have disappeared and are left with an equal amount of PECAM+ cells on all three conditions (data not shown). This may be due to the cells being cultured to over confluence during the experiment and in endothelial-specific media. The experiment was repeated using mESC-R1 and observed similar results to the mESC-A3 line.

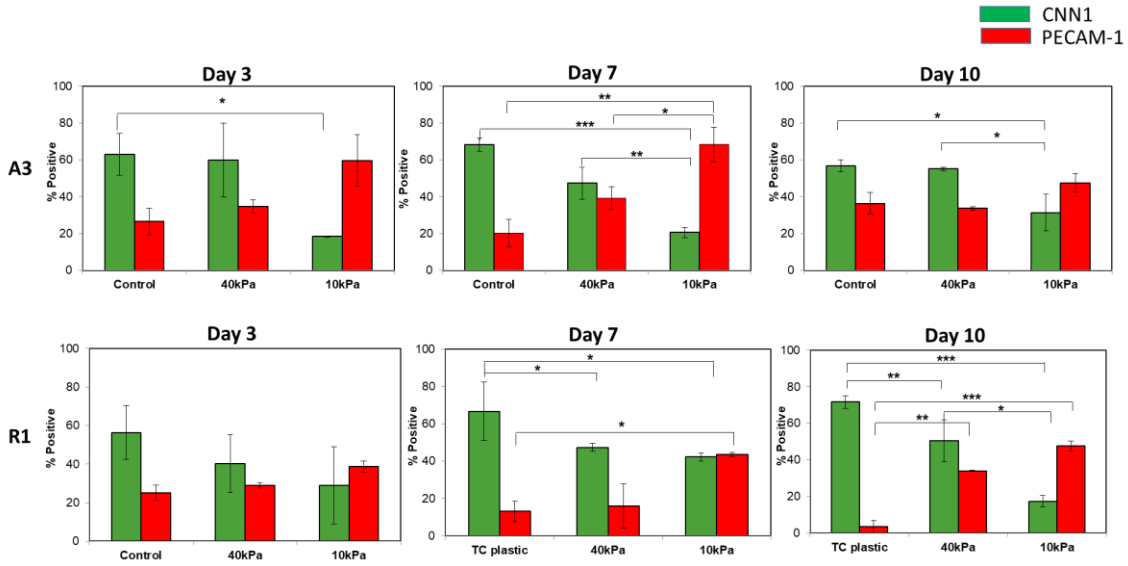

Figure 11: Flk-1+ VPC-A3 and R1 differentiation on single stiffness substrates from day 3-10 in stage 2 . We observed a trend of more PECAM-1 positive cells on lower stiffness and CNN1 on higher stiffness in both the A3 and R1 mESC lines. * p-value < 0.05 ** p-value < 0.005 *** p-value < 0.0005

To identity gene expression signatures associated with the varying stiffness, we performed RNA-Seq of the 10 kPa, 40 kPa, and TCP populations. 10 and 40 kPa populations display distinct expression profiles compared to TCP populations, with a total of 25 genes exhibiting more than a twofold expression changes (Figure 12A). Compared to the TCP population 11 genes were upregulated and 22 genes were downregulated in 10 kPa (Figure 12B), while only 14 genes were downregulated in 40 kPa compared to TCP (data not shown). Compared with gene expression profiles in TCP populations, the gene expressions in 10 kPa had higher expression in those known to be associated with vascular development, like: migration, vasculature, blood vessel, and angiogenesis.

The ability of the cell to sense its environment and convert that into cellular processes is the study of mechanotransduction and various mechanosensors have been implicated, such as integrins (transmembrane proteins) and focal adhesions (link between cytoskeleton and extracellular matrix). To further investigate the role of stiffness on vascular differentiation, inhibitors and antibodies were used to block the signaling pathways that may be affected stiffness directed differentiation. Based on the literature,

we chose FAK 14 (prevents FAK phosphorylation) [103-105], anti-αvβ3 (integrin that supports mesoderm differentiation, binds to vitronectin and fibrinogen) [106], anti-αvβ1 (integrin that stimulates angiogenesis and binds to fibronectin) [106, 107], and anti-αvβ6 (integrin that binds to several ECM proteins and affects vascular proliferation). Anti-αvβ3 inhibits or competitively binds αvβ3 integrin and blocks the crosstalk between αvβ3 and Flk-1 or VEGFR2, thereby down regulating VEGF signaling [41]. Both αvβ3 and αvβ1 have been shown to provide signals that regulate EC [108] and vascular lumen formation [109, 110].

After 48 h of treatment, the cells were stained with PECAM-1 and CNN-1 and counterstained with DAPI to observe any changes. FAK inhibitor 14, αvβ1, and αvβ1+ αvβ3 mitigated stiffness directed differentiation and, in some cases, up-regulated PECAM-1 expression, compared to the control (no inhibitor). However, their effect on PECAM-1 and CNN1 were not significant on the varying stiffness. αvβ3 and αvβ6 followed stiffness directed differentiation trend, but αvβ3 upregulated PECAM-1 expression, while downregulating CNN1 expression. αvβ6 saw similar expression levels as the control.

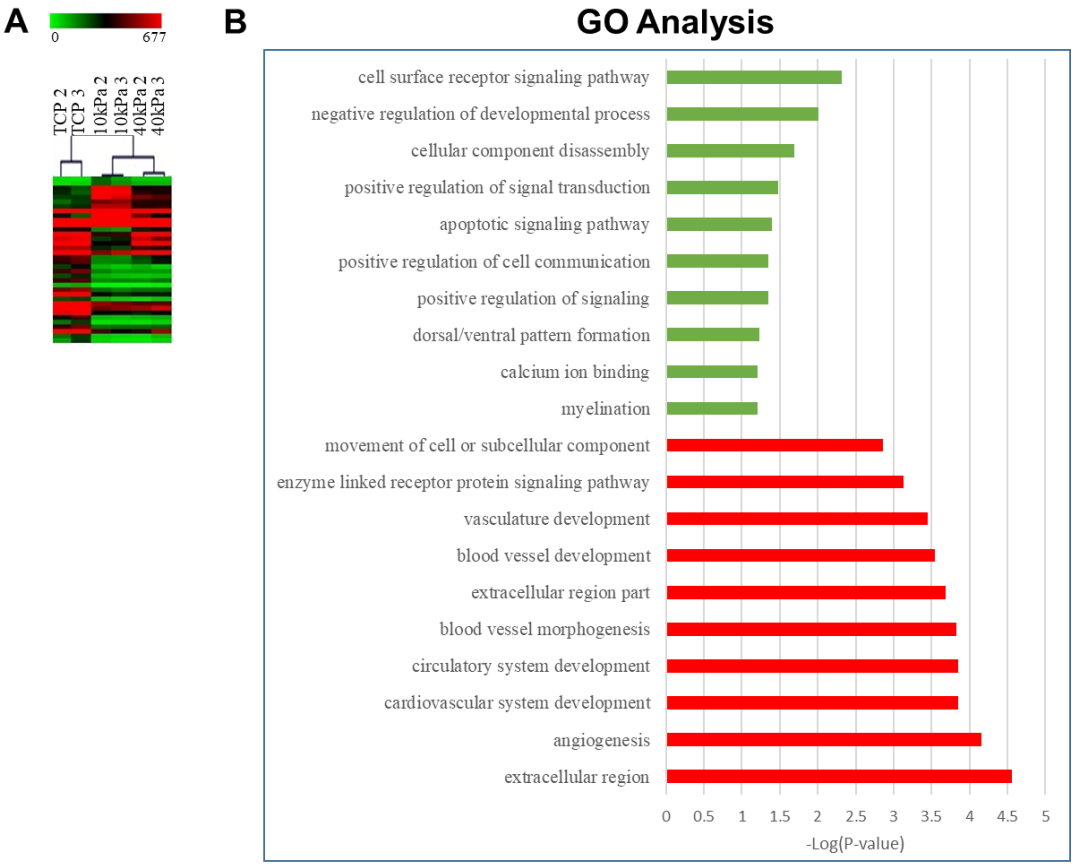

Figure 12: Gene expression of 10 kPa compared to TCP populations. A) Hierarchical clustering analysis of genes upregulated (red) and downregulated (green). Genes with

expression differences more than twofold were selected for analysis (P < 0.05). B) Gene ontology Analysis of the differentially expression genes. x-axis: -log(*P* value).

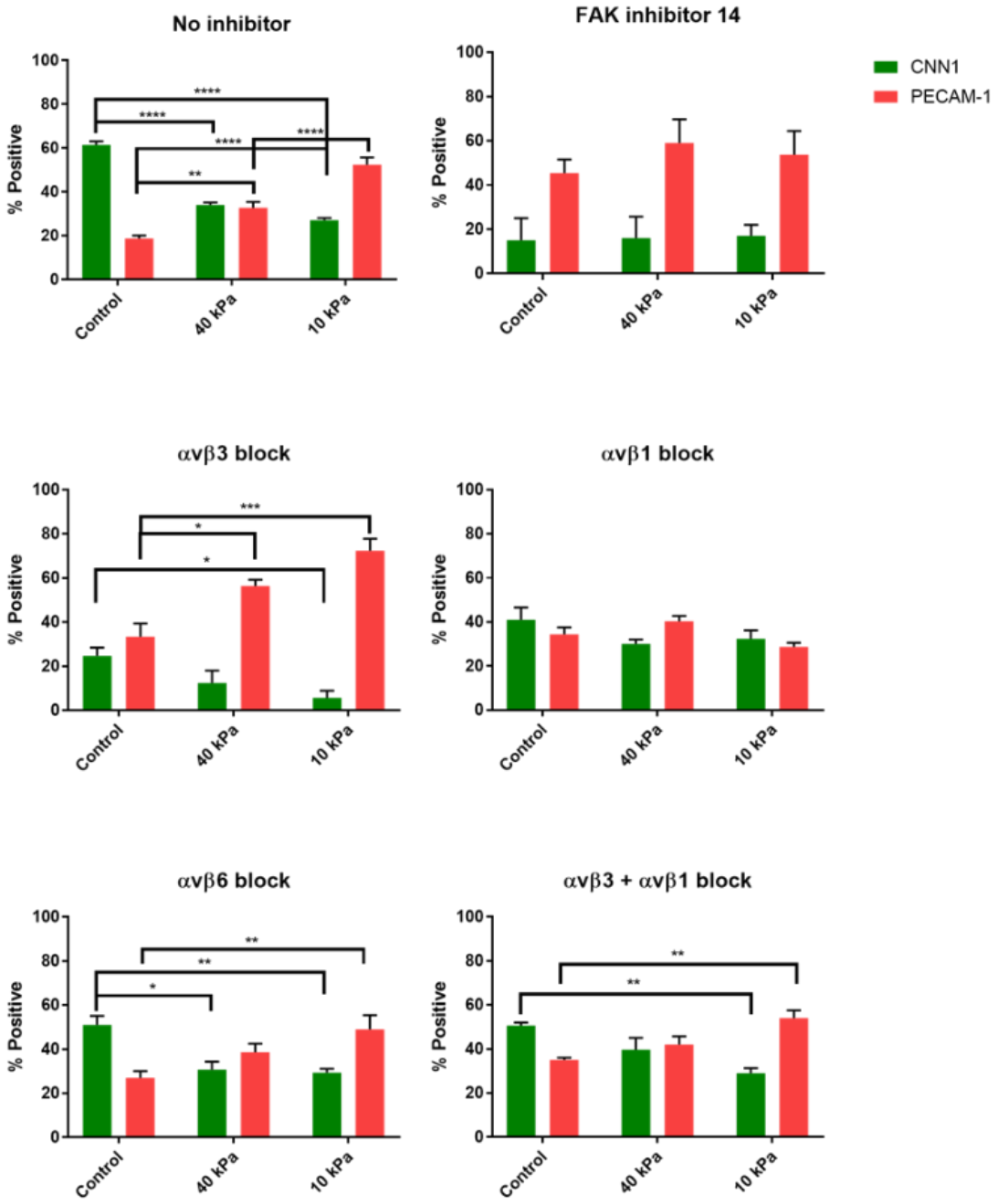

Figure 13: Inhibitor assay on Flk-1+ VPC-A3 outgrowths on day 5 after 24 hr treatment. Compared to the control (no inhibitor added), stiffness-directed differentiation was not seen when FAK inhibitor 14, αvβ1, or αvβ1+ αvβ3 were added. However, when αvβ3 was blocked, we saw an enhanced trend of PECAM-1 on lower stiffness and a decrease in over all levels of CNN-1. αvβ6 did not have an effect compared to the control. * p-value < 0.05 ** p-value < 0.005 *** p-value < 0.0005 **** p-value < 0.00005

2.4 Discussion

Initial studies on Zebraxis showed that Flk-1+ VPC preferred to adhere to the elevated surface, which happened to be the stiffer surface. Due to design constraints that required the stiffer material to be on a raised surface, we moved to single-stiffness surfaces. Those studies showed that the outgrowths of Flk-1+ VPC were observed as PECAM-1+ EC islands surrounded by CNN1+ SMC. From day 3-10, we see that SMC fate is greatest on the stiffer substrates and EC fate greatest on low stiffness. RNA-Seq data shows a clear difference between 10 and 40 kPa populations compared to TCP, with more vascular development related genes upregulated on low stiffness. Various mechanosensors were inhibited, which were seen to either negate stiffness directed differentiation or enhance endothelial differentiation.

Compared to TCP, *TEK* was upregulated on low stiffness (10 kPa) which encodes angiopoietin-1 receptor or Tie-2, a protein associated with regulating embryonic vascular development and angiogenesis [111]. Integrins αvβ1 and αvβ3 have been reported to congregate by Ang-1/Tie-2 and Ang2/Tie-2 and form complexes which result in different cellular outcomes in EC [112, 113] (Figure 14). Ang-1 and Ang-2 are ligands that are agonistic and antagonistic to Tie-2 receptor, respectively. Ang-1 binding to Tie-2 leads to Akt activation which promotes survival and endothelial quiescence, while Ang-2 will interfere with Ang-1/Tie-2. Both Ang-1 and Ang-2 recruit αvβ3 to Tie-2, but only Ang-2 results in the complex formed with Tie-2/αvβ3/FAK [112]. αvβ3 has been shown to be necessary in EC differentiation [26], rescue EC from apoptosis [114], regulates actin cytoskeleton in EC and aids in endothelial barrier integrity (decreased permeability) [115]. However, in our study, when antibody-blocked, we saw an increase of PECAM-1 expression (and a decrease in CNN1 expression) compared to our control (no inhibitor added) (Figure 13). Integrin blocking antibodies have been shown to result in integrin clustering on the cell surface, which can lead to signaling events [116, 117]. We suspect that αvβ3 was not activated due to our ECM substrate being fibronectin, but adding anti-αvβ3 allowed clustering and complexing with VEGFR2 to further promote endothelial differentiation [14, 50, 82]. It is interesting to note that high levels of Tie-2, found in our low stiffness populations, is a marker for phalanx or a quiescent EC phenotype compared to low levels of Tie-2 being expressed in tip cells of an angiogenic sprout [118, 119].

If Ang-1 is not present in high concentrations Tie-2 will associate with αvβ1 (binds to fibronectin) and leads to Tie-2 being phosphorylated [113, 120]. By blocking αvβ1 with no added Ang-1 we saw a decrease in both PECAM-1 and CNN1 expression compared to our control (no inhibitor added), which may be due to the antibody blocking the response of fibronectin as well as the underlying stiffness. αvβ1 has been shown to rescue αvβ3 signaling [121, 122], so we blocked both. We observed a recovery effect,

where PECAM-1 expression was suppressed by anti-αvβ1 but recovered through anti-αvβ3. Our data shows αvβ3 activation through the addition of anti-avb3, but αvβ1 requires the underlying stiffness/force from attachment to fibronectin to be activated.

Another upregulated gene in low stiffness is *TSPAN8*, which encodes for tetraspanin proteins that are found on the cell surface and forms complexes with integrins. TSPAN8 plays a role in cell development, motility, and angiogenesis [123]. Tetraspanins organize integrins into multiprotein complexes and has been shown to associate with a3b1 and a6b4. TSPAN8 is present in exosomes and enhances EC proliferation, migration, sprouting, and maturation of endothelial progenitors [124]. When internalized, EC have elevated levels of VWF, VEGF, VEGFR2 and other factors that drive EC proliferation, migration, sprouting and progenitor maturation [125].

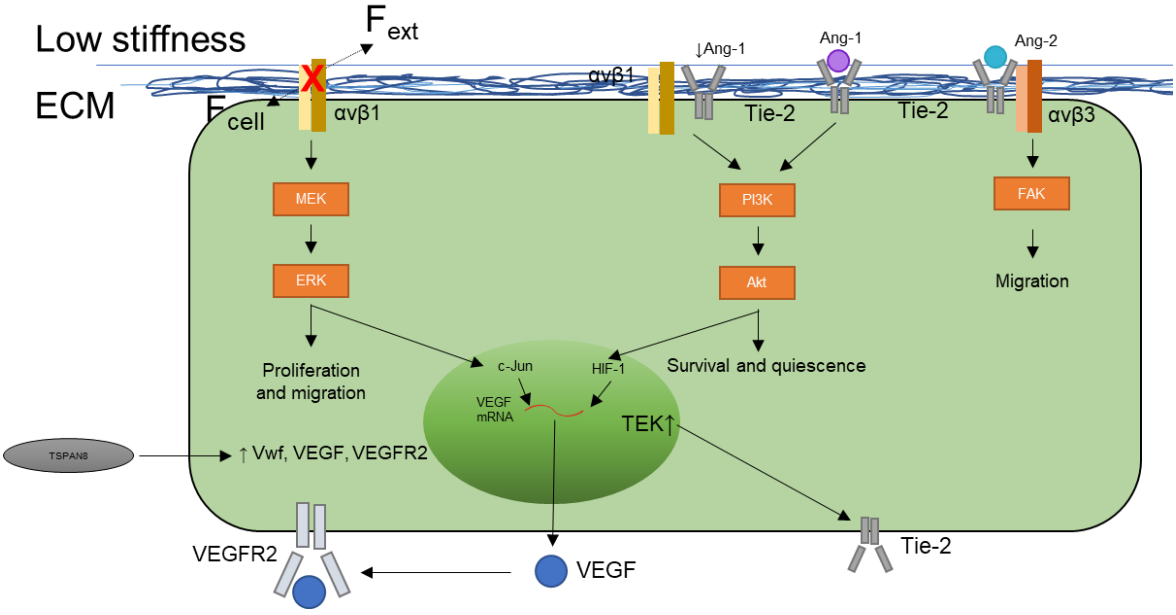

Figure 14: Proposed mechanism of low stiffness directed EC differentiation.

Chapter 3: Leaf-inspired microcontact printing vascular patterns

published in

Biofabrication

IOP Publishing Ltd, 2017

ABSTRACT

The vascularization of tissue grafts is critical for maintaining viability of the cells within a transplanted graft. Several strategies are currently being investigated including very promising microfluidics systems. Here, we explored the potential for generating a vasculature-patterned endothelial cells that could be integrated into distinct layers between sheets of primary cells. Bioinspired from the leaf veins, we generated a reverse mold with a fractal vascular-branching pattern that models the unique spatial arrangement over multiple length scales that precisely mimic branching vasculature. By coating the reverse mold with 50 μg/mL of fibronectin and stamping enabled selective adhesion of the human umbilical vein endothelial cells (HUVECs) to the patterned adhesive matrix, we show that a vascular-branching pattern can be transferred by microcontact printing. Moreover, this pattern can be maintained and transferred to a 3D hydrogel matrix and remains stable for up to 4 d. After 4 d, HUVECs can be observed migrating and sprouting into Matrigel. These printed vascular branching patterns, especially after transfer to 3D hydrogels, provide a viable alternative strategy to the prevascularization of complex tissues.

3.1 Introduction

A major obstacle in the development of tissue engineered products for clinical applications is the lack of perfusable prevascularization within the in vitro-generated tissue product. This is especially important for building large organs such as the heart, kidneys, and liver. Current strategies for in vitro prevascularization include: subtractive methods like stainless steel needle-based molding and dissolvable-network-based sacrificial molding, additive methods like soft lithography/PDMS stamping-based micromolding and layer-by-layer stacking, and hybrid methods like bioprinting and gel-based microfluidic systems [126]. These various vasculogenesis and angiogenesis-based strategies also utilize a number of techniques (reviewed in [127]) including: photolithography, microcontact printing, functionalization of scaffold material, growth factor gradients, and co-culture with mural cells [128, 129]. Specifically, microfluidic systems [47, 130, 131] have emerged as leading tools to overcome many of the challenges of developing microvasculature.

3.1.1 Generation of perfusable microvessels

Microfluidic platforms offer precise control over various aspects of the cellular microenvironment enabling the generation of perfusable microvessels, but the utility of these platforms remain limited. These platforms are limited to one length scale and are not currently designed to integrate the perfusable vasculature generated within the device with the primary tissue product. Moreover, it is becoming increasingly apparent that endothelial cells (EC) provided with a tissue co-culture are highly migratory and disruptive to the patterned tissue-specific cells [132]. Tissue co-cultures with ECs have been successfully used to generate functional in vitro models in the blood-brain barrier [133], skin [134] and the lung alveolar capillary barrier [135]. A remaining challenge in these co-culture models is the generation of a basement membrane for physically separating the EC from the tissue-specific cells.

Alternatively, decellularized matrix from heart [136], liver [137], and kidney [138] are especially promising strategies for organ replacement because these strategies preserve the native three-dimensional (3D) architecture and vascularity of the organ. However, the cell seeding often requires long culture times and tissue morphology and/or organization is difficult to reestablish [136]. Moreover, a failure to completely decellularize a tissue can lead to negative outcomes upon in vivo implantation, including a pro-inflammatory response with associated M1 macrophages and subsequent fibrosis. The complete endothelization of the entire vasculature is also a critical aspect for the success of a decellularized graft. Unless the graft is fully endothelialized to conceal the underlying collagen, coagulation and blockage will occur when the graft is exposed to circulating blood [137].

3.1.2 Microcontact printing

One potential alternative for providing semi-structured vasculature is to transfer patterned EC as distinct layers between sheets of cell/tissues or on the surface of biomaterials. Microcontact printing proteins is a well-known technique that is utilized to control spatial patterning and cell-cell interactions [53]. However, the successful biomimetic replicate of a highly branched vascular tree requires the anatomical structure

of the native vasculature include branching over various length scales. Analogous to the transport of oxygen and nutrients in the blood vessel, the leaf contains veins that transport food and water to the plant. The length scales in the leaf can also mimic our microcapillary system. The veins of the leaf can also branch into smaller and smaller tributaries, just like the vascular system. Specifically, net-veined or reticulate-veined leaves contain veins that branch from the main rib with subdivisions into finer veinlets, extending from a midrib to the edge (elm, peach, apple, cherry), or radiate fan-shaped (maple, grapes). Some leaves are even designed in a parallel configuration (tulip). These lessons from nature can be exploited to create innovative designs in building new tissues.

By generating a vascular fractal-like pattern reverse mold from the veins of a leaf, we were able to model the unique spatial arrangement of EC over several length scales that precisely mimic branching vasculature. Here, we show that this can be accomplished via 1) microcontact printing adhesive matrices in appropriate vascular-like patterns followed by 2) transfer of the patterned cells to a 3D gel. This pattern is maintained after transfer to the surface of a 3D hydrogel matrix. The unique design potential for this largely 2D pattern would be the ability to transfer patterned EC between layers of cell sheets, potentially providing a non-disruptive alternative to prevascularizing complex tissues.

3.2 Methods

3.2.1 Mask

The mask is prepared by boiling a fresh leaf from a White Alder (Alnus rhombifolia) in a 0.2 molar Na_2CO_3 solution for 2 hrs. After boiling, the excess cellulose material surrounding the leaf vascular structure is removed manually with a nylon brush, rinsed with dH_2O, and sandwiched between cardboard panels to dry overnight on the benchtop.

3.2.2 Leaf mold

The SU-8 2050 mold is soft baked on a hotplate at 65°C for 3 min and then 95°C for 6 minutes. The leaf mask is pressed flat against the SU-8 exposed to ultraviolet (ABM UV, I-line) for 15 seconds. A post exposure bake is performed on a hotplate at 65°C for 2 min and 95°C for 6 minutes. The SU-8 mold is then developed in SU-8 Developer (Microchem) for 5 minutes, rinsed with isopropyl alcohol (IPA) and air dried, then hard baked at 200°C for 30 minutes (Figure 15).

3.2.3 Vascular stamp

Polydimethylsiloxane (PDMS) prepolymer and a curing agent were thoroughly mixed in a 10:1 weight ratio (Sylgard 184 Silicon Elastomer Kit, Dow Corning) and degassed in a desiccator for 30 minutes to remove any air bubbles in the mixture. The prepolymer mixture was poured onto the leaf mold and set to cure at 60°C for 2 hours. The next day, the PDMS stamp was peeled off the mold, cut to desired stamp size (Figure 16), and sterilized following standard procedures.

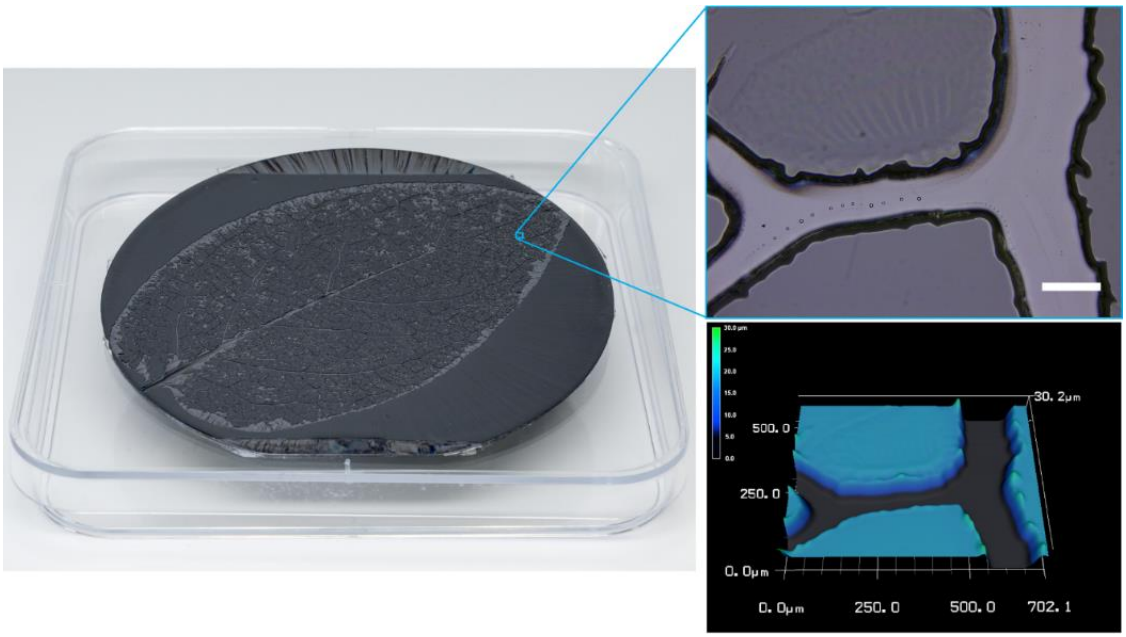

Figure 15: Leaf mask. After the mask is prepared by boiling a fresh leaf in a 0.2M Na_2CO_3 solution for 2 hrs and removing the excess cellulose material, the leaf is pressed into the surface of a SU-8 epoxy-based negative photoresist, treated with UV, baked and then developed. The resulting height profile of the patterned channels left in the mask measured ~25µm in height. Scale bar =100µm.

3.2.4 Microcontact printing

The PDMS stamping process (Figure 16) begins by coating (or "inking") the stamp surface with 50 µg/mL of fibronectin (FN; Corning) and incubated at 37°C. After 1 hour, the excess FN is removed by rinsing with distilled water followed by air drying. The FN-coated stamp is then applied directly to the surface of a non-tissue culture-treated dish using slight pressure and left in contact with the dish for 5 minutes before removal. The plate is incubated with 2% Pluronic® F-127 (Sigma) in phosphate buffered saline (PBS) solution for 1 hour before washing with PBS.

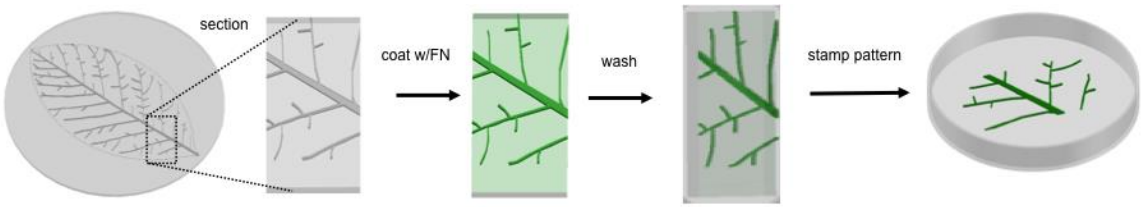

Figure 16: Schematic of the stamping process. A section of the PDMS leaf stamp is cut and coated with 50 µg/ml FN. After a gentle wash, the FN-coated stamp is pressed onto the surface of a non-tissue culture treated dish, thus transferring the FN pattern onto the surface of the dish.

3.2.5 Validation of printed fibronectin

To better visualize the stamped FN pattern, Alexa Fluor 488 succinimidyl ester (Life Technologies) was conjugated to FN (Corning) at a 10-fold molar excess of fluorophore-to-protein and developed on a nutation device for 90 minutes at room temperature. The protein-fluorophore mixture was then purified through a size-exclusion column (Amicon Ultra-15 Centrifugal Filter Unit with Ultracel-10 membrane; Millipore) and centrifuged according to manufacturer's directions. The final concentration of the protein-fluorophore was measured using a NanoDrop 1000 Spectrophotometer (Thermo Scientific). The 2.4mg/mL solution was then diluted down to 50 µg/mL for coating the stamp.

3.2.6 Cell culture

Human umbilical vein endothelial cell (HUVEC; Life Technologies) were cultured in a humidified incubator at 37°C under 5% CO_2 in fully supplemented Endothelial Cell Growth Medium (EGM™-2 with BulletKit™; Lonza). HUVEC (p3-5) were then seeded onto the FN-patterned surface in a non-tissue culture-treated dish at 10,000 cell per cm^2 and imaged after 24h.

3.2.7 Immunofluorescence staining and microscopy

The patterned HUVEC were fixed with 4% PFA for 20 minutes, permeabilized with 0.7% Triton X-100 for 5 minutes at room temperature, blocked for 20 minutes in 0.1% BSA in PBS, and then incubated with Fluorescein Phalloidin (1:200; Life Technologies) for 1 hour at room temperature. DAPI counterstain was added directly to the solution during the last 5 minutes of staining.

3.2.8 Collagen gels

Collagen gel solutions contained rat rail collagen type I (2 mg/mL; Corning), 0.1 M sodium hydroxide, 10% fetal bovine serum (Life Technologies), 20% 5x Dulbecco's Modified Eagle's medium (Life Technologies), and the remainder EGM-2 medium. The gel solution was then placed on patterned cells and cultured in a humidified incubator at 37°C and 5% CO_2 overnight. After 24 hours, the collagen gel is found compacted to 80% of its original size and floating in the medium with the cell pattern transferred from the cell culture dish to the lower surface of the gel.

3.2.9 Matrigel

Patterned HUVECs were coated in Matrigel™ Basement Membrane Matrix at 50 $\mu L/cm^2$ of growth surface and allowed to gel at 37°C for 30 minutes. Culture media was then added and observed over time. After 4 days, the gel was rinsed gently with PBS and fixed with 4% paraformaldehyde for 30 minutes at room temperature. After rinsing, phalloidin rhodamine (Invitrogen, 1:50) and DAPI (1:50) were added and allowed to stain for 24 hours at 4°C. Plates were rinsed twice before imaging using confocal microscopy (Nikon Eclipse C1).

3.3 Results

Using a leaf branching pattern, we were able to generate a mask, reverse mold, and stamp that retained the initial branch pattern (Figure 15). This branched pattern was then used to preferentially surface-treat (i.e. stamp) Alexa Fluor 488 succinimidyl ester-treated FN onto non-tissue culture-treated dishes retaining the same pattern (Figure 17A-C). Once HUVECs were seeded in the dish, they preferentially adhered only to the FN-stamped areas in the dish (Figure 17D-F), and thus retained the vascular-like branching pattern of the leaf. To further illustrate the structure and alignment of the cells, HUVECs were stained with phalloidin and counterstained with DAPI nuclear stain (Figure 17G-I).

Although a simple and elegant technique, microcontact printing using bulk stamps like our vascular leaf stamp comes with resolution limits. The upper limit is inherently set at the diameter of the largest vein in the leaf, measured at 229 µm. The lower resolution limit in our PDMS stamp was 29µm, respectively, and corresponded with stamped patterned vascular cells at 22 µm (Figure 18). Although leaf veins were present at lower diameters, the PDMS stamp was not able to transfer the printed pattern at this smaller resolution. However, this value is very close to the normal length scales for microvasculature which typically range from 5 to 10 µm in diameter, and therefore, are expected to be sufficient for clinical application.

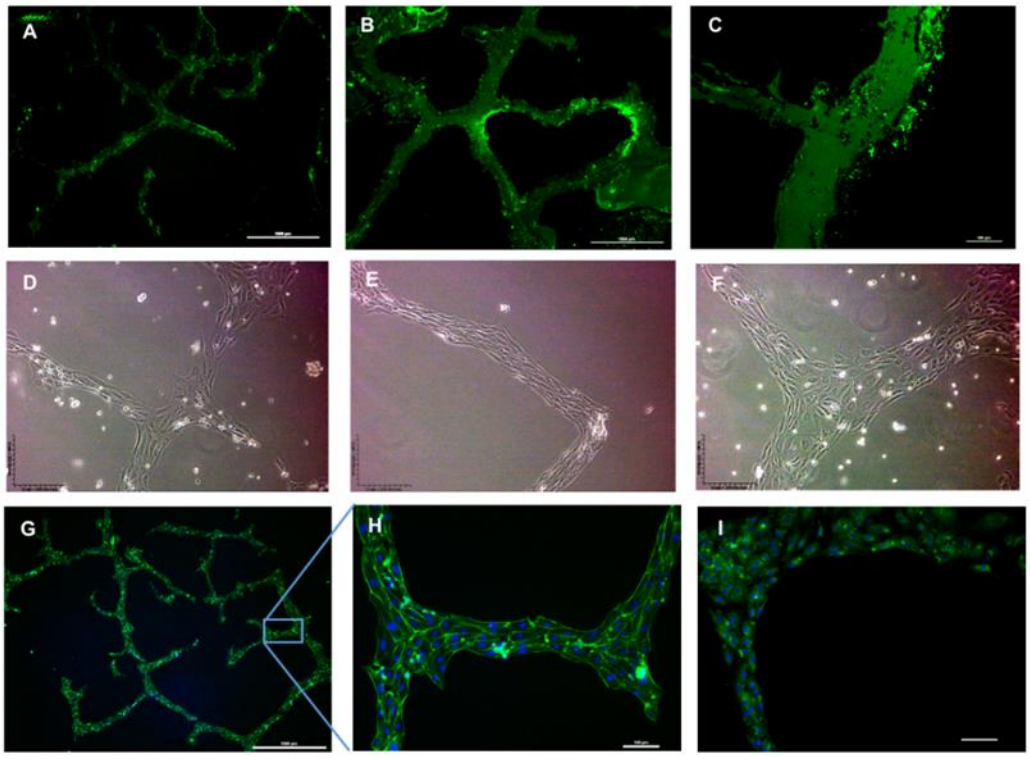

Figure 17: Images of the patterned cells. A-C) To verify the selective stamping of the FN, the stamp was coated with FN-treated Alexa 488 (green). Scale bars =1000µm, 1000µm and 100µm, respectively. D-F) After seeding with HUVECS, the cells adhere to

the stamped vascular pattern, but not to the non-stamped areas in the non-tissue culture-treated dishes. Scale bar = 200µm. G-I) The patterned were HUVECS stained with F-actin (green) and DAPI (blue) counterstain. Scale bars =1000µm, 100µm and 100µm, respectively. M-N) The HUVECs were then transferred to the surface of 3D collagen hydrogels. Scale bars = 200µm and 50µm, respectively.

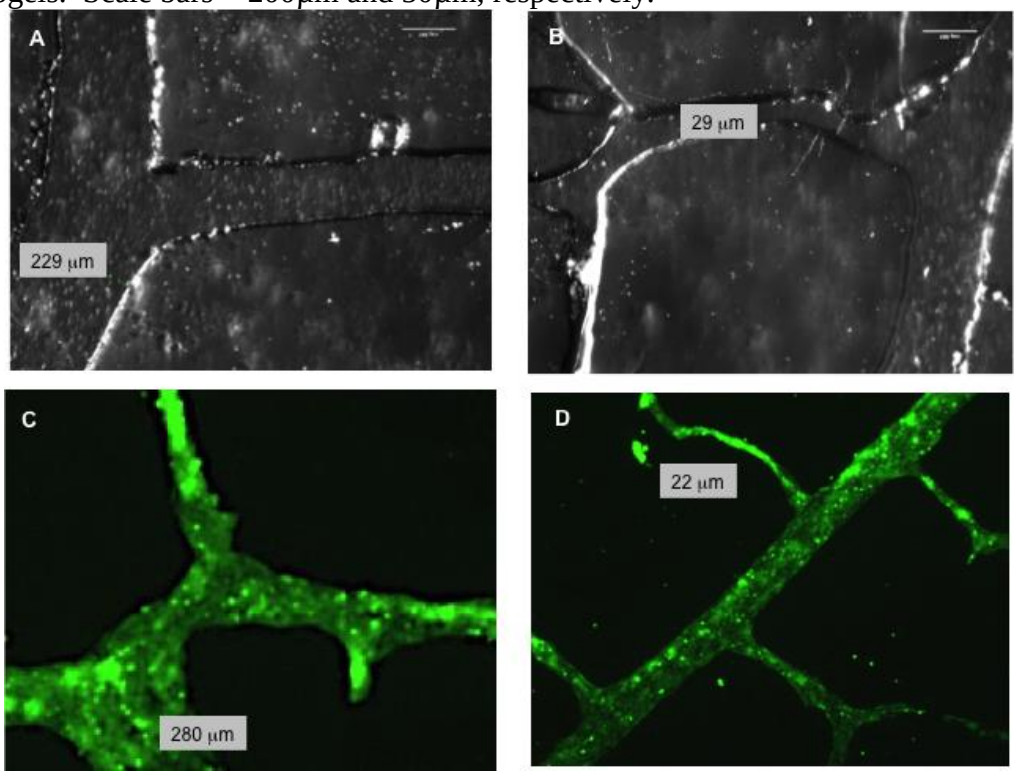

Figure 18: Resolution of the PDMS stamp is limited by the A) maximum vein diameter of the original leaf (229 µm) and the B) minimal size retained in the PDMS stamp (29 µm). Pattern transfer of Alexa 488-treated FN (green) can be C) slightly larger due to smudging or slightly smaller due to incomplete coverage. Note, the smallest printed thickness, 22 µm, is consistent an adhering EC.

After the cells reached confluence on the pattern (day 3-4), they were transferred onto a 3D collagen-type I gel by direct cell-to-gel contact (Figure 19A-B). Upon subsequent culture on the collagen-type I hydrogels, the HUVECs maintain their vascular patterns on the 3D gel surface with minimal EC invasion into the 3D gel with a maximal depth of 46 µm (Figure 19C-D) at 4 days. Interestingly, the maximal EC depths were observed at the nodes between branch points. To investigate invasion potential of the patterned EC, the cells were also transferred to softer Matrigel materials. Again, the patterned remained stable for up to 4 days. After 4 days, the EC began to migrate outside the pattern and invade into the Matrigel (Figure 20).

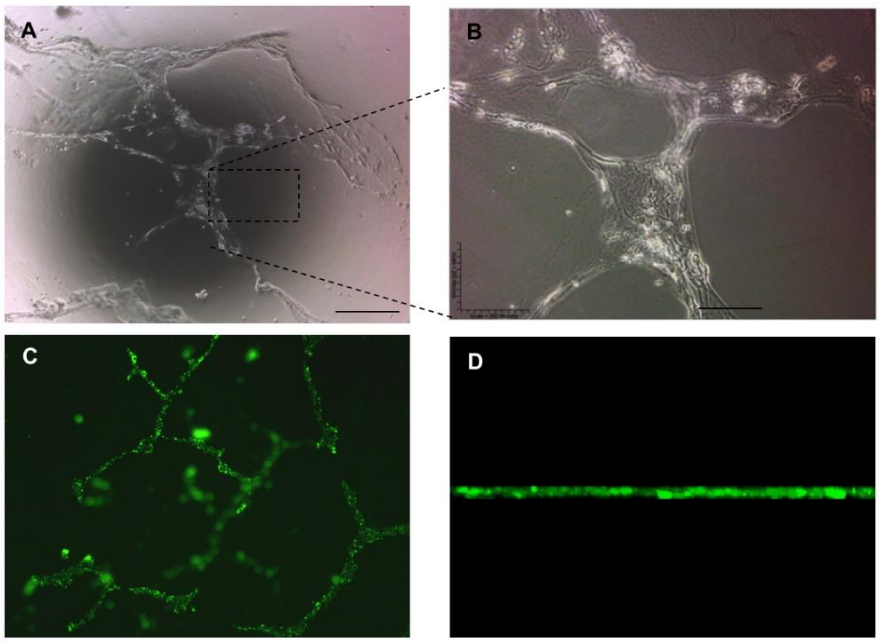

Figure 19: Pattern transfer to collagen gels. Patterned EC were transferred onto 3D collagen-type I gels by direct cell-to-gel contact A) scale bar = 500 µm and B) scale bar = 200 µm. Upon subsequent culture on the collagen-type I hydrogels, the HUVECs can C) maintain their vascular patterns on the gel surface for up to 4 days D) with minimal invasion into the 3D gel as seen by the Z-stacked image of the cells.

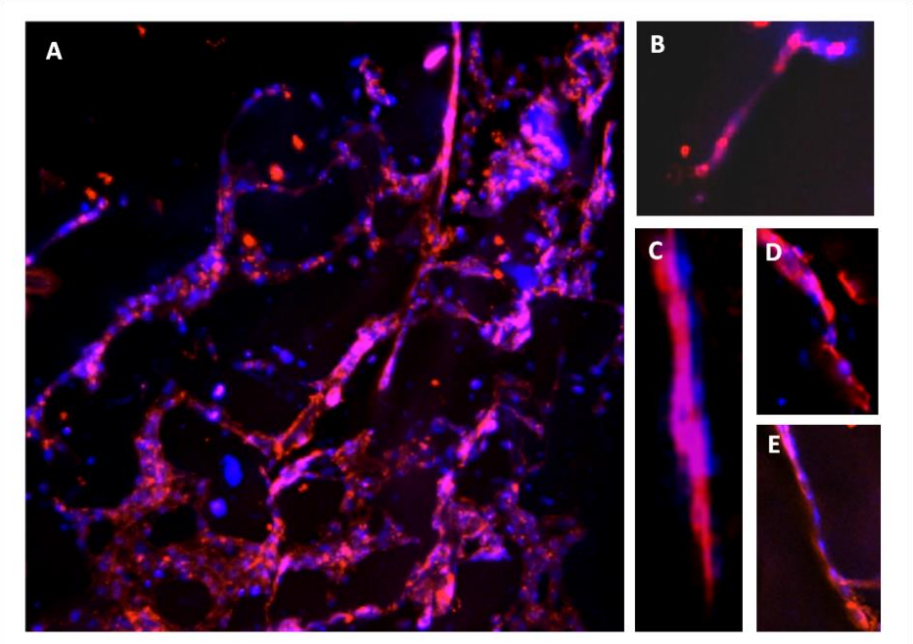

Figure 20: Pattern transfer to Matrigel. Patterned EC were transferred onto Matrigel by direct cell-to-gel contact. Individual cells can be seen by DAPI nuclear staining (blue) and phalloidin stain (red). Upon subsequent culture on the Matrigel, the HUVECs can

maintain their vascular patterns on the gel surface for up to 4 days (not shown), but then A) started to migrate (scale bar = 100 μm) and B-E) invade the 3D gel. Scale bar = 10 μm

3.4 Conclusions

The vascular patterns developed using our microcontact printing methods enable patterning cells into shapes mimicking the spatial scale of the microvasculature and the spatial organization of these cells is retained upon transfer into 3D gels. This is an alternative design approach to perfusable microfluidic systems [47, 130, 131] in which the dynamic ECs are disruptive to the primary tissue assembly and organ function. In cardiac tissue, for example, the alignment of the cardiac cells facilitates the rapid cell-to-cell signaling required for synchronous contractile forces [139]. However, when dynamic ECs and neo vessels are co-cultured with patterned cardiac cell sheets, the migratory ECs disrupt the cell-to-cell junctions of the cardiac cells [132]. In these types of in vitro cultures, dynamically sprouting neovessels, although perfusable, could disrupt the physiology of the primary tissue. Using the methods presented, patterned EC can be transferred onto 3D surfaces – potentially including cell/tissue/material grafts - enabling more rapid vascularization of implanted graft constructs and may, as recently shown from bioprinting 3D vascular channels with alternating primary tissue, facilitate a more robust vascularization of the transplanted graft in vivo [140].

Chapter 4: Generation of Endothelial Cells from Human Stem Cells to Form Perfusable Vascular Networks

4.1 Introduction

One of the goals of tissue engineering is to generate a functional tissue that can facilitate organ regeneration and may serve as models for studying diseases, drug screening and delivery. However, most cell cultures start in 2D systems, and translation into 3D systems it not a direct process. Despite significant advances in the field of regenerative medicine, the *in vitro* generation of patient-matched tissues/organoids remains hindered by the lack of a perfusable vasculature - required to meet the high nutritional and metabolic demands of the primary engineered tissue/organoids. To address this unmet need, many researchers focus their efforts towards forming and integrating perfusable vasculature with complex tissues or organoids.

Not only is the vasculature in tissues larger than oxygen's diffusion limit, but also required for tissue development, healing/regeneration, and appropriate immune responses to promote assimilation and survivability of tissue. All blood vessels are composed of endothelial cells, but their multifaceted nature can also be coupled with the presence of other important cell types distinct in each different blood vessel. Blood is pumped away from the heart through arteries composed of smooth muscle cells, a thick matrix, and sometimes additional blood vessels that feed the wall of the thick vessel and even fibroblasts in the adventitia. The arteries then branch into smaller vessels called arterioles, with pericytes, and capillaries. Capillaries, composed of only endothelial cells, allow the diffusion of oxygen, nutrients, and metabolic waste to the surrounding tissue. Then the blood flows through venules to the veins and back to the heart.

4.1.1 *In vitro* microvasculature

Perfusion of larger engineered biological tissues is required to ensure proper function and survival in its intended environment. Present limitations include the small size of lumen diameter, vessel length, complex geometries, and high vessel density requirements. Current approaches for generating in vitro vasculature include: subtractive methods like stainless steel needle-based molding and dissolvable-network-based sacrificial molding, additive methods like soft lithography/PDMS stamping-based micromolding [141] and layer-by-layer stacking, and hybrid methods like bioprinting and gel-based microfluidic systems [126]. These various vasculogenic and angiogenic-based strategies also utilize a number of techniques (reviewed in [127]) including: photolithography, microcontact printing, functionalization of scaffold material, growth factor gradients, and co-culture with mural cells [128, 129]. Of these approaches, microfluidic systems [47, 130, 131] have emerged as leading tools to overcome many of the challenges of developing microvasculature. Human umbilical vein endothelial cells (HUVEC) co-cultured with normal human lung fibroblasts (NHLF) seeded within a fibrin gel are the current cell combination most successful in building microvasculature *in vitro*, but the use of stem cells are a more versatile cell source for modeling tissue development,

and for iPS-derived EC, would allow for pathologies associated with patient-derived tissues to be examined [52].

Fibrin gels exhibit angiogenic properties that produce microvasculature-like networks and subjects cells to mechanical signaling through integrins that associate with the cytoskeleton [49]. Changing the concentration of fibrinogen allows for modifications of the gels' mechanical and viscoelastic properties that lead to increased vascular-like formation [49-51]. When HUVEC are co-cultured with stromal cells, networks do not regress as quickly and can maintain their stable morphology for up to 2 weeks [46]. Initial studies show that our stem cell-derived endothelial cells from both mouse ESC and human ESC can initially form vascular-like networks but are leaky and not stable past a few days. This may be due to matrix metalloproteinase and/or cathepsin activity which breaks down the fibrin gel [142] and inhibitors may be used to stabilize the networks.

4.2 Methods

4.2.1 Primary cell culture

Human umbilical vein endothelial cell (HUVEC; Life Technologies) were cultured in Endothelial Cell Growth Medium (EGM™-2 supplemented with BulletKit™; Lonza) on fibronectin coated plates (10 µg/mL; Corning) and used in experiments between passages 3-5. Norman human lung fibroblasts (NHLF; Lonza) were cultured in Fibroblast Growth Medium (FGM-2; Lonza) and used in experiments between passages 3-10. Human aortic smooth muscle cells (Lonza) were cultured in Smooth Muscle Growth Medium-2 (SmGM-2™ Bulletkit™; Lonza) on gelatin coated plates. Inactivated mouse embryonic fibroblasts (MEFs) were cultured in 88% High Glucose DMEM, 10% FBS, 1% L-glutamine, and 1% penicillin-streptomycin on gelatin coated plates.

4.2.2 Mouse embryonic stem cell culture

R1 and A3 murine embryonic stem cells were maintained on 0.5% gelatin coated plates in serum-free medium containing Knockout Dulbecco's Modified Eagle Medium (KO-DMEM; Invitrogen), 15% Knockout Serum Replacer (KSR; Invitrogen), 1X Penicillin-Streptomycin (Invitrogen), 1X Non-essential Amino Acids (Invitrogen), 2mM L-glutamine (Invitrogen), 0.1mM 2-mercaptoethanol (Calbiochem), 2000 Units/ml of leukemia inhibitory factor (LIF-ESGRO; Chemicon), and 10 ng/ml of bone morphogenetic protein-4 (BMP-4; R&D Systems). A3 mESC were maintained in the same media on mouse embryonic fibroblasts (MEF). Full media changes occurred every other day and cells were passaged every four to five days.

4.2.3 Induction of mouse embryonic stem cells to mesodermal lineage

mESC were harvested from 0.5% gelatin coated dishes using TrypLE (ThermoFisher) and plated in 100mm tissue culture treated plates (Corning) coated with 50 µg/mL Fibronectin (Corning). A3 cells were disassociated from the MEF layer and purified through a gravity separation. mESC were placed in a basal media of alpha-MEM (Cellgro), 20% knockout serum replacement (ThermoFisher), 1X penicillin-streptomycin (ThermoFisher), 1X nonessential amino acids (ThermoFisher), 2 mM L-

glutamine (ThermoFisher), 0.05mM 2-mercaptoethanol (Calbiochem), 5 ng/mL BMP-4 (Peprotech), and 20 ng/mL, or 30 ng/mL of VEGF (Peprotech) for A3 and R1 respectively. Cells were cultured for 2 or 3 days, R1 and A3 for optimal number of Flk-1$^+$ cells. Adherent cells were harvested using cell dissociation buffer (ThermoFisher) and sorted using fluorescent activated cell sorting (BD, ARIA II) using Flk-1 PerCP (Biolegend).

4.2.4 Human stem cell culture

Both iPS cell line (DF19-9-7T, WiCell) transfected with puromycin resistance under MHCa promoter (courtesy of Dr. Chiamvimonvat, UC Davis) and human embryonic stem cell line H9-ESC (WiCell) were maintained in mTeSR™1 medium (StemCell Technologies) on Matrigel™ (BD)-coated plates and passed every 3-4 days with Accutase.

4.2.5 Human stem cell induction towards KDR+ VPC (stage 1)

Human ESC (hESC-H9) were detached using Versene (Thermo Fisher) for 8 minutes followed by physical dissociation by triturating with a pipette. An aliquot of the cells was counted and plated on 50 µg/mL fibronectin-coated dishes at 10,000 cells/cm^2. The stage 1 medium included: alpha-MEM (Cellgro), 20% KSR (Invitrogen), 1XPS, 1XNEAA, 2 mM L-glutamine, 0.05 mM 2-mercaptoethanol, 15 ng/mL VEGF and 5ng/mL BMP-4 (Peprotech). Cells were fed with a full media change every third day until day 6, then it was fed every day and were sorted for KDR$^+$ (Biolegend) expression with a BD FACS Aria III on day 10 (Figure 21).

4.2.6 Human stem cell induction towards VE-cadherin+ EC (stage 2)

KDR$^+$ VPC were plated on dishes coated with 50 µg/mL fibronectin-coated dishes and plated at 20,000 cells/cm^2 and supplemented with 5uM ROCKi (Stem Cell Technologies) for the first 24 hours. The stage 1 medium consisted of: 70% alpha-MEM and 30% DMEM, 2X Nutridoma CS, 1% penicillin-streptomycin, 1% NEAA, 2 mM L-glutamine, 0.05 mM 2-mercaptoethanol, 30 ng/mL VEGF, and 10 ng/mL bFGF (Peprotech). After 7 days (day 17 of total differentiation), 5uM SB431542 was added to the medium. Cells were fed with a full media change every third day. On day 25 of total differentiation (8 days later), VPC were sorted for VE-Cadherin (eBioscience) and re-plated on 50 µg/mL fibronectin-coated dishes.

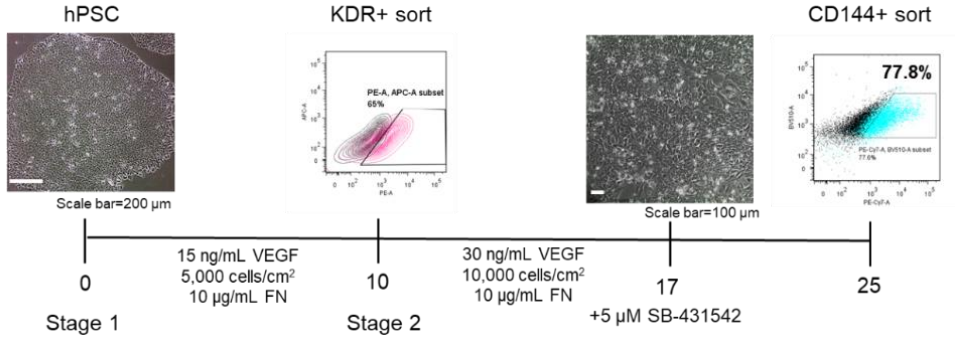

Figure 21: Optimized protocol for hESC-H9 for EC. In stage 1, hESC-H9 are plated on fibronectin and sorted for KDR expression on day 10. The KDR+ cells are then re-plated onto fibronectin. On day 17 of total differentiation, SB-431542 is added and the EC are sorted for CD144 expression on day 25 of total differentiation.

4.2.7 Induction of human stem cells towards smooth muscle cells

The McCloskey laboratory has also been optimizing the induction of smooth muscle cells from pluripotent stem cells using serum-free medium (Figure 22). For this study, undifferentiated stem cells were harvested and plated at 10,000 cells/cm^2 on dishes coated with 10 µg/mL fibronectin and cultured in stage 1 induction medium consisting of alpha-minimal essential medium (a-MEM), 20% KSR, 1x AAS, 1x NEAA, 2mM L-glutamine, and supplemented with 5ng/ml BMP-4, and 15ng/ml of VEGF. After 10 days, the KDR+ cells from stage 1 were isolated and seeded on 10 µg/mL fibronectin and expanded in stage 2 SMC induction medium consisting of alpha-minimal essential medium (a-MEM), 20% KSR, 1x AAS, 1x NEAA, 2mM L-glutamine supplemented with 0.1, 1, or 10 ng/mL PDGF-BB. Cells were collected for microvascular co-cultures on day 24 and the varying concentrations of PDGF-BB were pooled.

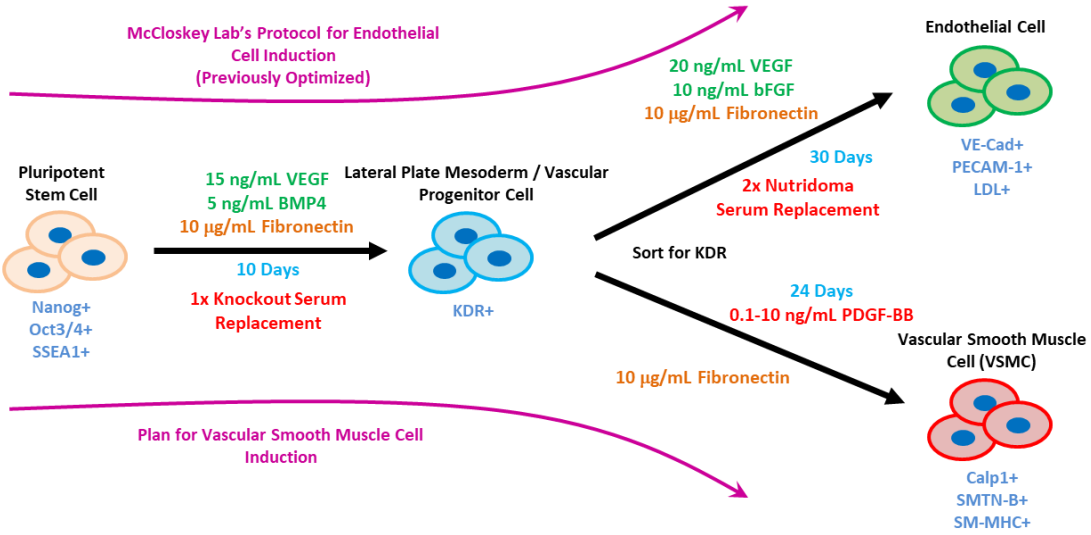

Figure 22: Differentiation protocol for hIPS for SMC. In stage 1, hIPS follow the endothelial cell induction protocol seen in [23]and sorted for KDR expression on day 10. The KDR+ cells are re-plated onto fibronectin and fed with stage 2 media supplemented with varying concentrations of PDGF-BB. On day 24, the derived hIPS cells were analyzed for Calp1, SMTN-B, and SM-MHC and were used for the following study. Image provided by Edwin Shen.

4.2.8 Human stem cell induction towards cardiomyocytes

hESC-H9 were detached using Versene for 8 minutes following by physical dissociation by triturating with a pipette. An aliquot of the cells was counted and re-plated onto Matrigel-coated plates in mTeSR1^{TM} (Stem Cell Technologies). When the cells reached confluency, the medium was replaced with RPMI supplemented with 2% B27 without insulin (RPMI/B27 w/o insulin) and 12 µM GSK3 inhibitor (CHIR99021)

on day 0. 24 hours later the medium was replaced with RPMI/B27 w/o insulin. On day 3, the medium was replaced again with RPMI/B27 w/o insulin supplemented with 5μM Wnt inhibitor (IWP2). On day 5, the medium is replaced with RPMI/B27 w/o insulin. From day 7-14 the cells were fed with RPMI/B27 w/ insulin every third day. Cardiac troponin T expression was analyzed on day 21 and 26 (Figure 23).

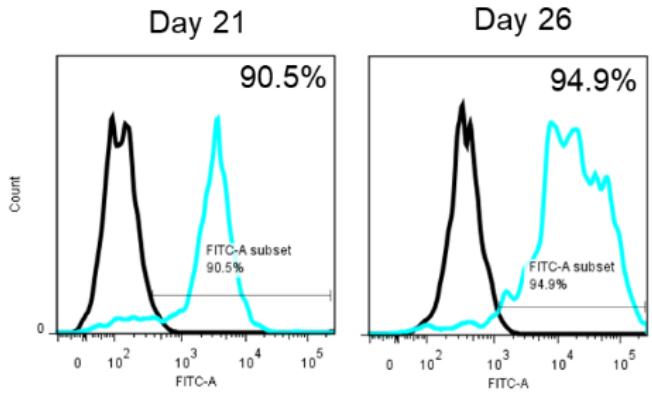

Figure 23: hESC-H9 derived cardiomyocytes stained with cTNT and analyzed using flow cytometry.

4.2.9 Microfluidic device fabrication

The molds for the microfluidic devices were generously provided by our collaborator, Dr. Roger Kamm (MIT). The devices were made by desiccating PDMS at a ratio of 1g of curing agent to 10g of base. The PDMS was then poured into the molds and baked in an oven at 75°C for 2 hours. There are three channels (width=0.4cm, length=2.1cm, and height=1cm). The device ports were generated using a biopsy punch (ID: 1mm) to create inlet and outlet ports. Both the PDMS devices and glass slides were plasma treated in a plasma cleaner (Harrick) for 1 minute and 20 seconds at approximately 600 mTorr and bonded together (Figure 24) to form the microfluidic device used in these studies.

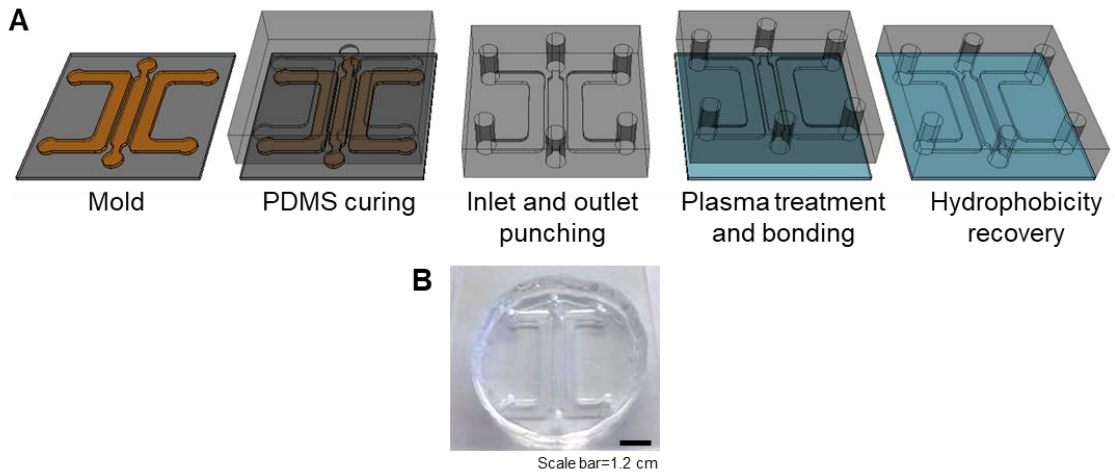

Figure 24: Microfluidic device fabrication. PDMS was mixed and desiccated at 10:1 base to curing agent before being poured into the mold and baked at 75°C for 2 hours.

The device was removed from the mold and ports were made with a biopsy punch. The device and a glass slide are placed in a plasma cleaner to be bonded together.

4.2.10 Microvascular network formation

Fibrinogen solution was prepared by reconstituting 6 mg/mL of bovine fibrinogen in PBS and dissolving the mixture in 37°C water bath for 4 hours. The solution was then filtered using 0.22 μm filter and stored at 4°C. Cells were lifted with trypsin and resuspended at various concentrations (Table 2) with 2 U/mL thrombin. The cell suspensions were then mixed in a 1:1 ratio of 6 mg/mL fibrinogen and immediately injected into the cell channel. Devices were placed in a humidity box at room temperature to allow the gels to cure for 20 minutes before filling the media channels with supplemented EGM2. Media was replenished every 24 hours for the duration of the culture. In the study where E-64 was used, 2 μM was added to the fibrin gel.

Cell combinations	Total number of cells (million/mL)	Ratio
HUVEC+NHLF	8 to 4	2 to 1
mESC-derived tip/stalk EC+NHLF	4 to 1	4 to 1
mESC-derived phalanx EC+NHLF	4 to 1	4 to 1
VPC-R1+HUVEC+NHLF	4 to 4 to 4	1 to 1
VPC-A3+HUVEC+NHLF	4 to 4 to 4	1 to 1
hESC-H9 VEC+NHLF	8 to 4	2 to 1
HUVEC+MEF	8 to 4	2 to 1
HUVEC+hIPS-derived SMC	8 to 4	2 to 1
HUVEC+hESC-derived CM+NHLF	4 to 4 to 4	1 to 1
HUVEC+hESC-derived CM	8 to 4	2 to 1

Table 2: Cell combinations used in microfluidic devices with their respective concentrations and ratios.

4.2.11 Vessel quantification

The quantification of vessel length, diameter, density, and branching points over time (Figure 25A) was accomplished using a quantitative tool called AngioTool [143]. AngioTool allows the user to threshold brightness depicting the outline of the vascular networks (green-yellow line, Figure 25B). Once the program is run, it identifies vascular pathways and junctions, as well as, spreadsheets of data for generating graphs and statistics.

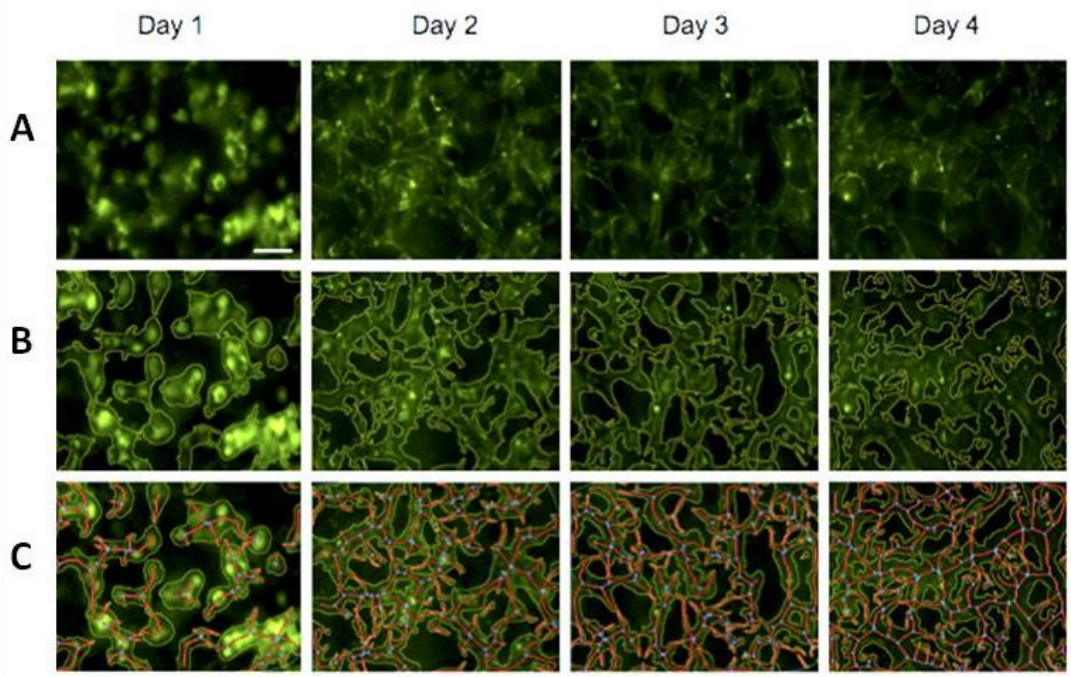

Figure 25: Quantification of vessel statistics is accomplished by A) first imaging the vasculature using a fluorescent microscope. B) The second line illustrates the green-yellow overlay while the C) red line shows the junctions and pathways after running AngioTool.

4.2.12 Statistical analysis

Statistical analyses were conducted with GraphPad Prism 7 software. One-way ANOVA with Student's unpaired t-test was used to compare two groups. Differences at $P \leq 0.05$ were considered statistically significant. *P* values were calculated by analysis of variance for multiple pairwise comparisons. The data are reported as mean ± SEM.

4.3 Results

First, we set out to replicate previous studies that show that HUVEC and NHLF form perfusable vasculature when embedded in a fibrin gel [46]. By day 3 of culture, we can already see that HUVEC self-assemble into a vascular-like structures (Figure 25 and Figure 26). By day 4, we can perfuse the tissue with 2.2 µm beads (not shown). Using AngioTool, we analyzed the average vessel length and vessel percentage area and used this data as our standard for the next experiments, in addition to perfusion.

The first set up experiments used co-cultures of our mESC- derived EC subpopulations, phalanx EC, with NHLF in the microfluidic devices (Figure 27). Within 48 hours, the cells form connections but regress the following day. The fibrin gels compact in the channel and the experiment can no longer progress. It was suspected that the mouse EC may not have been able to fully integrate with the human fibroblasts for complete vasculogenesis and/or stabilization of the neovessels.

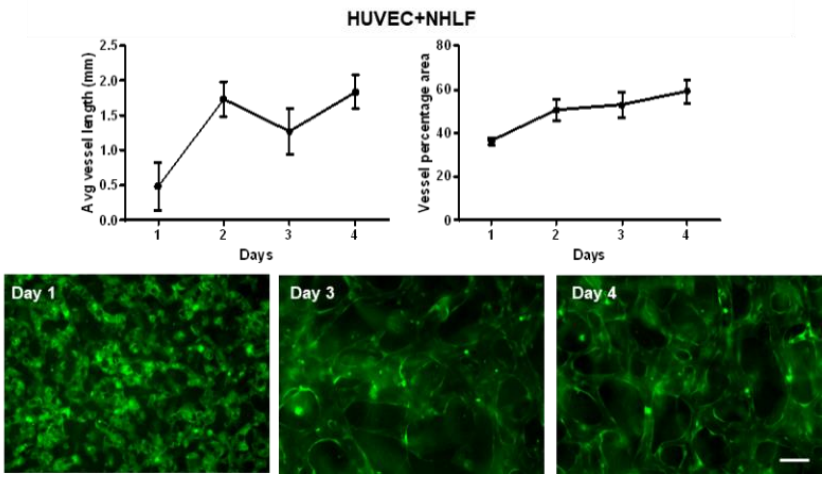

Figure 26: HUVEC and NHLF form perfusable microvasculature. Green=HUVEC CellTracker green dye. Scale bar=100µm. n=2

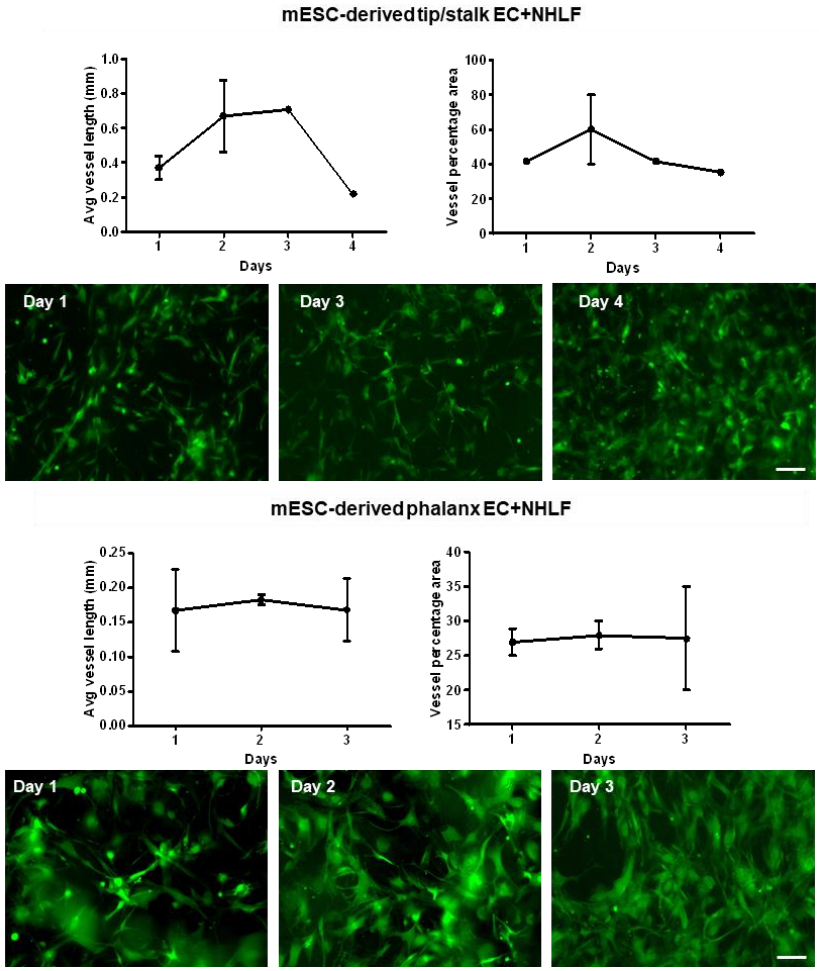

Figure 27: mESC-derived tip/stalk and phalanx EC and NHLF in fibrin gels form connections but are not stable. Green=mESC-derived tip/stalk or phalanx EC CellTracker green dye. Scale bar=100µm. n=2

Next, we attempted to compare VPC from two different mouse ESC lines, mESC-A3 and mESC-R1, with HUVEC and NHLF as a triculture. By supplementing the devices with known mature EC that are from a human, we suspected this may aid the VPC in forming perfusable vasculature. Although a developing vascular network is initiated, these vessels they are much less robust and stable, compared to the devices with only HUVEC and NHLF. It appears that the VPC might destabilize the structures, perhaps due to their highly angiogenic nature (Figure 28) [65].

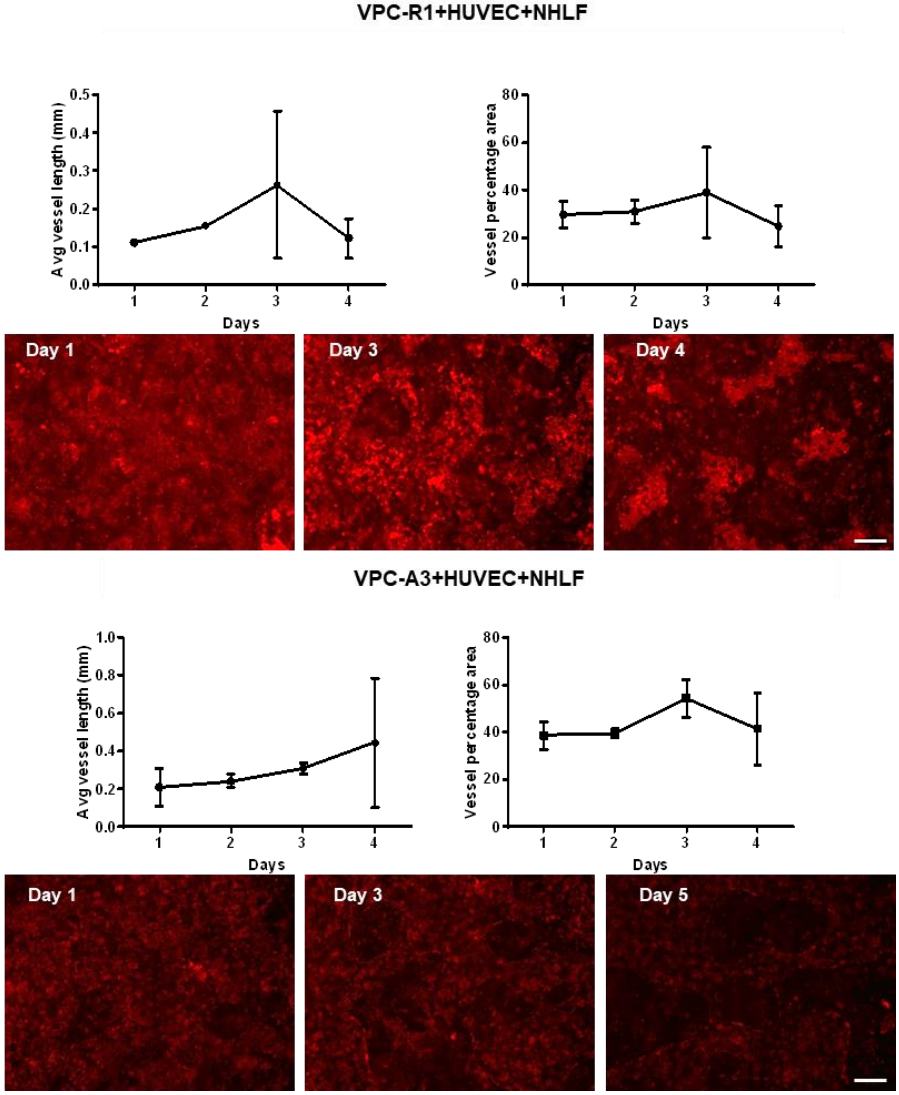

Figure 28: Vascular progenitor cells in fibrin gels. The addition of the VPC-R1 to the HUVEC+NHLF inhibit vasculature formation. By day 4, all the cells have regressed, and the gel has compacted. No visual evidence of lumen formation was seen. Red=VPC-R1 or VPC-A3 CellTracker red dye. Scale bar=100µm. n=2

Because it was suspected that the mouse ESC-derived EC might not be fully integrating with the human fibroblasts, we set out to examine the vascular assembly using

hESC-derived EC. These studies first required adapting our mouse ESC induction for human ESC. Human ESC cells were first examined for optimal induction time, seeding density, and VEGF treatment for stage 1. The greatest percentage of KDR+ cells from hESC-H9 cells was obtained at day 8 from cells seeding at 1,000 cells/cm^2, with VEGF treatment between 15 and 30 ng/ml insignificant (Figure 29) [23]. However, in order to generate enough EC for our experiments, we chose to use a cell density at 5,000 cells and collect on day 10. In stage 2, we also adapted our protocols to introduce a TGF-β receptor type 1 inhibitor (SB431542) at 7 days post sort to minimize smooth muscle cell proliferation in differentiating EC cultures [144]. On day 25 of total differentiation, the cells were sorted for VE-cadherin and expanded to passage 2 for our microfluidic device experiments.

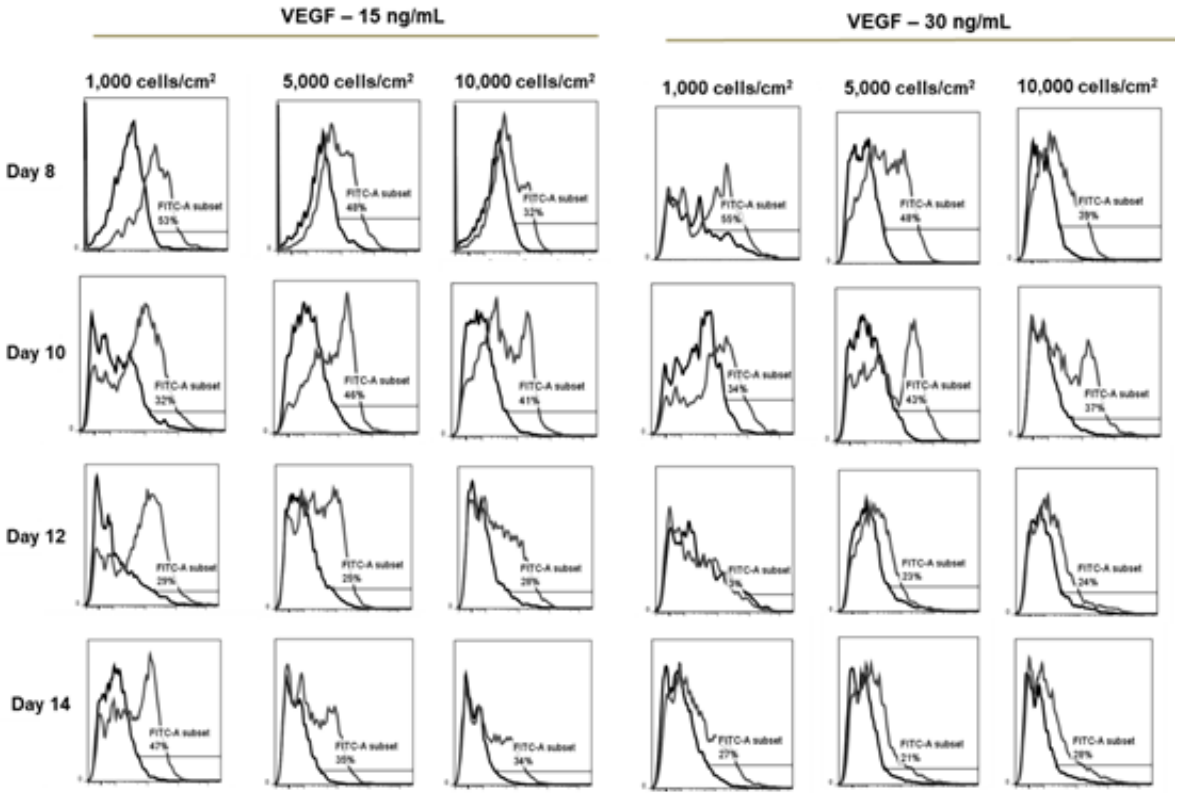

Figure 29: Induction of human ESC cells into VPC (stage 1) into KDR+ cells, varying seeding density, VEGF treatment, and examined for optimal induction time.

Combining the VE-cadherin+ cells with the NHLF in the fibrin gels and devices, we see that vascular connections started to form in the first 24 hours, but by day 3 have completely regressed. At this point, we thought that the issue might not be with the cells, but with the highly angiogenic cells migrating and degrading the fibrin gels. To block the activity of one potential source of fibrin degradation, we decided to add a cysteine protease inhibitor, E-64, to inhibit the breakdown of the fibrin gel (Figure 30). It appears as if the protease inhibitor might be aiding the vessel stability, but the concentration of the inhibitor required per cell source would still need to be optimized.

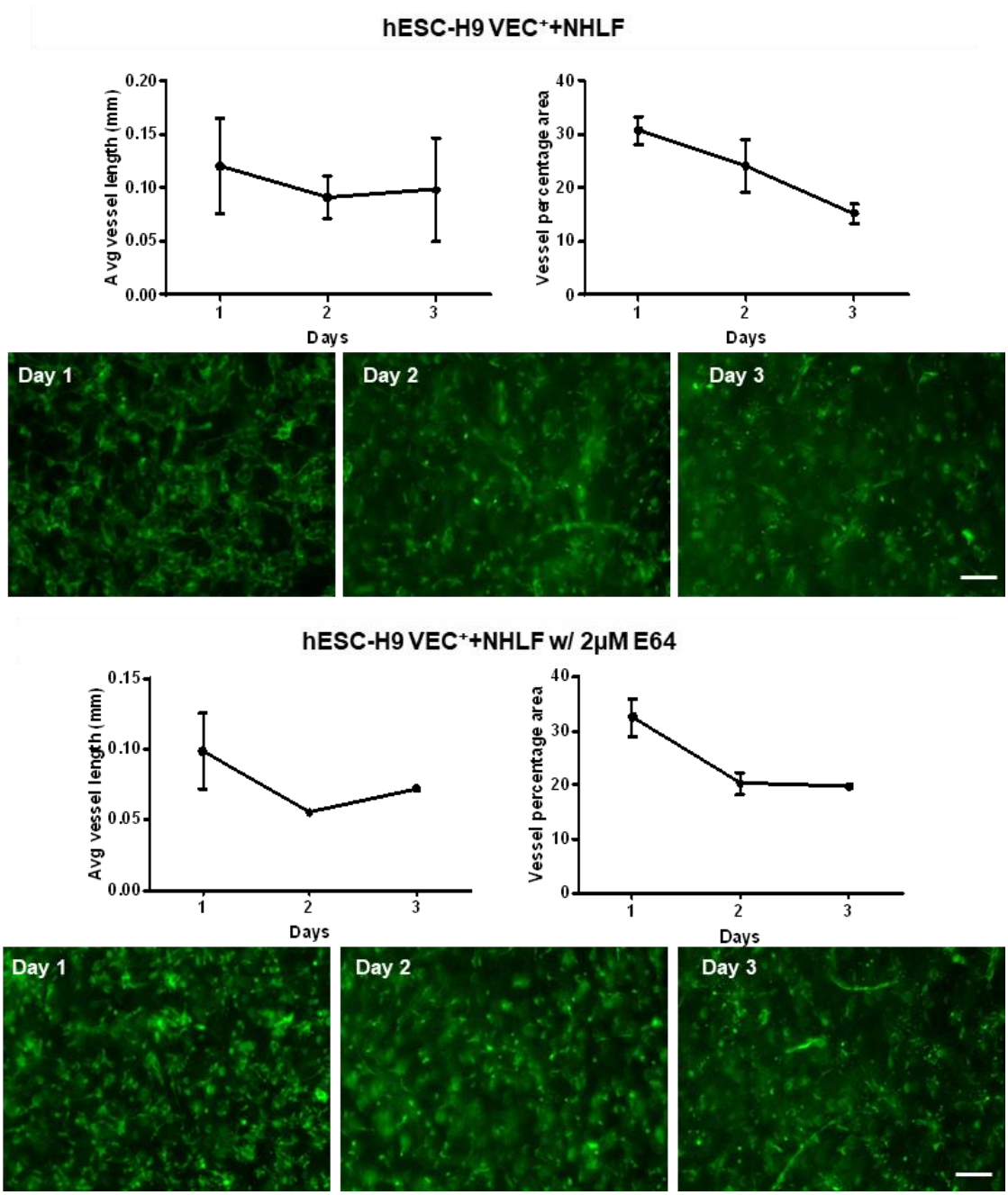

Figure 30: hESC-H9 derived EC and NHLF in fibrin gels. Similarly, to the mouse-ESC derived EC and VPC, the hESC-H9 derived EC form connections in the first 24 hours, but quickly regress over the next 48 hours and then curiously rebound formations. The addition of E-64 might be aiding not aid in the formation of vasculature up to day 3 and will require further studies. Green=hESC-H9 VEC^+ CellTracker green dye. Scale bar=100µm. n=2

Lastly, we decided to investigate the effect of co-culture with alternative stromal or accessory cell types including: inactivated mouse embryonic fibroblasts (MEF), hiPS-

derived SMC, and hESC-derived CM, with HUVEC and NHLF as our control and examine the vessels formation on day 4. Devices seeded with MEF co-cultured with HUVED did not form vessel-like structures and regressed by day 4, and according to data obtained by Angiotool, with low average vessel length, vessel percentage area, and total number of junctions (Figure 31). However, devices seeded with hIPS-derived SMC co-cultured with HUVEC exhibited more promising results, generating more vessel-like structures that appeared to be perfusable. However, these vessel-like structures were not stable past day 4. Devices seeded with HUVEC co-cultured with hESC-H9-derived cardiomyocytes (CM) and NHLF showed formation of vasculature and, compared to the control, the vessel network did not appear to be interrupted significantly by the presence of the hESC-H9 derived cardiomyocytes. The vessel percentage area was also similar to the control HUVECs co-cultured with NHLFs, but the average vessel lengths and total number of junctions remained inferior. Moreover, the vessel diameters were larger (data not shown) explaining the high vessel percentage area without high vessel length or numbers of junctions. Lastly, when devices were seeded with only HUVEC and hESC-H9 derived CM without the addition of NHLF, we did not observe vessel formation compared to the control. We conclude that although the presence of the CM did not significantly interrupt the vascular formations of HUVEC and NHLF, they did not enhance the vascular assembly or stability of neovessels.

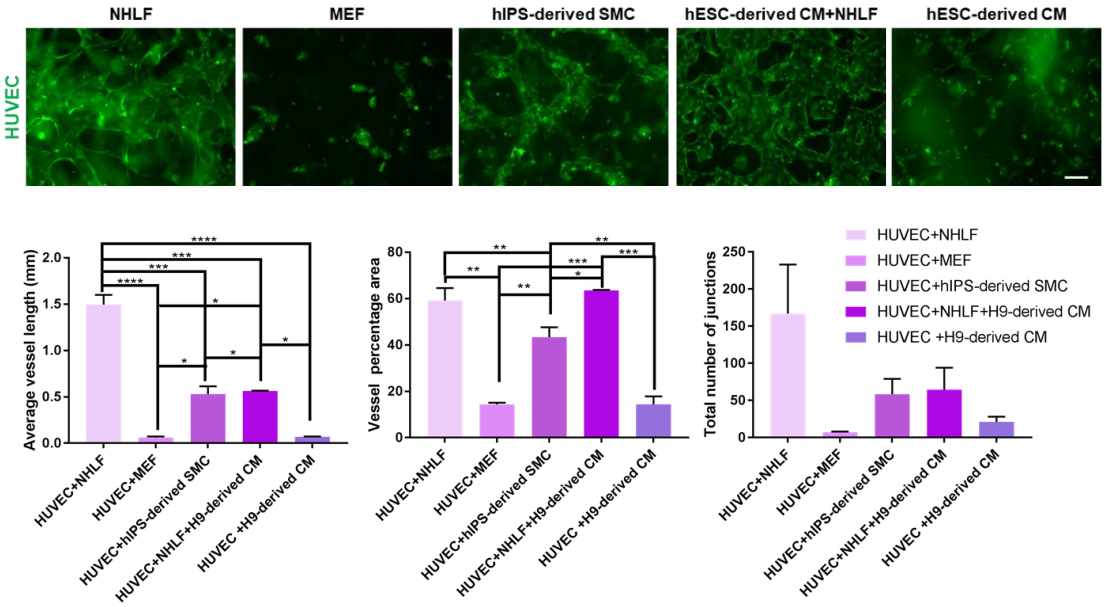

Figure 31: Investigating different accessory cell types co-cultured with HUVEC in microfluidic devices. Day 4 data presented for average vessel length, vessel percentage area, and total number of junctions. The addition of the stem cell-derived SMC produce vessel like structures, and hESC-derived CM with NHLF, but the average vessel length and total number of junctions varies significantly from the HUVEC and NHLF networks. Without the addition of NHLF with hESC-derived CM, vessel-like structures are not formed. n=2 * p-value < 0.05 ** p-value < 0.005 *** p-value < 0.0005 **** p-value < 0.00005

4.6 Discussion

In this chapter, fibrin is used as a three-dimensional structure to study the formation of vasculature in co- or tri-cultures. Fibrin is an insoluble protein which plays a role in blood clotting and is formed through the enzymatic polymerization of fibrinogen through thrombin. For therapeutic purposes, it is used as a sealant and adhesive in surgery. Once the wound starts to heal, fibrin is degraded and remodeled. *In vitro* studies have reported that fibrin gels might also promote proliferation and matrix synthesis through the release of platelet-derived growth factors and transforming growth factor beta [145]. In addition, fibrin gels have angiogenic properties that produces microvasculature-like networks and subjects cells to mechanical signaling through integrins that associate with the cytoskeleton [49]. The polymerization of fibrin forms a dense network that is impermeable to cell infiltration but is opposed by fibrinolysis, the degradation of fibrin through cell-secreted enzymatic proteases. Aprotinin is a proteinease inhibitor which slows down the degradation of fibrin (fibrinolysis). Aprotinin acts as an inhibitor by forming complexes with human trypsin, plasmin, and plasma. It blocks fibrinolysis by inhibiting plasmin. Plasmin is a serine protease that is secreted to rapidly degrade fibrin [146]. Cystine cathepsins are lysosomal proteases that degrade intracellular and extracellular matrix proteins, like collagenase and elastase [147]. Other proteases such as matrix metalloproteinases (MMPs) also contributes to fibrinolysis and degrading multiple ECM proteins [147]. Cathepsins and MMPs have been implicated in vasculogenic and angiogenic activities, normal and dysfunctional. Specifically, cathepsin L has been associated with cell invasion, neovascularization, and its activity is upregulated in endothelial progenitor cells compared to mature EC [148]. And in tumor studies, MMPs have been implicated to play a critical role in 'vasculogenic mimicry', which is a term to describe how malignant tumors form microvasculature [149, 150]. Zhang et al. shows that with the formation of microvasculature in melanoma tissues, there is an increase of MMP-2 secretion and a decrease of E-cadherins, which plays a role in cellular adhesion [150]. In another study, MMP-2 and MMP-9 were shown to increase in hypoxic conditions and promote angiogenesis in pulmonary arterial endothelial cells [151]. MMP-9 can also release VEGF from the ECM, which is an inducer of tumor angiogenesis [152].

A vascular network is needed to generate a functional tissue *in vitro* if larger than 100-200 μm because deeper than that the cells are deprived of oxygen and cell viability decreases [61, 153]. However, Shimizu et al. reports that only a maximum thickness of 80 μm can be used for successful transplantation of a cardiac construct [154]. To overcome this limit, primary cells have been used, like HUVEC and stromal cells to increase vascularity in *in vitro* tissues [130, 155, 156]. In these studies, sheets of cardiac tissue are made and placed on top of each other to form a thicker sheet. In between these sheets, vascular cells were placed and a vascular network forms within 24 hours. Even though microvessels self-assemble in these tissues, it is unclear whether the connection to host-derived vessels is fast enough to allow survival of the implanted tissue. This may explain why our hESC-derived CM did not integrate well in the microfluidic device as the fibrin gel channel is 4000 μm wide. However, when the device was tri-cultured with

HUVEC+NHLF+hESC-derived CM, we were able to observe the microvessels self-assemble. The viability of the hESC-derived CM was not assessed, but clusters were observed to be contracting (data not shown).

Within the branching sprout during angiogenesis are specialized EC: tip, stalk, and phalanx [118, 142]. The tip EC are found at the leading edge of a sprouting vessel and are distinct in their DLL4/Notch1 signaling [157]. Tip cells have more organized stress fibers compared to stalk and phalanx EC with probing filopodia and migrate towards angiogenic stimuli [158]. Stalk cells trail behind tip cells and are characterized through the suppression of Dll4 through Notch signaling. Stalk cells also readily proliferate, form lumens and do not extend filopodia [159]. Phalanx EC are less migratory and have high levels of Flt-1, which is thought to mitigate signals of VEGF, keeping phalanx EC stable [160]. This is also aided in high levels of VE-cadherin, which tightens the EC-to-EC junctions. We set out to examine these subpopulations of EC and their ability to form vasculature, as well as their vascular progenitors to mimic vasculogenesis further. Tip/stalk EC are thought to be more angiogenic than phalanx EC, so we expected that tip/stalk EC would readily form vessel-like structures, as they do in Matrigel assays [118]. However, we found that both EC subpopulations and VPC degrade the fibrin faster than they can form these connections. We suspect that these subpopulations are either too proliferative or too migratory for the fibrin gel. We also suspect the mouse cells do not integrate with the human fibroblasts. It is possible that the secreted soluble factors by either cell types may not have the appropriate receptors due to the different animal origins. The mechanism of how NHLF signal EC to self-assembly is still unclear, we know it occurs when the cells are cultured in direct fibroblast-endothelial contact (juxtacrine) and indirectly through secreted soluble factors (paracrine). Although, the juxtacrine culture has improved vascularity compared to paracrine, there are signals specifically from NHLF that have yet to be explored [46, 161].

During vasculogenesis, the endothelial precursor cells (EPC) form a primitive vascular plexus. These EPC then go on to differentiate into EC, which forms the first blood vessel network [2]. As the network undergoes further remodeling (angiogenesis) and matures, mural cells (pericytes and SMC) stabilize the network and provide contractile support and integrity to the newly formed vessels [3, 4]. Mural cells can be found surrounding the endothelium, with multiple layers of vascular SMC found on blood vessels and pericytes on small-diameter vessels [162]. In the absence of mural cells, embryos would not survive due to vessel permeability and destabilization, which is also found in the leaky vasculature formed by tumors due to their inability to recruit mural cells [163, 164]. Interestingly, there are reports suggesting that pericytes can differentiate into vascular SMC [165, 166], which proposes plasticity among mural cells. However, characterizing pericytes has been difficult as their behavior *in vivo* and *in vitro* are different. *In vivo* pericytes are multipotent, but *in vitro* they do not act as stem cells [162], and currently, pericytes have only been generated as a subpopulation in mesoderm EC differentiation studies in $CD31^-$ populations [167, 168]. Pericytes and vascular SMC share some markers and arise from the same embryonic origins, such as αSMA and

Calponin-h1 (CNN-1) *in vitro*, but pericytes do not express CNN-1 *in vivo* [162], further complicating their phenotypes.

Surprisingly, contrary to the *in vivo* surroundings during vasculogenesis, the most robust self-assembled microvasculature *in vitro* co-cultures EC with NHLF and is routinely used in numerous microfluidic studies [46, 169, 170], but there are some studies that use pericytes instead [171, 172]. In general, fibroblasts are the most common cell in connective tissue that maintains extracellular matrices and provides physical support to tissues [173, 174]. Even though these self-assembled microvessel networks do not completely mimic the complex *in vivo* microenvironment, they have been shown to behave similarly in terms of permeability, vasoactive response, and barrier function [48, 171]. Shown by Bichsel et al, the pericytes in culture surround the self-organized microvessel network and show mural-like behavior, but whether these cells function like vascular smooth muscle cells was not studied. To date, there are no studies characterizing why NHLF robustly make microvasculature *in vitro*, and no other studies using other types of fibroblasts found in other tissues. When recapitulating the vascular plexus *in vitro*, we examined the use of hIPS-derived SMC instead of lung fibroblasts since their roles in development and maintenance are significant *in vivo*. We found that devices seeded with hIPS-derived SMC co-cultured with HUVEC offered promising results but were not stable passed day 4. This may be due to not having a pure population of vascular SMC, so other cell types in the population may be proliferating and/or migrating and disrupting the newly formed networks.

4.4 Conclusions

Using microfluidic devices as our platform to form vasculature, we have investigated the potential of our mESC-derived EC and VPC and hESC-derived EC. These cell types seem to be able to form networks and connections, but quickly degrade their 3D environment. By comparing NHLF to other stromal cell types we see that NHLF provide the necessary cues to HUVEC to form perfusable vasculature. hIPS-derived SMC and hESC-derived CM with NHLF form some networks but are less stable. Future work will be needed to optimize seeding devices with alternative cell types like hESC-derived endothelial cells and eliminating the use of primary endothelial cells/HUVEC. Further optimization of microfluidic device protocols and medium formulations will also be necessary to generate stable vasculature from the stem cell derived endothelial cells. Further experimentation is also needed to determine if the vasculature is perfuasble.

Chapter 5: Electrospinning *Bombyx Mori* Silk with Poly(ethylene oxide)

5.1 Introduction

Cardiovascular diseases remain the leading cause of death in humans. Arthrosclerosis, the hardening and thickening of blood vessels, are a primary contributing factor in development of cardiovascular disease. An arterial blood vessel is composed of three distinct layers, an endothelial layer lining the lumen of the vessel, a medial layer with smooth muscle cells and thick matrix in the middle, and an outer adventitial layer of connective tissue. When the artery providing blood to the heart muscle is compromised, a bypass surgery will take a saphenous vein from the leg to reroute the blood flow around the occluded region. For patients who fail to arterialize following bypass surgery or patients with multiple bypass surgeries, synthetic or in vitro-derived vascular grafts are a necessity. Therefore, the development of small-diameter vascular grafts, for providing larger-scale blood flows (inner diameter > 6 mm), have been a subject of intense investigation in recent years. These have been made from synthetic materials like polytetrafluoroethylene, polyester (Dacron®) [175], polylactic acid, or polyglycolide [176]. However, synthetic grafts have the tendency to lead to thrombosis and eventual occlusion. Some products, like GORE® PROPATEN® Vascular Graft, include anti-coagulants to alleviate this problem. However, over time the drug will dissipate and, if not completely reendothelialized, the graft will occlude and require further replacement surgeries.

Newer small-diameter grafts made from polylactic acid [177] and polyurethane [178] have been widely accepted to be suitable for use as tissue-engineered vascular grafts, but they are not conducive to cell adhesion [179]. Only grafts seeded with endothelial cells will have properties that can excrete anti-thrombotic factors, and are considered vital for long term graft survival [55, 56]. Natural biopolymers like collagen and fibrin have been explored. These exhibit good biocompatibility and promote cell adhesion and differentiation [180, 181], but these natural grafts exhibit limited mechanical integrity complicating their integration *in vivo* [57]. Specifically, the burst strength of these constructs is much lower compared with bypass grafts from a patients' own blood vessel [182].

5.1.1 Silk fibroin

Silk fibroin, derived from *Bombyx mori* cocoons, is a naturally occurring polymer that can be blended with different ECM proteins, growth factors, or other polymers through electrospinning techniques and has been widely examined as a biomaterial [58, 183]. It is compatible with cells [184], blood [185], non-immunogenic [186], and the rate of degradation can also be tuned and has been shown to be replaced by collagen and other ECM proteins within the body [59, 60]. The use of silk fibroin has been reported in constructing vessels by electrospinning [187] or freeze drying [182], and the biocompatibility has been tested *in vitro* and *in vivo* [188]. Most importantly, electropun silk vascular grafts have been reported to have comparable mechanical properties to those of native blood vessels [58, 188].

5.1.2 Electrospinning

Electrospinning fibers, due to their long fibers and high surface area, are an excellent strategy that can provide tube-like structures that can sustain high levels of mechanical stress. An electrospinning set up requires high-voltage power supply, a syringe pump, a collecting plate, and an electrostatically charged fluid. A charge difference is established between the spinneret and grounded plate. The liquid will form a Taylor cone which produces an electrospun fiber. In addition to the setup, certain parameters must be optimized. These include: the distance between spinneret and ground, viscosity of the fluid, and flow rate that will form the Taylor cone. The fiber diameters formed can also be altered by adjusting these parameters.

Once the material is prepared through electrospinning, the secondary structures of silk fibroin (β-sheet, three-fold helix (β-turn), or random coil) can be altered depending on the processing [189]. Treatment with organic solvents like alcohols can be used to convert the crystallization from random coil to β-sheet, which has been shown to be highly effective and the transition to alcohol vapor and sterility for cell cultures purposes is effective as well [189, 190].

5.1.3 Lumenized muscle

The self-assembly of skeletal muscle strips under tension has been recently developed [191, 192]. Briefly, a hollow tube is created by allowing a high concentration of gelatin mixed with sodium hydroxide and thrombin to form around a 0.5mm diameter wire (Figure 32). After allowing the solution to solidify at 4°C, the wire is removed. Another solution made of fibrinogen, Matrigel™, cells, aminocaproic acid, and media is pipetted through the cavity from the displaced wire. The device is placed at 37°C, allowing the gelled thrombin to diffuse into the cell-fibrinogen solution to form the muscle strip in fibrin.

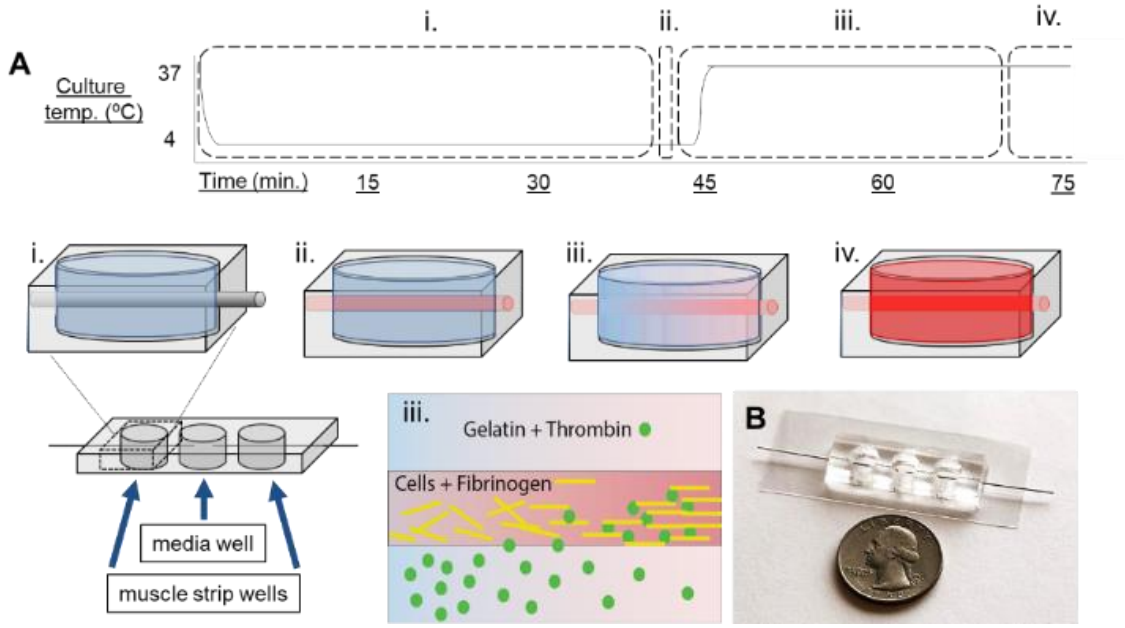

Figure 32: Muscle strip device. A) A gelatin solution is added to the device and allowed to solidify around a wire (i), a cell-fibrinogen solution is added (ii), placed at 37°C to allow thrombin to diffuse through and form fibrin (iii), and media is replaced surrounding the newly formed muscle strip (iv). B) A representative device with a quarter for scale.

This technology is required to be in tension axially, which aligns the cells, however, when the tissue under tension is detached, the muscle strip will contract. Moreover, without providing perfusion to the tissue, the size of these muscle strips remains limited. Our laboratory has explored the addition of a perfusable lumen through the length of the muscle. This required the addition of a second sacrificial gelation step for providing spatially segregated endothelial cells within the lumen. This new device design requires a series of molds cast using polydimethylsiloxane (PDMS) and degradable polymers to guide tissue formation within a microfluidic chamber. By inserting electrospun silk fibroin between the muscle and endothelial layers, we also aim to prevent the tissue from collapsing upon removal from the device.

5.2 Methods

5.2.1 Silk processing and spinning solution

Bombyx mori cocoons were processed following the methods published by Jin, H. [193]. First, they were boiled in 0.02 M sodium carbonate for 30 minutes and rinsed with distilled water to remove the pro-inflammatory sericin protein (Silk 1). After boiling, the silk was dissolved in 9.3 M lithium bromide for 30 minutes and dialyzed for 48 hours. The electrospinning solution was prepared by dissolving 2.5% by weight of polyethylene oxide (PEO) into 5% silk solution, resulting in a 5% silk 2.5% w/v PEO solution and placed on a rotator overnight (Figure 33).

5.2.2 Electrospinning

A syringe pump set at 5 µL/min was connected to tubing filled with 10 mL of silk/PEO solution. A 23G dispensing tip was used and connected to a positive charge of 5 kV. The distance from ground was set to 9 cm. The silk scaffolds were submerged in 90/10 (v/v) methanol/water for sterilization and induction of β-sheet formation for 20 minutes and desiccated overnight (Silk 3).

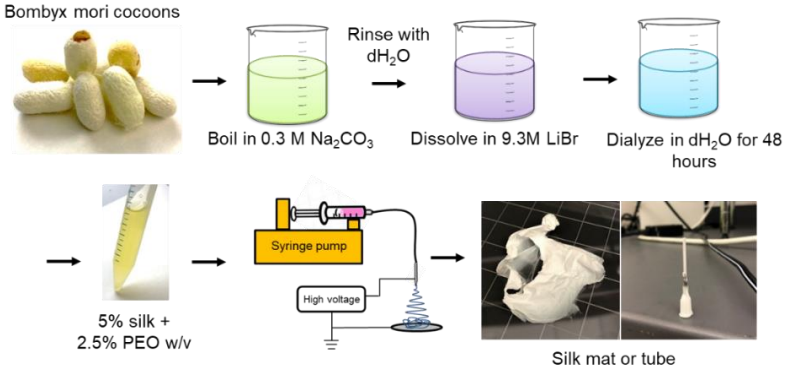

Figure 33: Processing *Bombyx mori* cocoons. The sericin was removed using sodium carbonate then dissolved in lithium bromide and dialyzed for 48 hours. Then 2.5%

polyethylene oxide was dissolved into 5% silk solution and electrospun to make silk mats or tubes.

5.2.3 Scanning electron microscopy (SEM)

Electrospun silk on glass coverslips were sputter coated with gold before analysis. Images of electrospun fibers coated with gold were obtained with a Zeiss Gemini 500. Average fiber diameters were determined by measuring 100 fibers selected randomly from each image using ImageJ software.

5.2.4 X-ray diffraction

An X-ray diffractometer (PANalytical X'Pert PRO Theta) with Co/Kα radiation (k=1.788965 nm) was used to analyze the crystallinity of the silk. Data were collected for 2θ values of 5-45° with a step size of 0.03° and a continuous time of 0.7 s per step, according to a previous study [194]. Bragg's Law was used to convert diffraction angles from Co/Kα to Cu/Kα. The D-spacing was calculated using the following equation: $D=\lambda/(2\times\sin(\theta))$, where θ=Bragg's angle.

5.2.5 Primary cell culture

Normal human lung fibroblasts (NHLF; Lonza) were cultured in Fibroblast Growth Medium (FGM™-2; Lonza) on gelatin-coated plates. To test attachment to our silk substrate, NHLF were lifted using trypsin and re-plated at 10,000 cells/cm^2 on tissue culture treated plastic, glass coverslips, and glass coverslips with electrospun silk. Gelatin was not used to coat any of these substrates. Murine C2C12 skeletal muscle cells were cultured on gelatin-coated dishes in medium containing: 88% High Glucose DMEM, 10% FBS, 1% L-glutamine, and 1% penicillin-streptomycin. Human umbilical vein endothelial cell (HUVEC; Life Technologies) were cultured in Endothelial Cell Growth Medium (EGM™-2 with BulletKit™; Lonza) on fibronectin coated plates (10 µg/mL; Corning) and used in experiments between passages 3-5. In the muscle strip device, C2C12 and HUVEC were injected at 20x10^6 cells/mL.

5.2.6 Quantifying Cell Alignment

Images were processed via custom MATLAB (MathWorks, Inc) scrips. Actin labeled images were analyzed by transforming them into 8-bit images. A 2-by-2 median filtering (medilt2) operation was carried out to ensure proper identification of edges. Image threshold values were calculated (graythresh) and used when turning the images into binary. The binary images were then dilated and eroded separately, and their difference became the cell membrane or actin skeleton. The binary outline was then analyzed for its properties (regionprops) from which the orientation was extracted. Cells were defined as "aligned" if they are within ± 30° of the principal axis, which was found by maximizing percent alignment.

5.2.7 Muscle-endothelial bundle device

The microfluidic devices (Figure 34) were made by desiccating PDMS at a ratio of 1g of curing agent to 10g of base around concentric 17 G and 24 G needles and baked in an oven at 75°C for 2 hours or overnight. A well is created by using a biopsy punch and the device is bonded to a 18mm glass coverslip. The muscle and endothelial tissue are layered using a sacrificial hydrogel technique. First, a silk mat is wrapped around the 24 G needle and placed into the 17 G needle. Second, the outer layer of the muscle tissue is formed by injecting muscle cells through the 17G needle (coats the silk tube). The endothelial layer is then added by injecting the cells through the 20 G needle. C2C12 and HUVEC are dyed with CellTracker Red/Green, respectively.

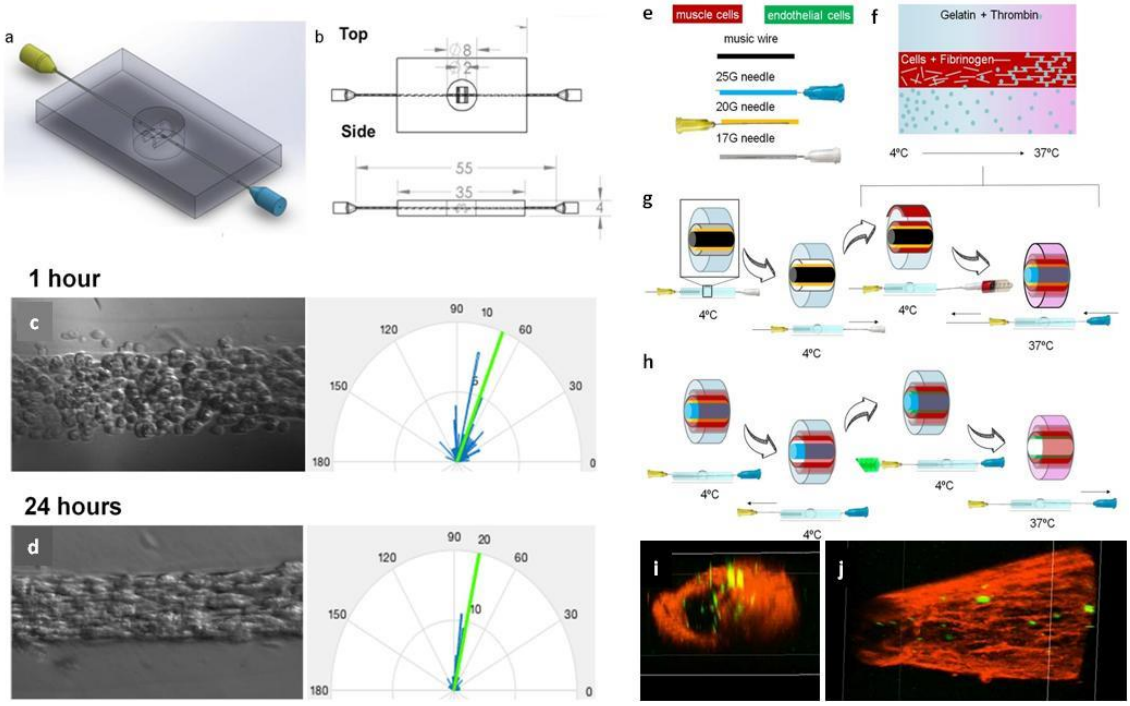

Figure 34: Muscle-endothelial bundle device. (a-b) Schematics of the device. (c-d) The cells that were injected after 1 hour are less aligned compared to 24 hours later. (e-h) The formation of the muscle-endothelial bundle is similar to the muscle strip device, however there is an additional needle in the cavity that allows the muscle cells to form around it before injecting endothelial cells in the new cavity. (i-j) C2C12 (red) form connections with each other and surround HUVEC (green) in a cavity.

5.3 Results

5.3.1 Silk characterization using SEM

The morphology of Silk 2 and 3 were characterized by SEM at different magnifications to investigate the effects of methanol (Figure 35). An average fiber diameter of 408 ± 121 nm was measured (Figure 36) in the regions of the mats where no defects were present and only of Silk 2, due to ambiguity of specific fibers in Silk 3 samples (Figure 35 bottom). The inconsistency in fiber formation in Silk 2 can be attributed to the start of the electrospinning process/Taylor cone formation because the

defects are most likely formed when electrospraying are underneath the electrospun fibers.

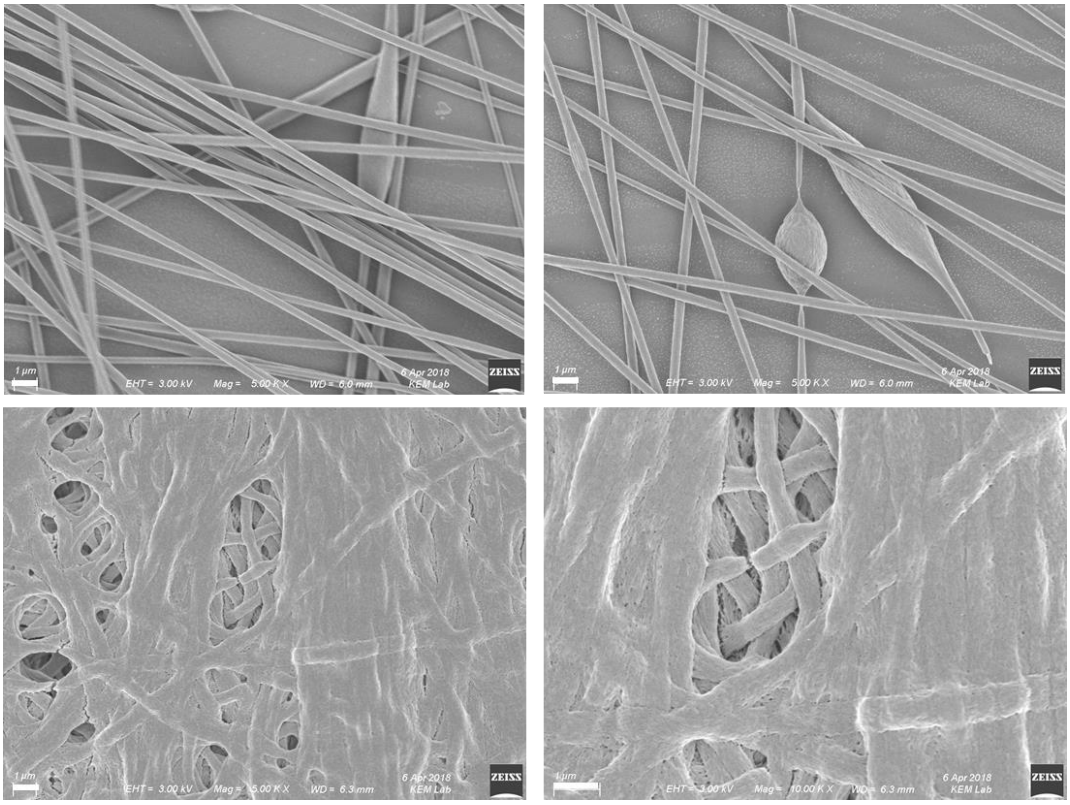

Figure 35: Scanning electron microscope images of Silk 2 (top) and Silk 3 (bottom). Scale bars=1µm

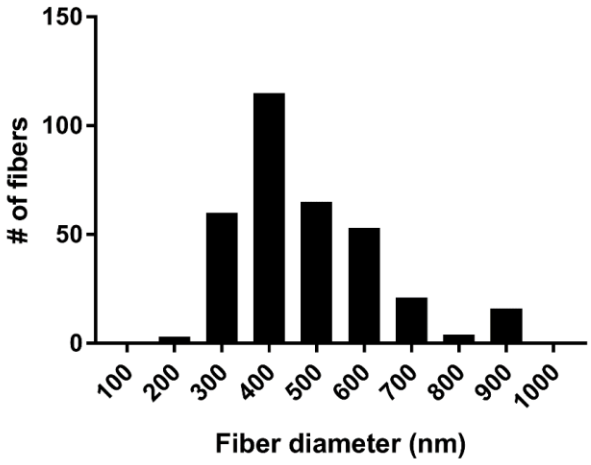

Figure 36: Histogram of diameter of electrospun fibers. Mean: 470 ± 150 nm

5.3.2 X-ray diffraction analysis

The main crystal structures are Silk 1 and 2, while Silk 3 is a relatively new structure that was observed to be formed in solutions of fibroin at an interface, like air-water [195]. Silk 1I is the natural fibroin that is emitted from *Bombyx mori* silk glands and is characterized by having β-turn structures that result in compact silk conformations [196]. Silk 2 is less compact than Silk 1 and is characterized by having antiparallel β-sheets of crystallized silk found in spun silk fibers, while Silk 3 is found to form a 3-fold extended helix at an interface [197]. The use of silk fibroin in research or commercial applications is usually made up of a mixture of these crystalline structures which can be tuned depending on the application [198]. The toughness and solubility in water of silk fibroin is dependent on their β-sheet composition. To study the composition of the silk produced, we used an X-ray diffraction method of analysis. Figure 37 shows the X-ray diffraction data of the silk fibroins produced in our studies: degummed fibroin (Silk 1), electrospun fibroin (Silk 2), and electrospun fibroin prepared in methanol (Silk 3). Silk 1 has a broad peak at 2θ = 21°, which corresponds to a crystalline spacing of 0.422 nm. Silk 2 and Silk 3 have similar 2θ diffraction peaks at 19° which corresponded to a crystalline spacing of 0.467 nm. However, Silk 3 showed an additional peak at 2θ = 24°, which corresponds with a crystalline spacing of 0.370 nm. A previous study demonstrated similar XRD pattern of the β-sheet crystalline structure at 0.370 nm, however they report two other diffraction peaks at 8.19° and 20.46° [194]. The peak for degummed silk was not as intense as the electrospun silk, indicating that these solutions contain decreased crystallization but increased organization.

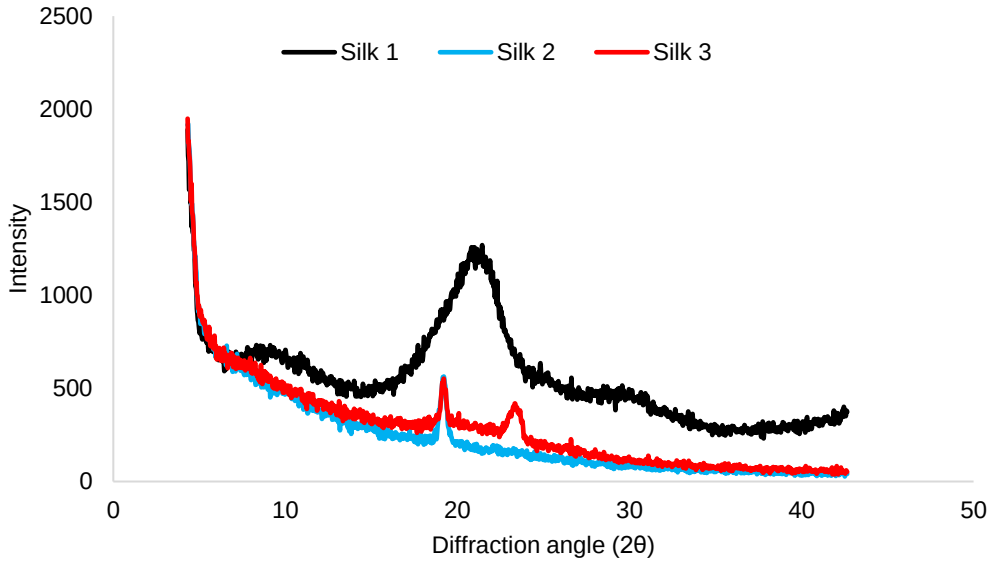

Figure 37: X-ray diffraction patterns of sericin-free silk (Silk 1), electrospun water-soluble silk (Silk 2), and electrospun water-insoluble silk (Silk 3).

5.3.3 In vitro cell interactions

Normal human lung fibroblasts were plated to examine cell attachment to the silk fibers. As controls, we plated NHLF on tissue culture plastic and glass coverslips. After 7 days, the cells were stained with F-actin and DAPI (Figure 38). Surprisingly, the NHLF appeared to be aligning to the substrate as early as 3 days, even though the fibers were spun randomly. We quantified the alignment using MatLab and found that the NHLF were more aligned on silk (84.6%) compared to TC plastic (67.7%) and glass (76.8%). This un-intended alignment can be observed in the XRD results, where the electrospun fibers (Silk 2) are more aligned than the raw silk (Silk 1). We also see the formation of aligned fibers after methanol treatment (Silk 3), so the cells are responding by aligning to these structures.

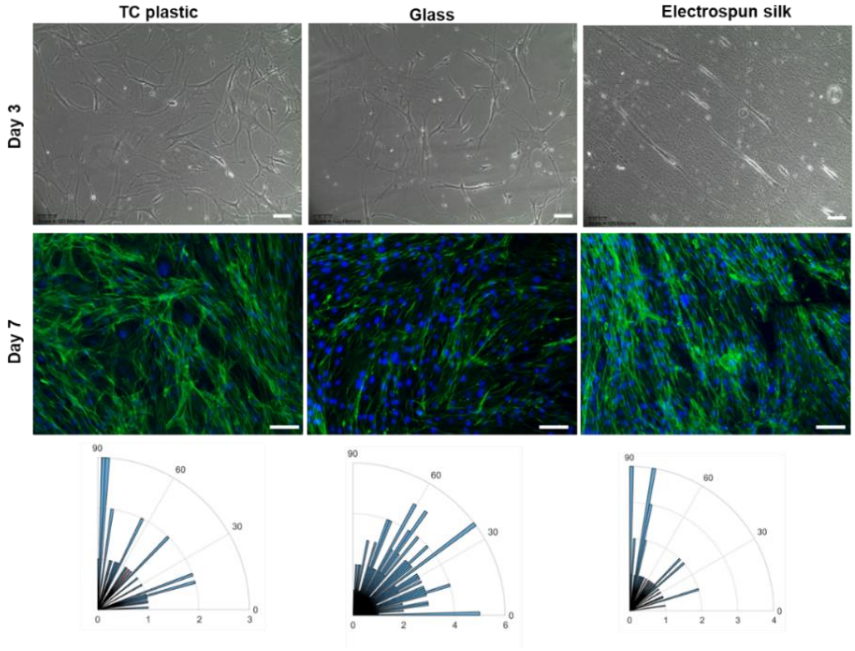

Figure 38: Normal human lung fibroblasts plated on tissue culture (TC) plastic, glass coverslips, and electrospun silk (Silk 3). Cells were stained with F-actin and DAPI. Using MatLab, we quantified alignment of F-actin fibers and found that, on average, the F-actin fibers are aligned more on the electrospun silk, then TC plastic, followed by glass. Scale bars=100μm

5.3.4 Muscle-endothelial bundle device

Figure 39 shows the development of muscle-endothelial bundle without (Figure 39A) and with (Figure 39B) the silk scaffold. After injecting the fibrinogen+C2C12 cells and allowing the thrombin to diffuse through at 37°C, the cells are also able to diffuse out into the well (Figure 39A). With the addition of the silk mat coating the 25G needle (blue), the C2C12 cells attach to the silk and remain from day 0-5. Since the C2C12 have attached so closely, we can also see that the silk has unwound itself in part of the device. The total length of the tissue is 8.87 mm, while the diameter of the muscle bundle starts at ~1.12 mm (day 0) and compacts to ~617 μm (day 5), a 45% change. The endothelial

bundle compacts from ~812 µm (day 0) to ~413 µm (day 5). As a previous study has reported [192], we observed that the bundles becomes taut, which indicates that there is internal tension between the two ends where the tissue is attached.

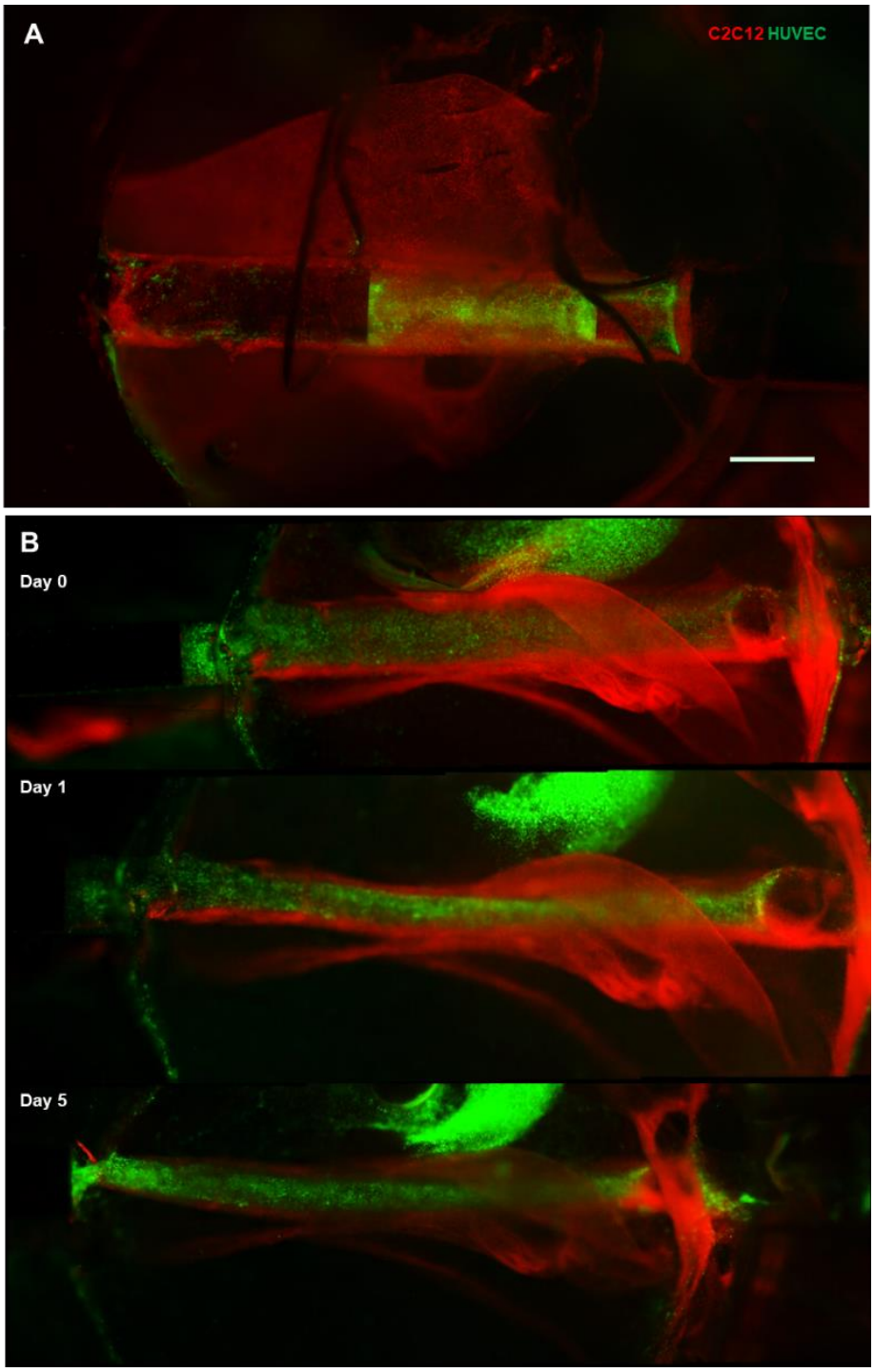

Figure 39: Muscle-endothelial bundle. A) HUVEC (green) and C2C12 (red) in muscle strip device, without the addition of silk. C2C12 leak into well of device after injection

but still forms a tube around the HUVEC. B) The addition of the silk tube allows the C2C12 to attach and prevents them from spreading into the well. After 24 hours, there is a clear border between the HUVEC and C2C12 cells, and the muscle-endothelial bundle further compacts through day 5. Scale bar=1000μm.

5.4 Conclusions

Using *Bombyx mori* cocoons, we have been able to repeat and demonstrate that we can electrospin in PEO into mats. We verify that fibers are formed using SEM and have an average diameter of 473 ± 147 nm. By using x-ray diffraction, we see there is a change in structure or organization of the fibers between Silk 1 (degummed silk) and Silk 2 and 3 (electrospun silk), due to the decreased broadness of the peaks at $2\theta = 19°$. By treating the electrospun mats in 90% methanol, we can induce a β-sheet change, and create water-insoluble silk, Silk 3. A structure change can be seen in the x-ray diffraction, at $2\theta = 24°$. We can also verify that the silk is water-insoluble when used in cell culture. We verified that NHLF will adhere to the silk mats, and interestingly align themselves compared to tissue-culture plastic and glass coverslip. Lastly, by wrapping the dispensing needle in the muscle-endothelial device with silk, we show that the C2C12 skeletal muscle cells will attach to the silk, with an endothelial tube bisecting the muscle tissue.

Chapter 6: Conclusions

The goal of tissue engineering is to generate a functional tissue that can facilitate organ regeneration. The field combines cells, materials, biochemical factors. However, a major obstacle is vascularizing these tissues. In the body, most cells are found no more than 100-200 μm from the nearest capillary [61]. This diffusion limitation restricts the size of tissues and organs that can be built and impedes successful integration after implantation. To build vasculature to overcome this obstacle, EC that line the lumen of blood vessels is required. Support cells, such as smooth muscle cells and fibroblasts, are also needed to synthesize matrix and control blood pressure. By studying EC differentiation and the factors that drive blood vessel formation, we can provide researchers with the ability to develop larger tissues. Embryonic and induced pluripotent stem cells are both valuable sources for generating specific cell types for its intended application due to their unlimited proliferation potential and ability to differentiate into any cell type. The goal of the work in this thesis is to investigate how the stiffness of the substrate affects VPC towards EC or SMC fate, microcontact printing using biomimicry, microvasculature formation in a 3D environment, and lastly *Bombyx mori* silk as a scaffolding for cells.

First, we were inspired by Dr. Engler's work on how the stiffness of polyacrylamide hydrogels can affect mesenchymal stem cells and wanted to examine its effects on VPC. Initially, we wanted to use a novel mouse ESC line that expresses GFP under Tie-2 promoter and RFP under the αSMA promoter on Zebraxis, which have low and high stiffness stripes, to see if their reporters would be expressed on the different stiffnesses. The results indicated that the VPC preferentially adhere to 10 kPa compared to 1 kPa, and 34 kPa compared to 10 kPa, which due to design constraints is elevated. There have been studies documenting cells migrating upward onto elevated ridges rather than in a downward direction, but is not well understood [36, 37]. Therefore, we moved to single-stiffness polyacrylamide hydrogels since the effect of stiffness on Zebraxis was inconclusive. Using 10 and 40 kPa single stiffness polyacrylamide hydrogels and tissue culture plastic as a control, we examined days 3-10 and found that VPC on lower stiffness expressed more PECAM-1, and more CNN-1 on higher stiffness. Next, we investigated mechanosensors such as integrins and focal adhesions to pinpoint signaling pathways that may be affecting stiffness directed differentiation. As expected, FAK 14, which prevents FAK phosphorylation, downregulated both PECAM-1 and CNN-1 on all varying stiffness. Integrin αV forms heterodimers with integrins β1, β3, and β6 which are expressed on EC. They interact with many ECM proteins and have a role in angiogenesis and leukocyte adhesion. Specifically, αvβ3 is an integrin that supports mesoderm differentiation. αvβ1 binds to several ECM proteins that affect vascular proliferation. It also associates with integrin α1-α6 chains and acts a fibronectin receptor that is involved in cell-cell and cell-matrix interactions. However, due to their associations with EC adhesion, migration and proliferation, variations of the αv integrin family are implicated in a number of diseases, including fibrosis and cancer [199, 200]. The same integrin mediated signals are exploited to manipulate the microenvironment to support tumor growth. In our studies, we surprisingly found that the addition of αvβ3

upregulated PECAM-1+ expression on all culture conditions, but αvβ1 suppressed PECAM-1+. Together, both αvβ3 and αvβ1 modulated the expression of PECAM-1. By analyzing RNA-Seq data we saw a clear difference between the 10 and 40 kPa populations compared to TCP. More vascular development related genes were upregulated on low stiffness compared to TCP. *TEK* was one of the genes upregulated on 10 kPa and encodes for Tie-2, an angiopoietin receptor that is associated with vascular development and angiogenesis [111]. The upregulation of Tie-2 leads to various signaling pathways that complex with αvβ3 and αvβ1. Tie-2 forms complexes with αvβ1 to activate subsequent signaling pathways. When comparing to our inhibitor assay, by blocking αvβ1 we see that stiffness-directed differentiation was repressed (decrease in PECAM-1). Interestingly, blocking αvβ3 did not lead to repressed PECAM-1 expression, but led to an increase. By blocking both αvβ3 and αvβ1, we concluded that αvβ3 is activated through the addition of anti-αvβ3, but αvβ1 needs the underlying stiffness/force from fibronectin to be activated.

In the next chapter (Chapter 3), we and collaborator, Michelle Khine (UCI), were inspired by leaf veins to generate a reverse mold. We explored the potential for generating a vasculature as patterned EC that could be provided as distinct layers between sheets of cells. The mask was prepared by boiling a fresh leaf and removing the excess cellulose material surrounding the leaf vascular structure. Standard photo lithography methods were applied, and the leaf mask was pressed flat against the photoresist. By using microcontact printing, we were able to preserve the branching vasculature and the unique spatial arrangement of EC over length scales that mimic branching vasculature. We showed that HUVEC adhere to the patterned matrix and can be transferred to 3D hydrogel matrices, like collagen and Matrigel. We observed migration of the cells and sprouting in the Matrigel, but to a lesser extent in collagen. That was expected due to the difference in stiffness between the matrices.

Chapter 4 explores the use of microfluidic devices to form perfusable vasculature. Our collaborator Roger Kamm (MIT) provided us both paracrine and juxtacrine molds for microfluidic devices to study whether cell secretion or cell-cell contact is necessary for the emergence of microvasculature. First, we set out to repeat his studies by using primary cell lines, HUVEC and NHLF. The co-culture of these cells in a fibrin gel robustly make perfusable vasculature as early as 4 days and stay stable for up to 14 days. However, the use of primary cells is not ideal to use for tissue engineering purposes because we need the vascularized tissue be able to connect to the host. Therefore, induced pluripotent stem cell derived-EC would be the optimal choice. In addition to cell type, matrix composition, cell concentration, cell ratio, stromal cell type, biochemical stimuli, can all be used to form perfusable vasculature [citations]. Starting with our mouse embryonic stem cell derived EC before moving to human stem cell derived cells, we investigated phalanx and tip/stalk EC subpopulations. Both subpopulations form connections but not perfusable vasculature and quickly de-stabilize, with phalanx EC destabilizing on day 3 and tip/stalk EC on day 4. Next, we cultured our mouse derived-VPC (mESC-R1 and A3) with HUVEC and NHLF and found similar results to the EC subpopulations. However, it was interesting to note that the mouse derived VPC, de-

stabilized the HUVEC from forming microvessels as well. We concluded that the mouse cells do not integrate with human fibroblasts since it is possible that the secreted soluble factors by either cell type may not have the appropriate receptors due to different animal origins. Subsequently, we attempted hESC-derived EC that were sorted for VE-cadherin. We see promising results on day 1 but the cells regress by day 2 and the fibrin gel dissipates. We attempted to add a protease inhibitor, E-64, to slow down the breakdown of the fibrin gel, it appears that there is a possibility of it aiding vessel stability, but the concentration of the inhibitor will need to be optimized. Lastly, we investigated the effect of alternative stromal or accessory cell types: inactivated MEF, hIPS-derived SMC, and hESC-derived CM. Unfortunately, the best accessory cell to HUVEC are NHLF, with a tri-culture with hESC-derived CM second, hIPS-derived SMC third, and MEF and hESC-derived CM last. Further examination on NHLF is needed to understand the synergistic effect with HUVEC to form microvessels.

Lastly, Chapter 5 investigates the use of *Bombyx mori* cocoons as a biomaterial through electrospinning. As both the material and method were new to the lab, specific parameters needed to be optimized. First, we followed a published protocol to process the cocoons into monomers. For our electrospinning solution, we combined the dissolved silk with polyethylene oxide (PEO) which has been shown to prevent conformational transitions while the silk is solubilizing and reprocessed into new fibers. Organic solvents like, hexafluoro-2-propanol, is commonly used to electrospin silk, but is not biocompatible and adds another removal step before introducing *in vitro* or *in vivo* [201]. Although, electrospinning parameters are published, it varies from set up to set up, such as height of the spinneret, voltage, viscosity of the solution, and the total time spent electrospinning, as well as the goal of the product (tubes, mats, etc). So, these parameters had to be optimized for our set up and our specific needs. First, a silk mat was produced to study the cytoxicity with cells *in vitro*, but we first had to change the silk into its secondary structure, so it would become insoluble using methanol. Next, we had to figure out how to make a silk tube. We tried to roll a silk mat into a tube and a rotating mandrel with a conductive dispensing tip attached. The electrospun silk on the dispensing tip was not removable compared to rolling a silk mat into a tube. The silk tube was then used to show that C2C12 skeletal muscle cells will attach to the silk with an endothelial bisecting the muscle tissue. Over the course of 5 days, compaction can be seen which has been reported from a previous study, which indicates that there is internal tension between the two ends where the tissue is attached [192].

References

1. Fioretta, E.S., et al., *Influence of substrate stiffness on circulating progenitor cell fate.* J Biomech, 2012. **45**(5): p. 736-44.
2. Drake, C.J. and P.A. Fleming, *Vasculogenesis in the day 6.5 to 9.5 mouse embryo.* Blood, 2000. **95**(5): p. 1671-9.
3. Hellstrom, M., et al., *Role of PDGF-B and PDGFR-beta in recruitment of vascular smooth muscle cells and pericytes during embryonic blood vessel formation in the mouse.* Development, 1999. **126**(14): p. 3047-55.
4. Carmeliet, P. and R.K. Jain, *Molecular mechanisms and clinical applications of angiogenesis.* Nature, 2011. **473**(7347): p. 298-307.
5. Downs, K.M., et al., *The Allantoic Core Domain: new insights into development of the murine allantois and its relation to the primitive streak.* Dev Dyn, 2009. **238**(3): p. 532-53.
6. Perez-Pomares, J.M., et al., *Origin of coronary endothelial cells from epicardial mesothelium in avian embryos.* Int J Dev Biol, 2002. **46**(8): p. 1005-13.
7. Yamashita, J., et al., *Flk1-positive cells derived from embryonic stem cells serve as vascular progenitors.* Nature, 2000. **408**(6808): p. 92-6.
8. Nishikawa, S.I., et al., *Progressive lineage analysis by cell sorting and culture identifies FLK1+VE-cadherin+ cells at a diverging point of endothelial and hemopoietic lineages.* Development, 1998. **125**(9): p. 1747-57.
9. Shalaby, F., et al., *Failure of blood-island formation and vasculogenesis in Flk-1-deficient mice.* Nature, 1995. **376**(6535): p. 62-6.
10. Rasmussen, T.L., et al., *VEGF/Flk1 signaling cascade transactivates Etv2 gene expression.* PLoS One, 2012. **7**(11): p. e50103.
11. Ferrara, N., et al., *Heterozygous embryonic lethality induced by targeted inactivation of the VEGF gene.* Nature, 1996. **380**(6573): p. 439-42.
12. Ferreira, L.S., et al., *Vascular progenitor cells isolated from human embryonic stem cells give rise to endothelial and smooth muscle like cells and form vascular networks in vivo.* Circ Res, 2007. **101**(3): p. 286-94.
13. Ferguson, J.E., 3rd, R.W. Kelley, and C. Patterson, *Mechanisms of endothelial differentiation in embryonic vasculogenesis.* Arterioscler Thromb Vasc Biol, 2005. **25**(11): p. 2246-54.
14. Kawasaki, K., et al., *Ras signaling directs endothelial specification of VEGFR2+ vascular progenitor cells.* J Cell Biol, 2008. **181**(1): p. 131-41.
15. Era, T., et al., *Multiple mesoderm subsets give rise to endothelial cells, whereas hematopoietic cells are differentiated only from a restricted subset in embryonic stem cell differentiation culture.* Stem Cells, 2008. **26**(2): p. 401-11.
16. Suzuki, Y., et al., *BMPs promote proliferation and migration of endothelial cells via stimulation of VEGF-A/VEGFR2 and angiopoietin-1/Tie2 signalling.* J Biochem, 2008. **143**(2): p. 199-206.
17. Guo, S., et al., *Endothelial progenitor cells derived from CD34+ cells form cooperative vascular networks.* Cell Physiol Biochem, 2010. **26**(4-5): p. 679-88.

18. Darland, D.C. and P.A. D'Amore, *TGF beta is required for the formation of capillary-like structures in three-dimensional cocultures of 10T1/2 and endothelial cells.* Angiogenesis, 2001. **4**(1): p. 11-20.
19. Lu, P., et al., *Extracellular matrix degradation and remodeling in development and disease.* Cold Spring Harb Perspect Biol, 2011. **3**(12).
20. Nakayama, K.H., L. Hou, and N.F. Huang, *Role of extracellular matrix signaling cues in modulating cell fate commitment for cardiovascular tissue engineering.* Adv Healthc Mater, 2014. **3**(5): p. 628-41.
21. Miranti, C.K. and J.S. Brugge, *Sensing the environment: a historical perspective on integrin signal transduction.* Nat Cell Biol, 2002. **4**(4): p. E83-90.
22. Schwartz, M.A. and M.H. Ginsberg, *Networks and crosstalk: integrin signalling spreads.* Nat Cell Biol, 2002. **4**(4): p. E65-8.
23. Glaser, D.E., et al., *Multifactorial Optimizations for Directing Endothelial Fate from Stem Cells.* PLoS One, 2016. **11**(12): p. e0166663.
24. Wijelath, E.S., et al., *Fibronectin promotes VEGF-induced CD34 cell differentiation into endothelial cells.* J Vasc Surg, 2004. **39**(3): p. 655-60.
25. Clarke, D.N., et al., *Perlecan Domain V induces VEGf secretion in brain endothelial cells through integrin alpha5beta1 and ERK-dependent signaling pathways.* PLoS One, 2012. **7**(9): p. e45257.
26. Lamalice, L., F. Le Boeuf, and J. Huot, *Endothelial cell migration during angiogenesis.* Circ Res, 2007. **100**(6): p. 782-94.
27. Stolberg, S. and K.E. McCloskey, *Can shear stress direct stem cell fate?* Biotechnol Prog, 2009. **25**(1): p. 10-9.
28. Polte, T.R., et al., *Extracellular matrix controls myosin light chain phosphorylation and cell contractility through modulation of cell shape and cytoskeletal prestress.* Am J Physiol Cell Physiol, 2004. **286**(3): p. C518-28.
29. le Noble, F., et al., *Flow regulates arterial-venous differentiation in the chick embryo yolk sac.* Development, 2004. **131**(2): p. 361-75.
30. Humphrey, J.D., *Vascular adaptation and mechanical homeostasis at tissue, cellular, and sub-cellular levels.* Cell Biochem Biophys, 2008. **50**(2): p. 53-78.
31. Bussolari, S.R., C.F. Dewey, Jr., and M.A. Gimbrone, Jr., *Apparatus for subjecting living cells to fluid shear stress.* Rev Sci Instrum, 1982. **53**(12): p. 1851-4.
32. Nomura, H., et al., *A disk-type apparatus for applying fluid shear stress on cultured endothelial cell.* Biorheology, 1988. **25**(3): p. 461-70.
33. Pries, A.R., T.W. Secomb, and P. Gaehtgens, *The endothelial surface layer.* Pflugers Arch, 2000. **440**(5): p. 653-66.
34. Pahakis, M.Y., et al., *The role of endothelial glycocalyx components in mechanotransduction of fluid shear stress.* Biochem Biophys Res Commun, 2007. **355**(1): p. 228-33.
35. Shi, Z.D. and J.M. Tarbell, *Fluid flow mechanotransduction in vascular smooth muscle cells and fibroblasts.* Ann Biomed Eng, 2011. **39**(6): p. 1608-19.
36. Nikmanesh, M., Z.D. Shi, and J.M. Tarbell, *Heparan sulfate proteoglycan mediates shear stress-induced endothelial gene expression in mouse embryonic stem cell-derived endothelial cells.* Biotechnol Bioeng, 2012. **109**(2): p. 583-94.

37. Engler, A.J., et al., *Matrix elasticity directs stem cell lineage specification.* Cell, 2006. **126**(4): p. 677-89.
38. Wingate, K., et al., *Compressive elasticity of three-dimensional nanofiber matrix directs mesenchymal stem cell differentiation to vascular cells with endothelial or smooth muscle cell markers.* Acta Biomater, 2012. **8**(4): p. 1440-9.
39. Hanjaya-Putra, D., et al., *Vascular endothelial growth factor and substrate mechanics regulate in vitro tubulogenesis of endothelial progenitor cells.* J Cell Mol Med, 2010. **14**(10): p. 2436-47.
40. Stroka, K.M. and H. Aranda-Espinoza, *Endothelial cell substrate stiffness influences neutrophil transmigration via myosin light chain kinase-dependent cell contraction.* Blood, 2011. **118**(6): p. 1632-40.
41. Engler AJ, R.L., Wong JY, Picart C, Discher D., *Surface probe measurements of the elasticity of sectioned tissue, thin gels and polyelectrolyte multilayer films: correlations between substrate stiffness and cell adhesion.* Surface Sci., 2004. **570**(1): p. 142-154.
42. Bae, Y.H., et al., *Measuring the Stiffness of Ex Vivo Mouse Aortas Using Atomic Force Microscopy.* J Vis Exp, 2016(116).
43. Kothapalli, D., et al., *Cardiovascular protection by ApoE and ApoE-HDL linked to suppression of ECM gene expression and arterial stiffening.* Cell Rep, 2012. **2**(5): p. 1259-71.
44. Peloquin, J., et al., *Indentation measurements of the subendothelial matrix in bovine carotid arteries.* J Biomech, 2011. **44**(5): p. 815-21.
45. Rossmann, J.S., *Elastomechanical properties of bovine veins.* J Mech Behav Biomed Mater, 2010. **3**(2): p. 210-5.
46. Whisler, J.A., M.B. Chen, and R.D. Kamm, *Control of perfusable microvascular network morphology using a multiculture microfluidic system.* Tissue Eng Part C Methods, 2014. **20**(7): p. 543-52.
47. Hsu, Y.H., et al., *A microfluidic platform for generating large-scale nearly identical human microphysiological vascularized tissue arrays.* Lab Chip, 2013. **13**(15): p. 2990-8.
48. Kim, S., et al., *Engineering of functional, perfusable 3D microvascular networks on a chip.* Lab Chip, 2013. **13**(8): p. 1489-500.
49. Vailhe, B., et al., *In vitro angiogenesis is modulated by the mechanical properties of fibrin gels and is related to alpha(v)beta3 integrin localization.* In Vitro Cell Dev Biol Anim, 1997. **33**(10): p. 763-73.
50. Brooks, P.C., R.A. Clark, and D.A. Cheresh, *Requirement of vascular integrin alpha v beta 3 for angiogenesis.* Science, 1994. **264**(5158): p. 569-71.
51. Gamble, J.R., et al., *Regulation of in vitro capillary tube formation by anti-integrin antibodies.* J Cell Biol, 1993. **121**(4): p. 931-43.
52. Belair, D.G., et al., *Human vascular tissue models formed from human induced pluripotent stem cell derived endothelial cells.* Stem Cell Rev, 2015. **11**(3): p. 511-25.
53. Agarwal, A., et al., *Micropatterning Alginate Substrates for Cardiovascular Muscle on a Chip.* Adv Funct Mater, 2013. **23**(30): p. 3738-3746.

54. Peck, M., et al., *The evolution of vascular tissue engineering and current state of the art.* Cells Tissues Organs, 2012. **195**(1-2): p. 144-58.
55. Thitiwuthikiat, P., et al., *A vascular patch prepared from Thai silk fibroin and gelatin hydrogel incorporating simvastatin-micelles to recruit endothelial progenitor cells.* Tissue Eng Part A, 2015. **21**(7-8): p. 1309-19.
56. Chlupac, J., E. Filova, and L. Bacakova, *Blood vessel replacement: 50 years of development and tissue engineering paradigms in vascular surgery.* Physiol Res, 2009. **58 Suppl 2**: p. S119-39.
57. Ravi, S. and E.L. Chaikof, *Biomaterials for vascular tissue engineering.* Regen Med, 2010. **5**(1): p. 107-20.
58. Lovett, M., et al., *Tubular silk scaffolds for small diameter vascular grafts.* Organogenesis, 2010. **6**(4): p. 217-24.
59. Kundu, J., et al., *Silk fibroin nanoparticles for cellular uptake and control release.* Int J Pharm, 2010. **388**(1-2): p. 242-50.
60. Sofia, S., et al., *Functionalized silk-based biomaterials for bone formation.* J Biomed Mater Res, 2001. **54**(1): p. 139-48.
61. Lovett, M., et al., *Vascularization strategies for tissue engineering.* Tissue Eng Part B Rev, 2009. **15**(3): p. 353-70.
62. Griffith, C.K., et al., *Diffusion limits of an in vitro thick prevascularized tissue.* Tissue Eng, 2005. **11**(1-2): p. 257-66.
63. Jain, R.K., et al., *Engineering vascularized tissue.* Nat Biotechnol, 2005. **23**(7): p. 821-3.
64. Blancas, A., Shih, AJ, Lauer, NE, McCloskey KE, *Endothelial Cells from Embryonic Stem Cells in a Chemically Defined Medium.* Stem Cells and Development, 2011.
65. Blancas, A.A., N.E. Lauer, and K.E. McCloskey, *Endothelial differentiation of embryonic stem cells.* Curr Protoc Stem Cell Biol, 2008. **Chapter 1**: p. Unit 1F 5.
66. Pelham, R.J., Jr. and Y. Wang, *Cell locomotion and focal adhesions are regulated by substrate flexibility.* Proc Natl Acad Sci U S A, 1997. **94**(25): p. 13661-5.
67. Totaro, A., et al., *YAP/TAZ link cell mechanics to Notch signalling to control epidermal stem cell fate.* Nat Commun, 2017. **8**: p. 15206.
68. Evans, N.D., et al., *Substrate stiffness affects early differentiation events in embryonic stem cells.* Eur Cell Mater, 2009. **18**: p. 1-13; discussion 13-4.
69. Wang, P.Y., W.B. Tsai, and N.H. Voelcker, *Screening of rat mesenchymal stem cell behaviour on polydimethylsiloxane stiffness gradients.* Acta Biomater, 2012. **8**(2): p. 519-30.
70. Her, G.J., et al., *Control of three-dimensional substrate stiffness to manipulate mesenchymal stem cell fate toward neuronal or glial lineages.* Acta Biomater, 2013. **9**(2): p. 5170-80.
71. Watt, F.M. and W.T. Huck, *Role of the extracellular matrix in regulating stem cell fate.* Nat Rev Mol Cell Biol, 2013. **14**(8): p. 467-73.
72. Wingate, K., et al., *Synergism of matrix stiffness and vascular endothelial growth factor on mesenchymal stem cells for vascular endothelial regeneration.* Tissue engineering. Part A, 2014. **20**(17-18): p. 2503-12.

73. Park, J.S., et al., *The effect of matrix stiffness on the differentiation of mesenchymal stem cells in response to TGF-beta.* Biomaterials, 2011. **32**(16): p. 3921-30.
74. Sack, K.D., M. Teran, and M.A. Nugent, *Extracellular Matrix Stiffness Controls VEGF Signaling and Processing in Endothelial Cells.* Journal of cellular physiology, 2016. **231**(9): p. 2026-39.
75. Riveline, D., et al., *Focal contacts as mechanosensors: externally applied local mechanical force induces growth of focal contacts by an mDia1-dependent and ROCK-independent mechanism.* J Cell Biol, 2001. **153**(6): p. 1175-86.
76. Mammoto, A., et al., *A mechanosensitive transcriptional mechanism that controls angiogenesis.* Nature, 2009. **457**(7233): p. 1103-8.
77. Juliano, R.L. and S. Haskill, *Signal transduction from the extracellular matrix.* J Cell Biol, 1993. **120**(3): p. 577-85.
78. Moursi, A.M., R.K. Globus, and C.H. Damsky, *Interactions between integrin receptors and fibronectin are required for calvarial osteoblast differentiation in vitro.* J Cell Sci, 1997. **110 (Pt 18)**: p. 2187-96.
79. Schaffner, F., A.M. Ray, and M. Dontenwill, *Integrin alpha5beta1, the Fibronectin Receptor, as a Pertinent Therapeutic Target in Solid Tumors.* Cancers (Basel), 2013. **5**(1): p. 27-47.
80. Ishida, T., et al., *MAP kinase activation by flow in endothelial cells. Role of beta 1 integrins and tyrosine kinases.* Circ Res, 1996. **79**(2): p. 310-6.
81. Fromigue, O., et al., *Peptide-based activation of alpha5 integrin for promoting osteogenesis.* J Cell Biochem, 2012. **113**(9): p. 3029-38.
82. Soldi, R., et al., *Role of alphavbeta3 integrin in the activation of vascular endothelial growth factor receptor-2.* EMBO J, 1999. **18**(4): p. 882-92.
83. Hermann, P., et al., *The vitronectin receptor and its associated CD47 molecule mediates proinflammatory cytokine synthesis in human monocytes by interaction with soluble CD23.* J Cell Biol, 1999. **144**(4): p. 767-75.
84. Kothapalli D, L.S., Byfield FJ, et al., *Apolipoprotein E controls matrix protein synthesis and arterial stiffness.* Poster presented at the American Society of Cell Biology Annual Meeting, 2010.
85. Gobaa, S., et al., *Artificial niche microarrays for probing single stem cell fate in high throughput.* Nat Methods, 2011. **8**(11): p. 949-55.
86. Parekh, S.H., et al., *Modulus-driven differentiation of marrow stromal cells in 3D scaffolds that is independent of myosin-based cytoskeletal tension.* Biomaterials, 2011. **32**(9): p. 2256-64.
87. Huebsch, N., et al., *Harnessing traction-mediated manipulation of the cell/matrix interface to control stem-cell fate.* Nat Mater, 2010. **9**(6): p. 518-26.
88. Banerjee, A., et al., *The influence of hydrogel modulus on the proliferation and differentiation of encapsulated neural stem cells.* Biomaterials, 2009. **30**(27): p. 4695-9.
89. Trappmann, B., et al., *Extracellular-matrix tethering regulates stem-cell fate.* Nat Mater, 2012. **11**(7): p. 642-9.

90. Shao, Y. and J. Fu, *Integrated micro/nanoengineered functional biomaterials for cell mechanics and mechanobiology: a materials perspective.* Adv Mater, 2014. **26**(10): p. 1494-533.
91. Choi, Y.S., et al., *The alignment and fusion assembly of adipose-derived stem cells on mechanically patterned matrices.* Biomaterials, 2012. **33**(29): p. 6943-51.
92. Tse, J.R. and A.J. Engler, *Preparation of hydrogel substrates with tunable mechanical properties.* Curr Protoc Cell Biol, 2010. **Chapter 10**: p. Unit 10 16.
93. Sirghi, L., et al., *Probing elasticity and adhesion of live cells by atomic force microscopy indentation.* Eur Biophys J, 2008. **37**(6): p. 935-45.
94. Grant, C.A. and P.C. Twigg, *Pseudostatic and dynamic nanomechanics of the tunica adventitia in elastic arteries using atomic force microscopy.* ACS Nano, 2013. **7**(1): p. 456-64.
95. S., A. *FastQC A Quality Control tool for High Throughput Sequence Data*. 2010; Available from: www.bioinformatics.babraham.ac.uk/projects/fastqc.
96. Krueger, F. *Trim Galore!: A wrapper tool around Cutadapt and FastQC to consistently apply quality and adapter trimming to FastQ files*. Available from: www.bioinformatics.babraham.ac.uk/projects/trim_galore/.
97. Martin, M., *Cutadapt removes adapter sequences from high through-put sequencing reads.* EMBnet, 2011. **J**(17): p. 10-12.
98. Dobin, A., et al., *STAR: ultrafast universal RNA-seq aligner*. Bioinformatics, 2013. **29**(1): p. 15-21.
99. Love, M.I., W. Huber, and S. Anders, *Moderated estimation of fold change and dispersion for RNA-seq data with DESeq2.* Genome Biol, 2014. **15**(12): p. 550.
100. Huang da, W., B.T. Sherman, and R.A. Lempicki, *Systematic and integrative analysis of large gene lists using DAVID bioinformatics resources.* Nat Protoc, 2009. **4**(1): p. 44-57.
101. Huang da, W., B.T. Sherman, and R.A. Lempicki, *Bioinformatics enrichment tools: paths toward the comprehensive functional analysis of large gene lists.* Nucleic Acids Res, 2009. **37**(1): p. 1-13.
102. Skardal, A., et al., *Substrate elasticity controls cell proliferation, surface marker expression and motile phenotype in amniotic fluid-derived stem cells.* J Mech Behav Biomed Mater, 2013. **17**: p. 307-16.
103. Katsumi, A., et al., *Integrins in mechanotransduction.* J Biol Chem, 2004. **279**(13): p. 12001-4.
104. Collins, C., et al., *Localized tensional forces on PECAM-1 elicit a global mechanotransduction response via the integrin-RhoA pathway.* Curr Biol, 2012. **22**(22): p. 2087-94.
105. Shih, Y.R., et al., *Matrix stiffness regulation of integrin-mediated mechanotransduction during osteogenic differentiation of human mesenchymal stem cells.* J Bone Miner Res, 2011. **26**(4): p. 730-8.
106. Plow, E.F., et al., *Ligand binding to integrins.* J Biol Chem, 2000. **275**(29): p. 21785-8.
107. Boudreau, N.J. and J.A. Varner, *The homeobox transcription factor Hox D3 promotes integrin alpha5beta1 expression and function during angiogenesis.* J Biol Chem, 2004. **279**(6): p. 4862-8.

108. Stupack, D.G. and D.A. Cheresh, *ECM remodeling regulates angiogenesis: endothelial integrins look for new ligands.* Sci STKE, 2002. **2002**(119): p. pe7.
109. Bayless, K.J., R. Salazar, and G.E. Davis, *RGD-dependent vacuolation and lumen formation observed during endothelial cell morphogenesis in three-dimensional fibrin matrices involves the alpha(v)beta(3) and alpha(5)beta(1) integrins.* Am J Pathol, 2000. **156**(5): p. 1673-83.
110. Zovein, A.C., et al., *Beta1 integrin establishes endothelial cell polarity and arteriolar lumen formation via a Par3-dependent mechanism.* Dev Cell, 2010. **18**(1): p. 39-51.
111. Jeltsch, M., et al., *Receptor tyrosine kinase-mediated angiogenesis.* Cold Spring Harb Perspect Biol, 2013. **5**(9).
112. Thomas, M., et al., *Angiopoietin-2 stimulation of endothelial cells induces alphavbeta3 integrin internalization and degradation.* J Biol Chem, 2010. **285**(31): p. 23842-9.
113. Cascone, I., et al., *Stable interaction between alpha5beta1 integrin and Tie2 tyrosine kinase receptor regulates endothelial cell response to Ang-1.* J Cell Biol, 2005. **170**(6): p. 993-1004.
114. Brooks, P.C., et al., *Integrin alpha v beta 3 antagonists promote tumor regression by inducing apoptosis of angiogenic blood vessels.* Cell, 1994. **79**(7): p. 1157-64.
115. Su, G., et al., *Effective treatment of mouse sepsis with an inhibitory antibody targeting integrin alphavbeta5.* Crit Care Med, 2013. **41**(2): p. 546-53.
116. Humphries, M.J., *Monoclonal antibodies as probes of integrin priming and activation.* Biochem Soc Trans, 2004. **32**(Pt3): p. 407-11.
117. Mould, A.P., et al., *Regulation of integrin function: evidence that bivalent-cation-induced conformational changes lead to the unmasking of ligand-binding sites within integrin alpha5 beta1.* Biochem J, 1998. **331 (Pt 3)**: p. 821-8.
118. Blancas, A.A., et al., *Specialized tip/stalk-like and phalanx-like endothelial cells from embryonic stem cells.* Stem Cells Dev, 2013. **22**(9): p. 1398-407.
119. Felcht, M., et al., *Angiopoietin-2 differentially regulates angiogenesis through TIE2 and integrin signaling.* J Clin Invest, 2012. **122**(6): p. 1991-2005.
120. Hunter, T., *Signaling--2000 and beyond.* Cell, 2000. **100**(1): p. 113-27.
121. Ruegg, C. and A. Mariotti, *Vascular integrins: pleiotropic adhesion and signaling molecules in vascular homeostasis and angiogenesis.* Cell Mol Life Sci, 2003. **60**(6): p. 1135-57.
122. Retta, S.F., et al., *Cross talk between beta(1) and alpha(V) integrins: beta(1) affects beta(3) mRNA stability.* Mol Biol Cell, 2001. **12**(10): p. 3126-38.
123. Zoller, M., *Tetraspanins: push and pull in suppressing and promoting metastasis.* Nat Rev Cancer, 2009. **9**(1): p. 40-55.
124. Nazarenko, I., et al., *Cell surface tetraspanin Tspan8 contributes to molecular pathways of exosome-induced endothelial cell activation.* Cancer Res, 2010. **70**(4): p. 1668-78.
125. Webber, J., V. Yeung, and A. Clayton, *Extracellular vesicles as modulators of the cancer microenvironment.* Semin Cell Dev Biol, 2015. **40**: p. 27-34.

126. Chen, Y.C., et al., *Functional Human Vascular Network Generated in Photocrosslinkable Gelatin Methacrylate Hydrogels.* Adv Funct Mater, 2012. **22**(10): p. 2027-2039.
127. Hasan, A., et al., *Microfluidic techniques for development of 3D vascularized tissue.* Biomaterials, 2014. **35**(26): p. 7308-25.
128. Boyd, N.L., et al., *Microvascular mural cell functionality of human embryonic stem cell-derived mesenchymal cells.* Tissue Eng Part A, 2011. **17**(11-12): p. 1537-48.
129. Kitahara, T., et al., *Mesangial cells stimulate differentiation of endothelial cells to form capillary-like networks in a three-dimensional culture system.* Nephrol Dial Transplant, 2005. **20**(1): p. 42-9.
130. Sakaguchi, K., et al., *In vitro engineering of vascularized tissue surrogates.* Sci Rep, 2013. **3**: p. 1316.
131. Vickerman, V., et al., *Design, fabrication and implementation of a novel multi-parameter control microfluidic platform for three-dimensional cell culture and real-time imaging.* Lab Chip, 2008. **8**(9): p. 1468-77.
132. Turner, W.S., et al., *Cardiac tissue development for delivery of embryonic stem cell-derived endothelial and cardiac cells in natural matrices.* J Biomed Mater Res B Appl Biomater, 2012. **100**(8): p. 2060-72.
133. Ma, S.H., et al., *An endothelial and astrocyte co-culture model of the blood-brain barrier utilizing an ultra-thin, nanofabricated silicon nitride membrane.* Lab Chip, 2005. **5**(1): p. 74-85.
134. Dai, N.T., et al., *A co-cultured skin model based on cell support membranes.* Biochemical and biophysical research communications, 2005. **329**(3): p. 905-8.
135. Hermanns, M.I., et al., *Lung epithelial cell lines in coculture with human pulmonary microvascular endothelial cells: development of an alveolo-capillary barrier in vitro.* Laboratory investigation; a journal of technical methods and pathology, 2004. **84**(6): p. 736-52.
136. Sanchez, P.L., et al., *Acellular human heart matrix: A critical step toward whole heart grafts.* Biomaterials, 2015. **61**: p. 279-289.
137. Faulk, D.M., J.D. Wildemann, and S.F. Badylak, *Decellularization and cell seeding of whole liver biologic scaffolds composed of extracellular matrix.* Journal of clinical and experimental hepatology, 2015. **5**(1): p. 69-80.
138. Orlando, G., et al., *Discarded human kidneys as a source of ECM scaffold for kidney regeneration technologies.* Biomaterials, 2013. **34**(24): p. 5915-25.
139. Luna, J.I., et al., *Multiscale biomimetic topography for the alignment of neonatal and embryonic stem cell-derived heart cells.* Tissue Eng Part C Methods, 2011. **17**(5): p. 579-88.
140. Jang, J., et al., *3D printed complex tissue construct using stem cell-laden decellularized extracellular matrix bioinks for cardiac repair.* Biomaterials, 2017. **112**: p. 264-274.
141. Wong, L., et al., *Leaf-inspired microcontact printing vascular patterns.* Biofabrication, 2017. **9**(2): p. 021001.
142. Madfis, N., et al., *Co-emergence of Specialized Endothelial Cells from Embryonic Stem Cells.* Stem Cells Dev, 2018.

143. Zudaire, E., et al., *A computational tool for quantitative analysis of vascular networks.* PLoS One, 2011. **6**(11): p. e27385.
144. James, D., et al., *Expansion and maintenance of human embryonic stem cell-derived endothelial cells by TGFbeta inhibition is Id1 dependent.* Nat Biotechnol, 2010. **28**(2): p. 161-6.
145. Ye, Q., et al., *Fibrin gel as a three dimensional matrix in cardiovascular tissue engineering.* Eur J Cardiothorac Surg, 2000. **17**(5): p. 587-91.
146. Prentice, C.R., *Basis of antifibrinolytic therapy.* J Clin Pathol Suppl (R Coll Pathol), 1980. **14**: p. 35-40.
147. Chapman, H.A., R.J. Riese, and G.P. Shi, *Emerging roles for cysteine proteases in human biology.* Annu Rev Physiol, 1997. **59**: p. 63-88.
148. Reiser, J., B. Adair, and T. Reinheckel, *Specialized roles for cysteine cathepsins in health and disease.* J Clin Invest, 2010. **120**(10): p. 3421-31.
149. Folberg, R., M.J. Hendrix, and A.J. Maniotis, *Vasculogenic mimicry and tumor angiogenesis.* Am J Pathol, 2000. **156**(2): p. 361-81.
150. Zhang, W., et al., *Down-regulating Myoferlin inhibits the vasculogenic mimicry of melanoma via decreasing MMP-2 and inducing mesenchymal-to-epithelial transition.* J Cell Mol Med, 2018. **22**(3): p. 1743-1754.
151. Liu, Y., et al., *MMP-2 and MMP-9 contribute to the angiogenic effect produced by hypoxia/15-HETE in pulmonary endothelial cells.* J Mol Cell Cardiol, 2018. **121**: p. 36-50.
152. Bergers, G., et al., *Matrix metalloproteinase-9 triggers the angiogenic switch during carcinogenesis.* Nat Cell Biol, 2000. **2**(10): p. 737-44.
153. Radisic, M., et al., *Oxygen gradients correlate with cell density and cell viability in engineered cardiac tissue.* Biotechnol Bioeng, 2006. **93**(2): p. 332-43.
154. Shimizu, T., et al., *Polysurgery of cell sheet grafts overcomes diffusion limits to produce thick, vascularized myocardial tissues.* FASEB J, 2006. **20**(6): p. 708-10.
155. Zhang, J., *Engineered Tissue Patch for Cardiac Cell Therapy.* Curr Treat Options Cardiovasc Med, 2015. **17**(8): p. 399.
156. Tulloch, N.L., et al., *Growth of engineered human myocardium with mechanical loading and vascular coculture.* Circ Res, 2011. **109**(1): p. 47-59.
157. Hellstrom, M., et al., *Dll4 signalling through Notch1 regulates formation of tip cells during angiogenesis.* Nature, 2007. **445**(7129): p. 776-80.
158. Huber, A.B., et al., *Signaling at the growth cone: ligand-receptor complexes and the control of axon growth and guidance.* Annu Rev Neurosci, 2003. **26**: p. 509-63.
159. Gerhardt, H., et al., *VEGF guides angiogenic sprouting utilizing endothelial tip cell filopodia.* J Cell Biol, 2003. **161**(6): p. 1163-77.
160. Mazzone, M., et al., *Heterozygous deficiency of PHD2 restores tumor oxygenation and inhibits metastasis via endothelial normalization.* Cell, 2009. **136**(5): p. 839-851.
161. Velazquez, O.C., et al., *Fibroblast-dependent differentiation of human microvascular endothelial cells into capillary-like 3-dimensional networks.* FASEB J, 2002. **16**(10): p. 1316-8.

162. Shen, E.M. and K.E. McCloskey, *Development of Mural Cells: From In Vivo Understanding to In Vitro Recapitulation.* Stem Cells Dev, 2017. **26**(14): p. 1020-1041.
163. Lindblom, P., et al., *Endothelial PDGF-B retention is required for proper investment of pericytes in the microvessel wall.* Genes Dev, 2003. **17**(15): p. 1835-40.
164. Abramsson, A., et al., *Analysis of mural cell recruitment to tumor vessels.* Circulation, 2002. **105**(1): p. 112-7.
165. Majesky, M.W., et al., *Vascular smooth muscle progenitor cells: building and repairing blood vessels.* Circ Res, 2011. **108**(3): p. 365-77.
166. Crisan, M., et al., *A perivascular origin for mesenchymal stem cells in multiple human organs.* Cell Stem Cell, 2008. **3**(3): p. 301-13.
167. Kusuma, S., et al., *Self-organized vascular networks from human pluripotent stem cells in a synthetic matrix.* Proc Natl Acad Sci U S A, 2013. **110**(31): p. 12601-6.
168. Orlova, V.V., et al., *Functionality of endothelial cells and pericytes from human pluripotent stem cells demonstrated in cultured vascular plexus and zebrafish xenografts.* Arterioscler Thromb Vasc Biol, 2014. **34**(1): p. 177-86.
169. Alonzo, L.F., et al., *Microfluidic device to control interstitial flow-mediated homotypic and heterotypic cellular communication.* Lab Chip, 2015. **15**(17): p. 3521-9.
170. Ehsan, S.M., et al., *A three-dimensional in vitro model of tumor cell intravasation.* Integr Biol (Camb), 2014. **6**(6): p. 603-10.
171. Bichsel, C.A., et al., *Primary Human Lung Pericytes Support and Stabilize In Vitro Perfusable Microvessels.* Tissue Eng Part A, 2015. **21**(15-16): p. 2166-76.
172. Kim, J., et al., *Engineering of a Biomimetic Pericyte-Covered 3D Microvascular Network.* PLoS One, 2015. **10**(7): p. e0133880.
173. Coulombe, K.L., et al., *Heart regeneration with engineered myocardial tissue.* Annu Rev Biomed Eng, 2014. **16**: p. 1-28.
174. Radisic, M., et al., *Biomimetic approach to cardiac tissue engineering.* Philos Trans R Soc Lond B Biol Sci, 2007. **362**(1484): p. 1357-68.
175. Roll, S., et al., *Dacron vs. PTFE as bypass materials in peripheral vascular surgery--systematic review and meta-analysis.* BMC Surg, 2008. **8**: p. 22.
176. Hielscher, D., et al., *Stem Cell Sources and Graft Material for Vascular Tissue Engineering.* Stem Cell Rev, 2018.
177. Kurobe, H., et al., *Development of small diameter nanofiber tissue engineered arterial grafts.* PLoS One, 2015. **10**(4): p. e0120328.
178. Battiston, K.G., et al., *Monocyte/macrophage cytokine activity regulates vascular smooth muscle cell function within a degradable polyurethane scaffold.* Acta Biomater, 2014. **10**(3): p. 1146-55.
179. Schmidt, C.E. and J.M. Baier, *Acellular vascular tissues: natural biomaterials for tissue repair and tissue engineering.* Biomaterials, 2000. **21**(22): p. 2215-31.
180. Wu, H.C., et al., *Coculture of endothelial and smooth muscle cells on a collagen membrane in the development of a small-diameter vascular graft.* Biomaterials, 2007. **28**(7): p. 1385-1392.

181. Sreerekha, P.R., P. Divya, and L.K. Krishnan, *Adult stem cell homing and differentiation in vitro on composite fibrin matrix.* Cell Proliferation, 2006. **39**(4): p. 301-312.
182. Wang, J.N., et al., *Cytocompatibility of a silk fibroin tubular scaffold.* Materials Science & Engineering C-Materials for Biological Applications, 2014. **34**: p. 429-436.
183. Nogueira, G.M., et al., *Preparation and characterization of ethanol-treated silk fibroin dense membranes for biomaterials application using waste silk fibers as raw material.* Bioresour Technol, 2010. **101**(21): p. 8446-51.
184. Vazquez, N., et al., *Silk Fibroin Films for Corneal Endothelial Regeneration: Transplant in a Rabbit Descemet Membrane Endothelial Keratoplasty.* Invest Ophthalmol Vis Sci, 2017. **58**(9): p. 3357-3365.
185. Adali, T. and M. Uncu, *Silk fibroin as a non-thrombogenic biomaterial.* Int J Biol Macromol, 2016. **90**: p. 11-9.
186. Mehrotra, S., S.K. Nandi, and B.B. Mandal, *Stacked silk-cell monolayers as a biomimetic three dimensional construct for cardiac tissue reconstruction.* Journal of Materials Chemistry B, 2017. **5**(31): p. 6325-6338.
187. Yen, K.C., et al., *Fabrication of keratin/fibroin membranes by electrospinning for vascular tissue engineering.* Journal of Materials Chemistry B, 2016. **4**(2): p. 237-244.
188. Tu, F.F., et al., *Vascular Cell Co-Culture on Silk Fibroin Matrix.* Polymers, 2018. **10**(1).
189. Wilson, D., R. Valluzzi, and D. Kaplan, *Conformational transitions in model silk peptides.* Biophys J, 2000. **78**(5): p. 2690-701.
190. Min, B.M., et al., *Regenerated silk fibroin nanofibers: water vapor-induced structural changes and their effects on the behavior of normal human cells.* Macromol Biosci, 2006. **6**(4): p. 285-92.
191. Neal, D., et al., *Mechanical Characterization and Shape Optimization of Fascicle-Like 3D Skeletal Muscle Tissues Contracted with Electrical and Optical Stimuli.* Tissue engineering. Part A, 2015. **21**(11-12): p. 1848-58.
192. Neal, D., et al., *Formation of elongated fascicle-inspired 3D tissues consisting of high-density, aligned cells using sacrificial outer molding.* Lab Chip, 2014. **14**(11): p. 1907-16.
193. Jin, H.J., et al., *Electrospinning Bombyx mori silk with poly(ethylene oxide).* Biomacromolecules, 2002. **3**(6): p. 1233-9.
194. Amirikia, M., et al., *Auto-fluorescence of a silk fibroin-based scaffold and its interference with fluorophores in labeled cells.* Eur Biophys J, 2018. **47**(5): p. 573-581.
195. Valluzzi, R., et al., *Orientation of silk III at the air-water interface.* Int J Biol Macromol, 1999. **24**(2-3): p. 237-42.
196. Asakura, T., et al., *Synthesis and characterization of water-soluble silk peptides and recombinant silk protein containing polyalanine, the integrin binding site, and two glutamic acids at each terminal site as a possible candidate for use in bone repair materials.* Biomacromolecules, 2013. **14**(10): p. 3731-41.
197. Seib, F.P., *Silk hydrogels for drug and cell delivery*. 2018.

198. Yucel, T., M.L. Lovett, and D.L. Kaplan, *Silk-based biomaterials for sustained drug delivery.* J Control Release, 2014. **190**: p. 381-97.
199. Song, K.H., S.J. Cho, and J.Y. Song, *alphavbeta1 integrin as a novel therapeutic target for tissue fibrosis.* Ann Transl Med, 2016. **4**(20): p. 411.
200. Weis, S.M. and D.A. Cheresh, *alphaV integrins in angiogenesis and cancer.* Cold Spring Harb Perspect Med, 2011. **1**(1): p. a006478.
201. Zhang, H., et al., *Preparation and characterization of silk fibroin as a biomaterial with potential for drug delivery.* J Transl Med, 2012. **10**: p. 117.